International Journal of Mechanical Sciences 286 (2025) 109794

Contents lists available at ScienceDirect

International Journal of Mechanical Sciences

journal homepage: www.elsevier.com/locate/ijmecsci

Enhanced high-frequency continualization scheme for inertial beam-lattice metamaterials

Andrea Bacigalupo *, Paolo Badino, Vito Diana, Luigi Gambarotta

DICCA, University of Genova, Italy

ARTICLE INFO

Keywords:
2D Lattices
Microstructured materials
Local resonators
Multifield continuum models
Frequency band structures
Band-gaps

ABSTRACT

A multifield continualization technique is introduced that offers a thermodynamically consistent description of the constitutive and dispersive properties of beam-lattice inertial metamaterials with periodic microstructures. The balance equations governing the mechanics of the discrete Lagrangian system are appropriately handled using an innovative continualization scheme to derive an equivalent integral-type continuum model. Based on formal Taylor series expansion of the integral kernels or the corresponding pseudo-differential functions incorporating shift operators and appropriate pseudo-differential downscaling laws, the proposed multifield enhanced continualization scheme allows the derivation of a gradient-type continuum model of given rank and equivalent to lattices. Two different resolution techniques are proposed. Firstly, the corresponding infinite-order average differential equations are tackled using a perturbative approach to describe the forced Bloch wave propagation in the metamaterial. Secondly, higher-order continuum models are employed through proper differential equation truncation to characterize the dispersive properties of the metamaterial in both high- and low-frequency regimes. Moreover, an energetically consistent generalized equivalent Micropolar continua, with non-local inertial terms, are here identified. The multifield continualization procedure is applied to two-dimensional periodic microstructures with tetrachiral, hexachiral, and hexa-tetrachiral topologies. Illustrative examples highlight the ability of the equivalent continuum model to accurately describe the effective constitutive properties of inertial metamaterials with periodic microstructures and to define a dynamic response consistent with the discrete Lagrangian model, validated and tested through virtual experimental verification under free and forced wave conditions.

1. Introduction

Periodic reticular micro-architectured materials represent a class of functionally engineered materials associated, in general, with lightweight properties and whose peculiar macroscopic physical/mechanical characteristics result from the unique combination of tailored microstructure and intrinsic material properties [1-4]. The advancements in three-dimensional printing and additive manufacturing technologies have now enabled the large-scale design and production of truss, beam-like, block-like, and other periodic reticulated lattices (micro) structures exhibiting unconventional and remarkable elastic and acoustic properties [5-12]. To achieve unique elastic properties such as auxeticity, bulk strain-rotation and axial/shear-bending couplings, a variety of lattice-like microstructures can be employed [13-20]. Additionally, recent advances in the use of periodic lattice-like materials have focused on the active and passive control of mechanical behavior using techniques like time-modulated tunable lattices and other frequency spectrum tuning devices [21-29].

Periodic reticulated materials characterized by rigid solid phases interconnected by elastic ligaments or interfaces, known as beam or block-lattice materials, represent a distinct class of lattice-like solids with profound similarities to blocky rock and masonry-like systems, granular materials, biological and bio-inspired microstructures, grids, honeycombs, and other heterogeneous composites [30-42]. A salient feature of artificial architectured materials of this kind lies in the possibility of periodically assembling lumped masses or rigid units of specified geometry with elastic elements or generic soft phases of varying characteristics, thereby achieving diverse overall mechanical and physical properties while providing simple and intuitive micro-macro correspondence [43-48]. Actually, from a mechanical perspective, beam-lattice materials (along with block-lattices and spring networks with lumped masses), can be effectively modeled as discrete

* Corresponding author.
E-mail address: andrea.bacigalupo@unige.it (A. Bacigalupo).

https://doi.org/10.1016/j.ijmecsci.2024.109794
Received 24 July 2024; Received in revised form 26 September 2024; Accepted 18 October 2024
Available online 20 October 2024

Lagrangian systems. In these systems, a node-centered periodic cell with specific size and lattice periodicity vectors can be identified, with generalized interactions between elements being derived from a properly defined elastic potential which turns out to be a function of pairwise defined kinematics and pairwise constitutive properties [49,50]. It is well established that due to the finite dimension of the periodic microstructure, these materials shows length-scale sensitivity which manifests itself in size/boundary layer effects and dispersion phenomena of elastic waves induced by diffuse Bragg scattering. However, the frequency band structures associated with the aforementioned architectured materials exhibit, in general, high spectral density.

To achieve low and full-frequency band gaps, the use of local resonators, typically consisting of a hard core surrounded by a soft coating, has proven particularly effective. Indeed, locally resonant materials (namely inertial metamaterials) may exhibit stop bands at frequencies close to that proper of the resonator and induced by both diffusive Bragg and localized Mie scattering, resulting in overall negative mass density and bulk modulus of the lattice [51-57]. Recently, chiral periodic architectured materials with internal locally resonant structures with tunable low-frequency band-gaps have been proposed by [58-64], demonstrating that the physical coupling of rotational and translational local resonances in chiral microstructures creates low-frequency stop bands and other exotic acoustic/elastic effects [65]. Numerical analysis and experimental validation confirmed hexachiral beam-lattices with softly coated heavy cylinder resonators achieve low-frequency band gaps [60,66].

Although discrete Lagrangian modeling provides a simple and accurate description of the mechanical behavior of lattice-like materials, the parallel identification of continuum models derived through specific homogenization schemes is needed to obtain an overall and synthetic characterization of the static and dynamic behavior of periodic architectured material [67]. Moreover, the definition of tensor-valued constitutive laws for continua equivalent to lattices allows for an accurate and effective description of material symmetries, direction-dependent mechanical properties, and elastic coupling effects. First-order continualization is the classical homogenization strategy for materials with a periodic lattice structure, which identifies constitutive parameters for the equivalent standard Cauchy continuum by replacing nodal displacements with first-order Taylor approximations. However, due to the intrinsic limits of classical elasticity, the corresponding equivalent continuum fails to capture elastic size effects and acoustic wave dispersion in discrete periodic materials [68]. Non-local homogenization schemes overcome these limitations by introducing characteristic lengths. Continualization of the Lagrangian functional approximates differences in node displacements, yielding fourth-order differential equations for the equivalent continuum. Despite the positive-definite potential energy density of the discrete model, this property is not retained in the continuous model, leading to ill-conditioning and instability phenomena [44,47,69]. Truncated series or shift and pseudo-differential operators are used in a dual strategy based on the continualization of the Lagrangian discrete governing equations. Partial-differential equations with non-local constitutive tensors and local inertial terms are produced by generalized continualization processes, retaining pathologies from non-positive-defined potential energy density in the analogous continua [70-72]. Regularized continualization methods offer solutions to these challenges. One common approach involves employing shift operators to convert discrete system equations into pseudo-differential equations, approximated using Padé approximants. This introduces non-local inertial terms indirectly, enriching the continuum models [73-77]. However, in some cases, this strategy may fail to ensure positive-definite elastic potential energy density in the homogenized continuum. Other continualization approaches, such as spatial discrete Fourier transforms or bilateral Z-transforms, yield integral-differential equations for non-local continua. Despite potential advantages, similar issues with elastic potential energy density persist [78-80]. Rosneau [69] proposed a first-order regularization method for monoatomic chains, using finite forward differences to relate continuous macro-displacement fields to nodal displacements in discrete Lagrangian models. This method modifies the governing equations of the equivalent continuum by introducing non-local inertial terms. Bacigalupo and Gambarotta have suggested a generalized improved continualization approach for one-dimensional beam lattices. This method used shift operators to generate macroscale-defined pseudo-differential field equations through the use of a first-order regularization technique based on central differences with second-order precision [67,81]. By employing formal power series expansion of the pseudo-differential equations, the resultant governing differential equations were derived, incorporating inertial and constitutive non-local terms with matching energetically compatible Lagrangian functionals. It has been demonstrated that using this method an equivalent non-local continuum is obtained that closely reproduces both the static and dynamic response of the discrete model. Gómez-Silva conducted a thorough analysis evaluating several continualization/homogenization procedures for one-dimensional lattices with first-nearest interactions [82,83].

In this scientific scenario, an enhanced high-frequency continualization technique for inertial metamaterials is proposed, providing a thermodynamically consistent characterization of the constitutive and dispersive properties of locally resonant metamaterials with generic periodic microstructures. It is important to highlight that the enhanced high-frequency continualization scheme, here presented, has been developed in a completely general and rigorous mathematical framework that consents to describe in a very accurate way the fundamental aspects of the physical problem at hand. By starting from periodic lattice-like metamaterials, realised by a regular assembling of rigid elements elastically connected to each other, continuum models, governed by integral-differential or averaged differential governing equations (with infinite and finite order), can be consistently identified. Once the equivalent continuum model is characterized, two distinct solution strategies of their field equations are proposed and discussed in detail. One technique employs a perturbative approach to tackle the infinite-order averaged differential equations, which are asymptotically equivalent to the discrete Lagrangian equations, to describe the forced Bloch wave propagation in the metamaterial. The other technique involves determining a higher-order continuum model by appropriately truncating the corresponding infinite-order averaged differential equations, to characterize the dispersive properties of the metamaterial in both high- and low-frequency regimes. The analytical formulation is applied to two-dimensional periodic structures with tetrachiral (Fig. 1b), hexachiral (Fig. 1c), and hexa-tetrachiral (Fig. 1d) topologies. Firstly, energetically consistent generalized micropolar continua with non-local inertial terms have been identified for these topologies, using the proposed enhanced multifield continualization scheme. Particular attention has been then devoted to the propagation of Bloch free waves, investigating how these identified continuum models can convergently approximate the actual frequency spectrum with increasing orders of truncation. Under these free dynamic conditions, a universal characterization of the frequency band structure of the metamaterials is provided for a generic lattice, represented by a monoatomic periodic cell elastically coupled with local resonators and elastically connected with the adjacent atoms/cells. For a fixed direction, the governing structure of the problem is explored, noting that a palindromic characteristic polynomial with respect to the Floquet multiplier governs the general lattice systems being analyzed. Furthermore, a virtual experimental test for the case of forced wave propagation in the first-order continualized model has been developed, extending the applicability of the continualization procedure results.

The paper is structured as follows. Section 2 outlines the dynamic problem formulation for the discrete Lagrangian model. Section 3 introduces the multifield continualization technique, resulting in non-homogeneous integral-differential equations characterized by pseudo-differential operators, which describe the non-local integral-type

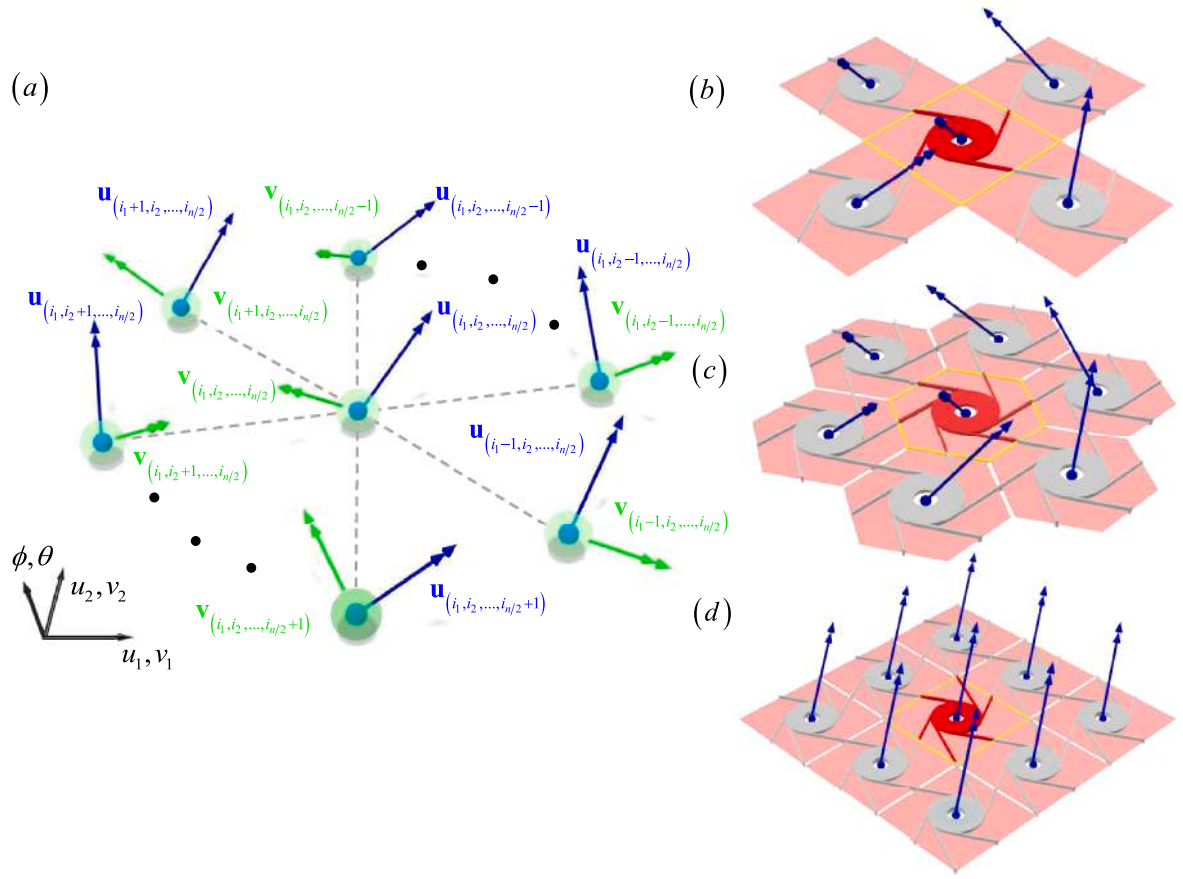

Fig. 1. a) Degrees of freedom associated with a lattice structure equipped with resonators, b) tetrachiral lattice's degrees of freedom, c) hexachiral lattice's degrees of freedom, d) tetra-hexachiral lattice's degrees of freedom.

generalized continuum models equivalent to the discrete Lagrangian lattices. In sub-Section 3.1, these equations are reformulated as non-homogeneous differential equations of infinite order using a Taylor series expansion and solved via a perturbative approach to characterize the forced dynamic response of the inertial metamaterials. Subsequently, Section 4 derives the governing equations for multifield gradient-type continuum models by truncating the previously mentioned infinite-order differential equations. Section 5 provides illustrative examples, including the identification of the global constitutive relation of equivalent generalized micropolar continua for simple non-resonant beam-lattice materials (sub-Section 5.1) and for various considered topologies. Additionally, the propagation of homogeneous free Bloch waves in the discrete Lagrangian system is examined (sub-Section 5.2). In sub-Section 5.3, the non-resonant beam-lattice materials, as well as the full inertial metamaterial, are considered, and the effectiveness of the multifield continualization is validated against the discrete Lagrangian solution for different microstructure topologies. In conclusion, sub-Section 5.4 presents a virtual experimental test aimed at the resolution of harmonic forced wave propagation in the continualized model governed by second-order differential equations, specifically focusing on the case of the hexachiral beam lattice.

2. Discrete Lagrangian model

Let's analyse a generic two-dimensional periodic lattice structure composed of rigid blocks connected by elastic elements, equipped with local resonators in each elementary cell. The dynamics of the cell are described by the vector of degrees of freedom $\mathbf{U}_{(i_1,\ldots,i_{n/2})}(t) = \left(\mathbf{u}_{(i_1,\ldots,i_{n/2})}(t) \quad \mathbf{v}_{(i_1,\ldots,i_{n/2})}(t)\right)^T$ whose components are shown in Fig. 1. The vector $\mathbf{u}_{(i_1,\ldots,i_{n/2})} = \left(u_1^{(i_1,\ldots,i_{n/2})} \quad u_2^{(i_1,\ldots,i_{n/2})} \quad \phi^{(i_1,\ldots,i_{n/2})}\right)^T$ represents the generalized displacement associated with the centroid $(i_1, \ldots, i_{n/2}) \in \mathbb{Z}^{n/2}$ of the elementary block, and the vector $\mathbf{v}_{(i_1,\ldots,i_{n/2})} = \left(v_1^{(i_1,\ldots,i_{n/2})} \quad v_2^{(i_1,\ldots,i_{n/2})} \quad \theta^{(i_1,\ldots,i_{n/2})}\right)^T$ is the generalized displacement of the resonator. The multi-index $(i_1, \ldots, i_{n/2})$ allows for a unique description of the lattice topology considered through the coordination number n (Fig. 2a). The differential equations governing the dynamic problem can be formulated as

$$\begin{aligned}
&\sum_{P(j_1,\ldots,j_{n/2})} \widetilde{\mathbf{K}}^{\mathbf{uu}}_{(j_1,\ldots,j_{n/2})}\mathbf{u}_{(i_1+j_1,\ldots,i_{n/2}+j_{n/2})} + \mathbf{K}^{\mathbf{uv}}\mathbf{v}_{(i_1,\ldots,i_{n/2})} + \mathbf{M}^{\mathbf{uu}}\ddot{\mathbf{u}}_{(i_1,\ldots,i_{n/2})} \\
&= \widetilde{\mathbf{K}}^{\mathbf{uu}}_{(-1,\ldots,0)}\mathbf{u}_{(i_1-1,\ldots,i_{n/2})} + \widetilde{\mathbf{K}}^{\mathbf{uu}}_{(0,\ldots,0)}\mathbf{u}_{(i_1,\ldots,i_{n/2})} + \widetilde{\mathbf{K}}^{\mathbf{uu}}_{(1,\ldots,0)}\mathbf{u}_{(i_1+1,\ldots,i_{n/2})} + \ldots + \\
&+ \widetilde{\mathbf{K}}^{\mathbf{uu}}_{(0,\ldots,-1)}\mathbf{u}_{(i_1,\ldots,i_{n/2}-1)} + \widetilde{\mathbf{K}}^{\mathbf{uu}}_{(0,\ldots,1)}\mathbf{u}_{(i_1,\ldots,i_{n/2}+1)} + \mathbf{K}^{\mathbf{uv}}\mathbf{v}_{(i_1,\ldots,i_{n/2})} + \\
&+ \mathbf{M}^{\mathbf{uu}}\ddot{\mathbf{u}}_{(i_1,\ldots,i_{n/2})} = \mathbf{f}_{(i_1,\ldots,i_{n/2})}, \\
&\mathbf{K}^{\mathbf{vu}}\mathbf{u}_{(i_1,\ldots,i_{n/2})} + \mathbf{K}^{\mathbf{vv}}\mathbf{v}_{(i_1,\ldots,i_{n/2})} + \mathbf{M}^{\mathbf{vv}}\ddot{\mathbf{v}}_{(i_1,\ldots,i_{n/2})} = \mathbf{0},
\end{aligned} \tag{1}$$

where $\widetilde{\mathbf{K}}^{\mathbf{uu}}_{(j_1,\ldots,j_{n/2})}$, $\mathbf{K}^{\mathbf{uv}}$, $\mathbf{K}^{\mathbf{vu}}$ and $\mathbf{K}^{\mathbf{vv}}$ are the 3×3 coefficient matrices dependent on the stiffnesses of the connecting elastic elements of the structure and the local resonator, $\mathbf{M}^{\mathbf{uu}}$ and $\mathbf{M}^{\mathbf{vv}}$ are the 3×3 inertia matrices of the cell and the resonator respectively, while $\mathbf{f}_{(i_1,\ldots,i_{n/2})}$ is the external force applied to the centroid $(i_1, \ldots, i_{n/2})$ of the elementary

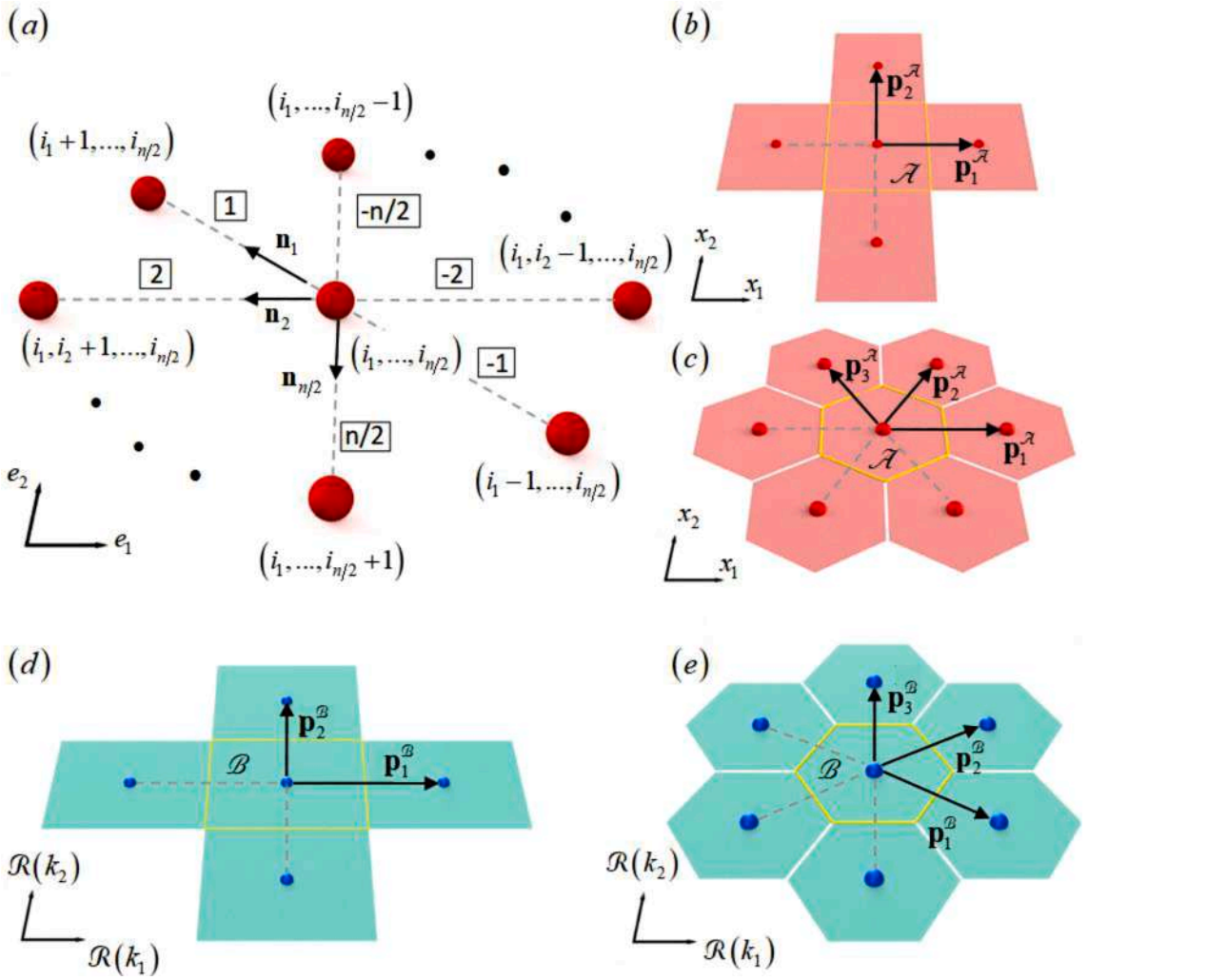

Fig. 2. a) Lattice's reference centroids, b) physical lattice for periodic tetrachiral structure, c) physical lattice for periodic hexachiral structure, d) reciprocal lattice for tetrachiral structure, e) reciprocal lattice for hexachiral structure. Regions *A* and *B* identified in physical and reciprocal lattices represent respectively the periodic elementary cell and the Brillouin zone for the various geometries.

block. The subgroup $\mathscr{P}_{(j_1,\ldots,j_{n/2})} = \left\{ j_1,\ldots,j_{n/2} : j_1,\ldots,j_{n/2} \in \mathbb{Z}^{\leq 1}_{\geq -1} \cup |j_1| + \ldots + |j_{n/2}| \leq 1 \right\}$ collects the $(j_1, \ldots, j_{n/2})$ increment values on the $(i_1, \ldots, i_{n/2})$ coordination lines, identified in the physical space by the periodicity vectors $\mathbf{p}_k^{\mathscr{A}} \in \mathscr{X} \doteq \{\mathbf{X} : \mathbf{X} = c_l \mathbf{w}_l^{\mathscr{A}};\ c_l \in \mathbb{Z},\ l = 1,2\} \in \mathbb{R}^2$ where $\mathbf{w}_l^{\mathscr{A}} = w_r^{\mathscr{A},l}\mathbf{e}_r$ with $r = 1, 2$ are the independent spatial periodicity vectors in the plane, and $\{\mathbf{e}_1,\mathbf{e}_2\}$ is the orthonormal basis, with $k = 1, \ldots, n/2$ indicating the $k-$th coordination direction (references in Fig. 2a–c). Firstly, the Eq. (1) presented are initially modified by introducing the bilateral Z-transform, which transforms a generic vector $\mathbf{y}_{(i_1,\ldots,i_{n/2})}$ defined for the discrete points of the domain $(i_1, \ldots, i_{n/2})$ into a vector dependent on the $n/2$ continuous complex variables $z_1, \ldots, z_{n/2} \in \mathbb{C}$, i.e.

$$\mathscr{Z}\left[\mathbf{y}_{(i_1,\ldots,i_{n/2})}(t)\right] = \sum_{i_1\in\mathbb{Z}} \ldots \sum_{i_{n/2}\in\mathbb{Z}} \mathbf{y}_{(i_1,\ldots,i_{n/2})} z_1^{-i_1} \ldots z_{n/2}^{-i_{n/2}} \doteq \widehat{\mathbf{y}}(z_1, \ldots, z_{n/2}, t). \tag{2}$$

Applying this definition to the variables defined in the differential equations formulated in (1) yields

$$\begin{aligned}
&\sum_{P(j_1,\ldots,j_{n/2})} \widetilde{\mathbf{K}}^{\mathbf{uu}}_{(j_1,\ldots,j_{n/2})} \widehat{\mathbf{u}}(z_1, \ldots, z_{n/2}, t) z_1^{j_1} \ldots z_{n/2}^{j_{n/2}} + \mathbf{K}^{\mathbf{uv}} \widehat{\mathbf{v}}(z_1, \ldots, z_{n/2}, t) + \mathbf{M}^{\mathbf{uu}} \ddot{\widehat{\mathbf{u}}}(z_1, \ldots, z_{n/2}, t) = \\
&= \widetilde{\mathbf{K}}^{\mathbf{uu}}_{(-1,\ldots,0)} \widehat{\mathbf{u}}(z_1, \ldots, z_{n/2}, t) z_1^{-1} + \widetilde{\mathbf{K}}^{\mathbf{uu}}_{(0,\ldots,0)} \widehat{\mathbf{u}}(z_1, \ldots, z_{n/2}, t) + \widetilde{\mathbf{K}}^{\mathbf{uu}}_{(1,\ldots,0)} \widehat{\mathbf{u}}(z_1, \ldots, z_{n/2}, t) z_1 + \ldots + \\
&\quad + \widetilde{\mathbf{K}}^{\mathbf{uu}}_{(0,\ldots,-1)} \widehat{\mathbf{u}}(z_1, \ldots, z_{n/2}, t) z_{n/2}^{-1} + \widetilde{\mathbf{K}}^{\mathbf{uu}}_{(0,\ldots,1)} \widehat{\mathbf{u}}(z_1, \ldots, z_{n/2}, t) z_{n/2} + \\
&\quad + \mathbf{K}^{\mathbf{uv}} \widehat{\mathbf{v}}(z_1, \ldots, z_{n/2}, t) + \mathbf{M}^{\mathbf{uu}} \ddot{\widehat{\mathbf{u}}}(z_1, \ldots, z_{n/2}, t) = \widehat{\mathbf{f}}(z_1, \ldots, z_{n/2}, t), \\
&\mathbf{K}^{\mathbf{vu}} \widehat{\mathbf{u}}(z_1, \ldots, z_{n/2}, t) + \mathbf{K}^{\mathbf{vv}} \widehat{\mathbf{v}}(z_1, \ldots, z_{n/2}, t) + \mathbf{M}^{\mathbf{vv}} \ddot{\widehat{\mathbf{v}}}(z_1, \ldots, z_{n/2}, t) = \mathbf{0},
\end{aligned} \tag{3}$$

and by defining $\mathbf{K}^{\mathbf{uu}}(z_1, \ldots, z_{n/2}) = \sum_{P(j_1,\ldots,j_{n/2})} \widetilde{\mathbf{K}}^{\mathbf{uu}}_{(j_1,\ldots,j_{n/2})} z_1^{j_1} \ldots z_{n/2}^{j_{n/2}}$, it is possible to express the Eq. (3) in the following compact form

$$\begin{bmatrix} \mathbf{K}^{\mathbf{uu}}(z_1, \ldots, z_{n/2}) & \mathbf{K}^{\mathbf{uv}} \\ \mathbf{K}^{\mathbf{vu}} & \mathbf{K}^{\mathbf{vv}} \end{bmatrix} \begin{Bmatrix} \widehat{\mathbf{u}}(z_1, \ldots, z_{n/2}, t) \\ \widehat{\mathbf{v}}(z_1, \ldots, z_{n/2}, t) \end{Bmatrix} + \\ + \begin{bmatrix} \mathbf{M}^{\mathbf{uu}} & \mathbf{0} \\ \mathbf{0} & \mathbf{M}^{\mathbf{vv}} \end{bmatrix} \begin{Bmatrix} \ddot{\widehat{\mathbf{u}}}(z_1, \ldots, z_{n/2}, t) \\ \ddot{\widehat{\mathbf{v}}}(z_1, \ldots, z_{n/2}, t) \end{Bmatrix} = \begin{Bmatrix} \widehat{\mathbf{f}}(z_1, \ldots, z_{n/2}, t) \\ \mathbf{0} \end{Bmatrix}. \tag{4}$$

Exploiting a polar-like representation of the complex variable, it is possible to define the expressions in the $\mathbf{k}-$space through the definition $z_\alpha = \exp\ (I\mathbf{k}\cdot\mathbf{x}_\alpha)$ with $\alpha \in \mathbb{N}_{\geq 1}^{\leq n/2}$, $\mathbf{k} = k_i\mathbf{e}_i \in \mathbb{C}^2$ being the complex wave vector, and $\mathbf{x}_\alpha = l_\alpha \mathbf{n}_\alpha$ the position vector relative to the centroid of the reference block (with α not summed index), which in this context coincides with the periodicity vector in the physical space $\mathbf{p}_k^A$. Additionally, l_α denotes the distance between the centroids concerning the direction of the α − th unit vector $\mathbf{n}_\alpha$. It is worth noting that in the space $\mathscr{R}(\mathbf{k}) = \mathscr{R}(k_i)\mathbf{e}_i \in \mathbb{R}^2$, The reciprocal lattice is also periodic and is characterized by periodicity vectors $\mathbf{p}_k^{\mathscr{B}} \in \mathscr{G} \doteq \{\mathbf{G} : \mathbf{G} = c_l \mathbf{w}_l^{\mathscr{B}};\ \ c_l \in \mathbb{Z},\ l = 1,2\} \in \mathbb{R}^2$ where $\mathbf{w}_l^{\mathscr{B}} = w_r^{\mathscr{B},l}\mathbf{e}_r$ for $r = 1, 2$ are the independent reciprocal periodicity vectors, with $k = 1, \ldots, n/2$ characterizing the corresponding coordination directions of the reciprocal lattice (Fig. 2d and e). Furthermore, the independent periodicity vectors of the reciprocal lattice are associated with their counterparts in the physical space lattice through the condition $\mathbf{w}_i^{\mathscr{A}} \cdot \mathbf{w}_j^{\mathscr{B}} = 2\pi\delta_{ij}$, where δ_{ij} represents the Kronecker delta. By substituting the complex terms with their corresponding polar forms, the Eq. (4) become

$$\begin{bmatrix} \mathbf{K}^{\mathbf{uu}}(\mathbf{k}) & \mathbf{K}^{\mathbf{uv}} \\ \mathbf{K}^{\mathbf{vu}} & \mathbf{K}^{\mathbf{vv}} \end{bmatrix} \begin{Bmatrix} \widetilde{\mathbf{u}}(\mathbf{k}, t) \\ \widetilde{\mathbf{v}}(\mathbf{k}, t) \end{Bmatrix} + \begin{bmatrix} \mathbf{M}^{\mathbf{uu}} & \mathbf{0} \\ \mathbf{0} & \mathbf{M}^{\mathbf{vv}} \end{bmatrix} \begin{Bmatrix} \ddot{\widetilde{\mathbf{u}}}(\mathbf{k}, t) \\ \ddot{\widetilde{\mathbf{v}}}(\mathbf{k}, t) \end{Bmatrix} = \begin{Bmatrix} \widetilde{\mathbf{f}}(\mathbf{k}, t) \\ \mathbf{0} \end{Bmatrix}, \tag{5}$$

and by utilizing the temporal bilateral Laplace transform applied to the Eq. (5) defined

$$\mathscr{L}[\widetilde{\mathbf{y}}(\mathbf{k}, t)] = \int_{\mathbb{R}} \widetilde{\mathbf{y}}(\mathbf{k}, t)\exp(-st)dt \doteq \widehat{\mathbf{y}}(\mathbf{k}, s), \tag{6}$$

where $\widetilde{\mathbf{y}}(\mathbf{k}, t)$ is a generic field, the governing equations in the complex frequency domain associated with the Laplace variable $s \in \mathbb{C}$ and in the $\mathbf{k}-$space are obtained

$$\begin{bmatrix} \mathbf{K}^{\mathbf{uu}}(\mathbf{k}) + s^2\mathbf{M}^{\mathbf{uu}} & \mathbf{K}^{\mathbf{uv}} \\ \mathbf{K}^{\mathbf{vu}} & \mathbf{K}^{\mathbf{vv}} + s^2\mathbf{M}^{\mathbf{vv}} \end{bmatrix} \begin{Bmatrix} \widehat{\mathbf{u}}(\mathbf{k}, s) \\ \widehat{\mathbf{v}}(\mathbf{k}, s) \end{Bmatrix} = \begin{Bmatrix} \widehat{\mathbf{f}}(\mathbf{k}, s) \\ \mathbf{0} \end{Bmatrix}. \tag{7}$$

The detailed analysis of the wave vector $\mathbf{k} \in \mathbb{C}^2$ allows for observations on the propagation and spatial attenuation of both homogeneous and non-homogeneous waves. For purely elastic problems, where $s = I\omega$ with $\omega \in \mathbb{R}$ the angular frequency, and under unforced wave conditions (i.e. $\mathbf{f} = \mathbf{0}$), the subsequent eigenproblem is determined from the Eq. (7)

$$\mathbf{C}^{lag}(\mathbf{k}, \omega)\widehat{\mathbf{U}}(\mathbf{k}, \omega) = \\ = \begin{bmatrix} \mathbf{K}^{\mathbf{uu}}(\mathbf{k}) - \omega^2\mathbf{M}^{\mathbf{uu}} & \mathbf{K}^{\mathbf{uv}} \\ \mathbf{K}^{\mathbf{vu}} & \mathbf{K}^{\mathbf{vv}} - \omega^2\mathbf{M}^{\mathbf{vv}} \end{bmatrix} \begin{Bmatrix} \widehat{\mathbf{u}}(\mathbf{k}, \omega) \\ \widehat{\mathbf{v}}(\mathbf{k}, \omega) \end{Bmatrix} = \begin{Bmatrix} \mathbf{0} \\ \mathbf{0} \end{Bmatrix}. \tag{8}$$

The dispersion spectra are obtained in an implicit form by enforcing the singularity of the matrix $\mathbf{C}^{lag}$ from Eq. (8), which means

$$D^{lag}(\mathbf{k}, \omega) = \det\left(\mathbf{C}^{lag}(\mathbf{k}, \omega)\right) = 0. \tag{9}$$

The wave vector $\mathbf{k} \in \mathbb{C}^2$ can be represented as the sum of two vector components $\mathbf{k} = \mathbf{k}_R + I\mathbf{k}_I = k_R\mathbf{n}_R + Ik_I\mathbf{n}_I$ with $\mathbf{k}_R, \mathbf{k}_I \in \mathbb{R}^2$ real part (characterizing spatial wave propagation) and imaginary part (characterizing spatial wave damping) respectively. In the case of non-homogeneous waves, the directions

$$\mathbf{n}_{\mathscr{R}} = \frac{\mathbf{k}_{\mathscr{R}}}{\|\,\mathbf{k}_{\mathscr{R}}\,\|_2} = \cos\varphi_{\mathscr{R}}\mathbf{e}_1 + \sin\varphi_{\mathscr{R}}\mathbf{e}_2, \\ \mathbf{n}_{\mathscr{I}} = \frac{\mathbf{k}_{\mathscr{I}}}{\|\,\mathbf{k}_{\mathscr{I}}\,\|_2} = \cos\varphi_{\mathscr{I}}\mathbf{e}_1 + \sin\varphi_{\mathscr{I}}\mathbf{e}_2, \tag{10}$$

of these components are generally distinct, hence $\varphi_R \neq \varphi_I$. The characteristic equation can be reinterpreted in the form $D^{lag}(k_R, k_I, \varphi_R, \varphi_I, \omega) = D_R^{lag} + ID_I^{lag} = 0$, thus obtaining the dispersion curves as the intersection of two hypersurfaces in implicit form, which are represented by the nullification of the real and imaginary parts of the characteristic equation to identify the following locus of points

$$\mathscr{S}^{lag} = \left\{(k_{\mathscr{R}}, k_{\mathscr{I}}, \varphi_{\mathscr{R}}, \varphi_{\mathscr{I}}, \omega) :\ \ \mathscr{D}_{\mathscr{R}}^{lag}(k_{\mathscr{R}}, k_{\mathscr{I}}, \varphi_{\mathscr{R}}, \varphi_{\mathscr{I}}, \omega) = 0 \ \cap\ \mathscr{D}_I^{lag}(k_{\mathscr{R}}, k_{\mathscr{I}}, \varphi_{\mathscr{R}}, \varphi_{\mathscr{I}}, \omega) = 0\right\}. \tag{11}$$

In the case of homogeneous waves where the equality $\varphi_R = \varphi_I = \varphi$ holds, the wave vector $\mathbf{k}$can be rewritten as $\mathbf{k} = (k_R + Ik_I)\mathbf{n} = k\mathbf{n}$ with $k \in \mathbb{C}$ the wave number and $\mathbf{n}$ the unique unit propagation vector. The dispersion curves can be obtained by imposing the intersection of the hypersurfaces $D_R^{lag} = 0$, $D_I^{lag} = 0$, thus obtaining the locus of points

$$\mathscr{S}^{lag} = \left\{(k_{\mathscr{R}}, k_{\mathscr{I}}, \varphi, \omega) :\ \mathscr{D}_{\mathscr{R}}^{lag}(k_{\mathscr{R}}, k_{\mathscr{I}}, \varphi, \omega) = 0 \cap \mathscr{D}_{\mathscr{I}}^{lag}(k_{\mathscr{R}}, k_{\mathscr{I}}, \varphi, \omega) = 0\right\}. \tag{12}$$

Note that, by fixing the propagation directions of the wave and spatial attenuation, identified by the angles φ_R, φ_I or φ in the case of homogeneous waves, the intersections expressed in (11) and (12) are imposed for surfaces immersed in $\mathbb{R}^3$. In the particular condition where $\mathbf{k} \in \mathbb{R}^2$, the pseudo-polar definition of the complex variable $z_\alpha = \exp\ (I\mathbf{k}\cdot\mathbf{x}_\alpha)$ defines a mapping onto the unit circle in the complex domain, a condition in which the Z transform coincides with the finite Fourier transform (or finite-domain Fourier transform), while the discrete sequences $\mathbf{u}_{(i_1,\ldots,i_{n/2})}$ and $\mathbf{v}_{(i_1,\ldots,i_{n/2})}$ represent the Fourier coefficients. The following standard eigenproblem can be formulated to obtain dispersion spectra for this particular case

$$\left(\mathbf{H}_{lag} - \lambda\mathbf{I}\right)\widehat{\mathbf{U}} = \\ = \left(\begin{bmatrix} (\mathbf{M}^{\mathbf{uu}})^{-1}\mathbf{K}^{\mathbf{uu}}(\mathbf{k}) & \mathbf{K}^{\mathbf{uv}} \\ \mathbf{K}^{\mathbf{vu}} & (\mathbf{M}^{\mathbf{vv}})^{-1}\mathbf{K}^{\mathbf{vv}} \end{bmatrix} - \lambda\begin{bmatrix} \mathbf{I} & \mathbf{0} \\ \mathbf{0} & \mathbf{I} \end{bmatrix}\right)\begin{Bmatrix} \widehat{\mathbf{u}}(\mathbf{k}, \omega) \\ \widehat{\mathbf{v}}(\mathbf{k}, \omega) \end{Bmatrix} = \mathbf{0}, \tag{13}$$

where $\lambda = \omega^2$ eigenvalue and $\widehat{\mathbf{U}}$ polarization vector. The $j-$ th coefficients I_j of the characteristic polynomial $\sum_{j=0}^{6} I_j\lambda^j = 0$ enforced to be null, are detailed as the trace of matrix $\mathbf{H}_{lag}$ and the powers of $\mathbf{H}_{lag}$, as described in the Appendix A through the Faddeev-Leverrier method [84-86].

3. Enhanced multi-field integral-differential continuum model

This Section aims to present a continuous multi-field model that extends the degrees of freedom of the structure to include those of the resonator, providing an equivalent representation of the previously described discrete Lagrangian system. Building on the enhanced continualization proposed for two-dimensional monoatomic lattices by

Bacigalupo and Gambarotta in [67], this procedure is now extended to these multi-field systems, understood as multiatomic lattices. In particular, a thermodynamically consistent multi-field continuous model can be defined by introducing the regularized field variable $\widetilde{\mathbf{Q}}^R(\mathbf{k},t) = \left(\widetilde{\mathbf{q}}^R(\mathbf{k},t) \quad \widetilde{\mathbf{p}}^R(\mathbf{k},t)\right)^T$ with $\widetilde{\mathbf{q}}^R(\mathbf{k},t)$ and $\widetilde{\mathbf{p}}^R(\mathbf{k},t)$ as the field variables related to the degrees of freedom of the structure and the resonator, respectively. Specifically, the variable $\widetilde{\mathbf{Q}}^R(\mathbf{k},t)$ is associated with the variable $\widetilde{\mathbf{U}}(\mathbf{k},t) = (\widetilde{\mathbf{u}}(\mathbf{k},t) \quad \widetilde{\mathbf{v}}(\mathbf{k},t))^T$ of the discrete Lagrangian system through the following bridging scale relationship in the $\mathbf{k}-$ space

$$\begin{aligned} &F(\mathbf{k})\widetilde{\mathbf{Q}}^R(\mathbf{k},t) = \widetilde{\mathbf{Q}}(\mathbf{k},t) = F[\mathbf{Q}(\mathbf{x},t)] \doteq \\ &\doteq \widetilde{\mathbf{U}}(\mathbf{k},t) = \mathscr{Z}\left[\mathbf{U}_{(i_1,\ldots,i_{n/2})}(t)\right]\Big|_{z_\alpha=\exp(I\mathbf{x}_\alpha\cdot\mathbf{k})}, \end{aligned} \tag{14}$$

where $F(\mathbf{k})$ is the regularization kernel defined as

$$\begin{aligned} F(\mathbf{k}) \quad &\doteq \prod_{\alpha=1}^{n/2} \frac{2I\mathbf{x}_\alpha\cdot\mathbf{k}}{\exp(I\mathbf{x}_\alpha\cdot\mathbf{k}) - \exp(-I\mathbf{x}_\alpha\cdot\mathbf{k})} = \\ &= \prod_{\alpha=1}^{n/2} \frac{\mathbf{x}_\alpha\cdot I\mathbf{k}}{\sinh(\mathbf{x}_\alpha\cdot I\mathbf{k})} = \prod_{\alpha=1}^{n/2} \frac{\mathbf{x}_\alpha\cdot\mathbf{k}}{\sin(\mathbf{x}_\alpha\cdot\mathbf{k})} = \prod_{\alpha=1}^{n/2} \operatorname{sinc}^{-1}(\mathbf{x}_\alpha\cdot\mathbf{k}), \end{aligned} \tag{15}$$

while $\mathbf{Q}(\mathbf{x},t) = (\mathbf{q}(\mathbf{x},t) \quad \mathbf{p}(\mathbf{x},t))^T$ is the auxiliary generalized displacement field correlated through the spatial Fourier transform with a complex argument

$$\mathscr{F}[\mathbf{y}(\mathbf{x},t)] = \int_{\mathbb{R}^2} \mathbf{y}(\mathbf{x},t)\exp(-I\mathbf{k}\cdot\mathbf{x})d\mathbf{x} \doteq \widetilde{\mathbf{y}}(\mathbf{k},t), \tag{16}$$

with $\mathbb{C}_\varsigma^2 = \left\{\mathbf{k} = k_j\mathbf{e}_j \ : \ k_j \in \lim_{\rho_j\to\infty}(\varsigma_j - I\rho_j;\ \varsigma_j + I\rho_j)\right\}$ and ς_j real constant chosen appropriately within the holomorphic domain of the function $\widetilde{\mathbf{y}}(\mathbf{k},t)$. It is worth to note that the inverse transform of the regularization kernel introduced in the Eq. (17) leads to an indicator function compactly supported on a rectangular region section that coincides with the periodic cell of the microstructured material. Proceeding by leveraging the definition (14) in the Eq. (5) formulated in the $\mathbf{k}-$ space, one obtains

$$\begin{aligned} &\mathbf{K}^{\mathbf{uu}}(\mathbf{k})\widetilde{\mathbf{q}}(\mathbf{k},t) + \mathbf{K}^{\mathbf{uv}}\widetilde{\mathbf{p}}(\mathbf{k},t) + \mathbf{M}^{\mathbf{uu}}\ddot{\widetilde{\mathbf{q}}}(\mathbf{k},t) = \widetilde{\mathbf{f}}(\mathbf{k},t), \\ &\mathbf{K}^{\mathbf{vu}}\widetilde{\mathbf{q}}(\mathbf{k},t) + \mathbf{K}^{\mathbf{vv}}\widetilde{\mathbf{p}}(\mathbf{k},t) + \mathbf{M}^{\mathbf{vv}}\ddot{\widetilde{\mathbf{p}}}(\mathbf{k},t) = \mathbf{0}, \end{aligned} \tag{19}$$

thus deriving the following relationships

$$\begin{aligned} &\mathbf{K}^{\mathbf{uu}}(\mathbf{k})F(\mathbf{k})\widetilde{\mathbf{q}}^R(\mathbf{k},t) + \mathbf{K}^{\mathbf{uv}}F(\mathbf{k})\widetilde{\mathbf{p}}^R(\mathbf{k},t) + \mathbf{M}^{\mathbf{uu}}F(\mathbf{k})\ddot{\widetilde{\mathbf{q}}}^R(\mathbf{k},t) = \widetilde{\mathbf{s}}(\mathbf{k},t), \\ &\mathbf{K}^{\mathbf{vu}}F(\mathbf{k})\widetilde{\mathbf{q}}^R(\mathbf{k},t) + \mathbf{K}^{\mathbf{vv}}F(\mathbf{k})\widetilde{\mathbf{p}}^R(\mathbf{k},t) + \mathbf{M}^{\mathbf{vv}}F(\mathbf{k})\ddot{\widetilde{\mathbf{p}}}^R(\mathbf{k},t) = \mathbf{0}, \end{aligned} \tag{20}$$

where the source term $\widetilde{\mathbf{s}}(\mathbf{k},t)$ is the complex-argument Fourier transform of the continuous field $\mathbf{s}(\mathbf{x},t)$, which satisfies the property

$$\widetilde{\mathbf{s}}(\mathbf{k},t) = \mathscr{F}[\mathbf{s}(\mathbf{x},t)] \doteq \mathscr{Z}\left[\mathbf{f}_{(i_1,\ldots,i_{n/2})}(t)\right]\Big|_{z_\alpha=\exp(I\mathbf{x}_\alpha\cdot\mathbf{k})} = \widetilde{\mathbf{f}}(\mathbf{k},t). \tag{21}$$

By applying the inverse of the transform (16) to each term of Eq. (20), it is possible to obtain the integral-differential relationships of the variables $\mathbf{q}^R(\mathbf{x},t)$ and $\mathbf{p}^R(\mathbf{x},t)$ in the physical and temporal domains, namely

$$\begin{aligned} &\mathscr{F}^{-1}\left[\mathbf{K}^{\mathbf{uu}}(\mathbf{k})F(\mathbf{k})\mathscr{F}\left[\mathbf{q}^R(\mathbf{x},t)\right] + \mathbf{K}^{\mathbf{uv}}F(\mathbf{k})\mathscr{F}\left[\mathbf{p}^R(\mathbf{x},t)\right] + \mathbf{M}^{\mathbf{uu}}F(\mathbf{k})\mathscr{F}\left[\ddot{\mathbf{q}}^R(\mathbf{x},t)\right]\right] = \mathscr{F}^{-1}[\widetilde{\mathbf{s}}(\mathbf{k},t)], \\ &\mathscr{F}^{-1}\left[\mathbf{K}^{\mathbf{vu}}F(\mathbf{k})\mathscr{F}\left[\mathbf{q}^R(\mathbf{x},t)\right] + \mathbf{K}^{\mathbf{vv}}F(\mathbf{k})\mathscr{F}\left[\mathbf{p}^R(\mathbf{x},t)\right] + \mathbf{M}^{\mathbf{vv}}F(\mathbf{k})\mathscr{F}\left[\ddot{\mathbf{p}}^R(\mathbf{x},t)\right]\right] = \mathbf{0}. \end{aligned} \tag{22}$$

with $\mathbf{y}(\mathbf{x},\ t)$ as a generic field defined in the physical space. It is important to note that for $F = 1$, the continualization procedure yields analogous results to those obtained from the standard continualization, which is derived from the Taylor series expansion centered concerning the position of the elementary cell of the generalized displacement field $\mathbf{Q}(\mathbf{x},\ t)$, which directly represents the macro-displacement. Invoking the property of the inverse spatial Fourier transform applied to the product and by exploiting the definition in the Eq. (14), it is possible to obtain the following up-scaling relation in the physical space

$$\begin{aligned} \mathbf{Q}^R(\mathbf{x},t) \quad &= \mathscr{F}^{-1}\left[F^{-1}(\mathbf{k})\widetilde{\mathbf{Q}}(\mathbf{k},t)\right] = \mathscr{F}^{-1}\left[F^{-1}(\mathbf{k})\right] * \mathbf{Q}(\mathbf{x},t) = \\ &= \mathscr{F}^{-1}\left[F^{-1}(\mathbf{k})\right] * \mathscr{F}^{-1}[\widetilde{\mathbf{U}}(\mathbf{k},t)] = \mathscr{F}^{-1}\left[F^{-1}(\mathbf{k})\right] * \mathscr{F}^{-1}\left[\mathscr{Z}\left[\mathbf{U}_{(i_1,\ldots,i_{n/2})}(t)\right]\Big|_{z_\alpha=\exp(I\mathbf{x}_\alpha\cdot\mathbf{k})}\right]. \end{aligned} \tag{17}$$

Here, the symbol * indicates the convolution in the space while F^{-1} denotes the inverse spatial Fourier transform with a complex argument, defined for the generic field $\widetilde{\mathbf{y}}(\mathbf{k},t)$ as

$$\mathscr{F}^{-1}[\widetilde{\mathbf{y}}(\mathbf{k},t)] = \frac{1}{(2\pi I)^2}\int_{\mathbb{C}_\varsigma^2} \widetilde{\mathbf{y}}(\mathbf{k},t)\exp(I\mathbf{k}\cdot\mathbf{x})d\mathbf{k} \doteq \mathbf{y}(\mathbf{x},t), \tag{18}$$

According with [87,88,81], the equation of the equivalent integral-type continuum model (22) can be reformulated using pseudo-differential notation. It is worth noting that the terms as functions of the wave vector $\mathbf{k}$ are reliant on the independent variable $I\mathbf{k}$, thereby open to being redefined as $F(\mathbf{k}) \equiv F_\diamond(I\mathbf{k})$, $\mathbf{K}^{\mathbf{uu}}(\mathbf{k}) \equiv \mathbf{K}_\diamond^{\mathbf{uu}}(I\mathbf{k})$ pseudo-differential operators that can be identified by introducing the following definitions

$$\begin{aligned} &\mathscr{F}^{-1}\left[\mathbf{K}_\diamond^{\mathbf{uu}}(I\mathbf{k})F_\diamond(I\mathbf{k})\mathscr{F}\left[\mathbf{q}^R(\mathbf{x},t)\right]\right] \doteq \mathbf{K}_\diamond^{\mathbf{uu}}[D_1,D_2]F_\diamond[D_1,D_2]\mathbf{q}^R(\mathbf{x},t), \\ &\mathscr{F}^{-1}\left[\mathbf{K}^{\mathbf{uv}}F_\diamond(I\mathbf{k})\mathscr{F}\left[\mathbf{p}^R(\mathbf{x},t)\right]\right] \doteq \mathbf{K}^{\mathbf{uv}}F_\diamond[D_1,D_2]\mathbf{p}^R(\mathbf{x},t), \\ &\mathscr{F}^{-1}\left[\mathbf{M}^{\mathbf{uu}}F_\diamond(I\mathbf{k})\mathscr{F}\left[\ddot{\mathbf{q}}^R(\mathbf{x},t)\right]\right] \doteq \mathbf{M}^{\mathbf{uu}}F_\diamond[D_1,D_2]\ddot{\mathbf{q}}^R(\mathbf{x},t), \\ &\mathscr{F}^{-1}\left[\mathbf{K}^{\mathbf{vu}}F_\diamond(I\mathbf{k})\mathscr{F}\left[\mathbf{q}^R(\mathbf{x},t)\right]\right] \doteq \mathbf{K}^{\mathbf{vu}}F_\diamond[D_1,D_2]\mathbf{q}^R(\mathbf{x},t), \\ &\mathscr{F}^{-1}\left[\mathbf{K}^{\mathbf{vv}}F_\diamond(I\mathbf{k})\mathscr{F}\left[\mathbf{p}^R(\mathbf{x},t)\right]\right] \doteq \mathbf{K}^{\mathbf{vv}}F_\diamond[D_1,D_2]\mathbf{p}^R(\mathbf{x},t), \\ &\mathscr{F}^{-1}\left[\mathbf{M}^{\mathbf{vv}}F_\diamond(I\mathbf{k})\mathscr{F}\left[\ddot{\mathbf{p}}^R(\mathbf{x},t)\right]\right] \doteq \mathbf{M}^{\mathbf{vv}}F_\diamond[D_1,D_2]\ddot{\mathbf{p}}^R(\mathbf{x},t), \end{aligned} \tag{23}$$

where $D_j(\mathbf{y}(\mathbf{x},t)) = \partial\mathbf{y}(\mathbf{x},t)/\partial x_j$, for $j = 1,\ 2$, being $\mathbf{y}(\mathbf{x},\ t)$ a generic

continuum field. It is interesting to observe that regarding the definition of the regularization kernel $F(\mathbf{k})$ in the Eq. (15) and reminding that $F(\mathbf{k}) \equiv F_\diamond(I\mathbf{k})$, the pseudo-differential operator $F_\diamond[D_1,D_2]$ defined in the Eq. (23) enables to notice that the partial derivatives with respect to the spatial field variables of the model (which are involved in the macro-directional derivative) are by definition equivalent to the first-order finite difference with second-order accuracy of the micro-displacement fields. From the relationships expressed in (23), it is possible to reformulate the equations of motion (22), obtaining the equivalent integral-differential equations in the form

$$\begin{aligned}&\mathbf{K}^{\mathbf{uu}}_\diamond[D_1,D_2]F_\diamond[D_1,D_2]\mathbf{q}^R(\mathbf{x},t)+\mathbf{K}^{\mathbf{uv}}F_\diamond[D_1,D_2]\mathbf{p}^R(\mathbf{x},t)+\\&\quad+\mathbf{M}^{\mathbf{uu}}F_\diamond[D_1,D_2]\ddot{\mathbf{q}}^R(\mathbf{x},t)=\mathbf{s}(\mathbf{x},t),\\&\mathbf{K}^{\mathbf{vu}}F_\diamond[D_1,D_2]\mathbf{q}^R(\mathbf{x},t)+\mathbf{K}^{\mathbf{vv}}F_\diamond[D_1,D_2]\mathbf{p}^R(\mathbf{x},t)+\\&\quad+\mathbf{M}^{\mathbf{vv}}F_\diamond[D_1,D_2]\ddot{\mathbf{p}}^R(\mathbf{x},t)=\mathbf{0}.\end{aligned} \tag{24}$$

It is worth noting that from the definitions of the regularized fields in (14), it follows that the equations of motion in (20) transformed into the frequency domain ω, are the same equations obtained starting from the discrete model (7) by imposing $\widehat{\mathbf{s}}(\mathbf{k},s)=\widehat{\mathbf{f}}(\mathbf{k},s)=\mathbf{0}$. Consequently, the frequency band structure of the integral-type continuum model is identical to that of the previously treated Lagrangian discrete model.

The pseudo-differential down-scaling law can be consistently defined in the following operatorial form

$$\mathbf{U}_{\left(i_1,\dots,i_{n/2}\right)}(t)=\left(F_\diamond[D_1,D_2]\mathbf{Q}^R(\mathbf{x},t)\right)\big|_{\mathbf{x}\in X}. \tag{25}$$

Based on the definition of the pseudo-differential operator referenced in Eq. (23) (see for details [81]) and considering the bridging relationship (14), the down-scaling law in differential form can be reformulated through the formal Taylor series expansion of the pseudo-differential operator $F_\diamond[D_1,D_2]$, which can be expressed in the following form

$$\begin{aligned}&\mathbf{K}^{\mathbf{uu}}_\diamond[D_1,D_2]F_\diamond[D_1,D_2]\sim\sum_{r\in\mathbb{N}}\sum_{\substack{|\alpha|=r\\l_1+l_2=r}}\frac{1}{r!}\binom{r}{l_1,l_2}\frac{\partial^{|\alpha|}\left(\mathbf{K}^{\mathbf{uu}}_\diamond[D_1,D_2]F_\diamond[D_1,D_2]\right)}{\partial\mathbf{D}^\alpha}\Big|_{\substack{D_1\Rightarrow0\\D_2\Rightarrow0}}\mathbf{D}^\alpha=\\&=\sum_{r\in\mathbb{N}}\sum_{\substack{|\alpha|=r\\l_1+l_2=r}}\frac{1}{r!}\binom{r}{l_1,l_2}\frac{\partial^{|\alpha|}\left(\mathbf{K}^{\mathbf{uu}}_\diamond[D_1,D_2]F_\diamond[D_1,D_2]\right)}{\partial D_{\alpha_1}\dots\partial D_{\alpha_r}}\Big|_{\substack{D_1\Rightarrow0\\D_2\Rightarrow0}}D_{\alpha_1}\dots D_{\alpha_r}=\\&=\sum_{l_1,l_2\in\mathbb{N}}\frac{1}{l_1!l_2!}\frac{\partial^{l_1+l_2}\left(\mathbf{K}^{\mathbf{uu}}_\diamond[D_1,D_2]F_\diamond[D_1,D_2]\right)}{\partial D_1^{l_1}\partial D_2^{l_2}}\Big|_{\substack{D_1\Rightarrow0\\D_2\Rightarrow0}}D_1^{l_1}D_2^{l_2},\\&F_\diamond[D_1,D_2]\sim\sum_{r\in\mathbb{N}}\sum_{\substack{|\alpha|=r\\l_1+l_2=r}}\frac{1}{r!}\binom{r}{l_1,l_2}\frac{\partial^{|\alpha|}(F_\diamond[D_1,D_2])}{\partial\mathbf{D}^\alpha}\Big|_{\substack{D_1\Rightarrow0\\D_2\Rightarrow0}}\mathbf{D}^\alpha=\\&=\sum_{r\in\mathbb{N}}\sum_{\substack{|\alpha|=r\\l_1+l_2=r}}\frac{1}{r!}\binom{r}{l_1,l_2}\frac{\partial^{|\alpha|}(F_\diamond[D_1,D_2])}{\partial D_{\alpha_1}\dots\partial D_{\alpha_r}}\Big|_{\substack{D_1\Rightarrow0\\D_2\Rightarrow0}}D_{\alpha_1}\dots D_{\alpha_r}=\sum_{l_1,l_2\in\mathbb{N}}\frac{1}{l_1!l_2!}\frac{\partial^{l_1+l_2}(F_\diamond[D_1,D_2])}{\partial D_1^{l_1}\partial D_2^{l_2}}\Big|_{\substack{D_1\Rightarrow0\\D_2\Rightarrow0}}D_1^{l_1}D_2^{l_2},\end{aligned} \tag{27}$$

$$\begin{aligned}\mathbf{U}_{\left(i_1,\dots,i_{n/2}\right)}(t)&\sim\sum_{r\in\mathbb{N}}\sum_{\substack{|\alpha|=r\\l_1+l_2=r}}\frac{1}{r!}\binom{r}{l_1,l_2}\frac{\partial^{|\alpha|}(F_\diamond[D_1,D_2])}{\partial\mathbf{D}^\alpha}\Big|_{\substack{D_1\Rightarrow0\\D_2\Rightarrow0}}\mathbf{D}^\alpha\mathbf{Q}^R(\mathbf{x},t)\big|_{\mathbf{x}\in X}=\\&=\sum_{l_1,l_2\in\mathbb{N}}\frac{1}{l_1!l_2!}\frac{\partial^{l_1+l_2}(F_\diamond[D_1,D_2])}{\partial D_1^{l_1}\partial D_2^{l_2}}\Big|_{\substack{D_1\Rightarrow0\\D_2\Rightarrow0}}D_1^{l_1}D_2^{l_2}\mathbf{Q}^R(\mathbf{x},t)\big|_{\mathbf{x}\in X}=\\&=\left(\sum_{l_1,l_2\in\mathbb{N}}\frac{1}{l_1!l_2!}\frac{\partial^{l_1+l_2}(F_\diamond[D_1,D_2])}{\partial D_1^{l_1}\partial D_2^{l_2}}\Big|_{\substack{D_1\Rightarrow0\\D_2\Rightarrow0}}\frac{\partial^{l_1+l_2}\mathbf{Q}^R(\mathbf{x},t)}{\partial x_1^{l_1}\partial x_2^{l_2}}\right)\Big|_{\mathbf{x}\in X},\end{aligned} \tag{26}$$

where $\mathbf{D}^\alpha=D_{\alpha_1}D_{\alpha_2}\dots D_{\alpha_r}=D_1^{l_1}D_2^{l_2}$ with $\alpha=(\alpha_1,\alpha_2,\dots,\alpha_r)\in\mathbb{N}^r$ the multi-index of length $|\alpha|=r$ such that $\alpha_1,\alpha_2,\dots,\alpha_r=1,2$ considering that l_1 and l_2 are integers denoting the repetition of D_1, D_2 to order $r=l_1+l_2$. In Appendix B, a specialization for the case of orthogonal coordination directions aligned with the coordinate axes $\mathbf{n}_1=\mathbf{e}_1$ and $\mathbf{n}_2=\mathbf{e}_2$ is detailed.

3.1. Average infinite order differential equations and perturbative solution approach

The integral-differential equations can be equivalently reformulated as infinite-order differential equations by applying Taylor expansion to pseudo-differential operators

Substituting expansions (27) into Eq. (24) yields the average infinite order governing equations, namely

$$\begin{aligned}
&\sum_{l_1,l_2\in\mathbb{N}} -\frac{1}{l_1!l_2!}\left[\mathbf{A}^{\mathbf{qq}}_{l_1l_2}\frac{\partial^{l_1+l_2}\mathbf{q}^R(\mathbf{x},t)}{\partial x_1^{l_1}\partial x_2^{l_2}}+\mathbf{A}^{\mathbf{qp}}_{l_1l_2}\frac{\partial^{l_1+l_2}\mathbf{p}^R(\mathbf{x},t)}{\partial x_1^{l_1}\partial x_2^{l_2}}\right]+\mathbf{s}(\mathbf{x},t)=\\
&\quad=\sum_{l_1,l_2\in\mathbb{N}}\frac{1}{l_1!l_2!}\mathbf{B}^{\mathbf{qq}}_{l_1l_2}\frac{\partial^{l_1+l_2}\ddot{\mathbf{q}}^R(\mathbf{x},t)}{\partial x_1^{l_1}\partial x_2^{l_2}},\\
&\sum_{l_1,l_2\in\mathbb{N}} -\frac{1}{l_1!l_2!}\left[\mathbf{A}^{\mathbf{pq}}_{l_1l_2}\frac{\partial^{l_1+l_2}\mathbf{q}^R(\mathbf{x},t)}{\partial x_1^{l_1}\partial x_2^{l_2}}+\mathbf{A}^{\mathbf{pp}}_{l_1l_2}\frac{\partial^{l_1+l_2}\mathbf{p}^R(\mathbf{x},t)}{\partial x_1^{l_1}\partial x_2^{l_2}}\right]=\\
&\quad=\sum_{l_1,l_2\in\mathbb{N}}\frac{1}{l_1!l_2!}\mathbf{B}^{\mathbf{pp}}_{l_1l_2}\frac{\partial^{l_1+l_2}\ddot{\mathbf{p}}^R(\mathbf{x},t)}{\partial x_1^{l_1}\partial x_2^{l_2}},
\end{aligned}\tag{28}$$

where the coefficient matrices are

$$\begin{aligned}
&\mathbf{A}^{\mathbf{qq}}_{l_1l_2}\doteq\frac{\partial^{l_1+l_2}\left(\mathbf{K}^{\mathbf{uu}}_{\diamond}[D_1,D_2]F_{\diamond}[D_1,D_2]\right)}{\partial D_1^{l_1}\partial D_2^{l_2}}\bigg|_{\substack{D_1\Rightarrow 0\\D_2\Rightarrow 0}},\ \mathbf{A}^{\mathbf{qp}}_{l_1l_2}\doteq\mathbf{K}^{\mathbf{uv}}\frac{\partial^{l_1+l_2}(F_{\diamond}[D_1,D_2])}{\partial D_1^{l_1}\partial D_2^{l_2}}\bigg|_{\substack{D_1\Rightarrow 0\\D_2\Rightarrow 0}},\\
&\mathbf{A}^{\mathbf{pq}}_{l_1l_2}\doteq\mathbf{K}^{\mathbf{vu}}\frac{\partial^{l_1+l_2}(F_{\diamond}[D_1,D_2])}{\partial D_1^{l_1}\partial D_2^{l_2}}\bigg|_{\substack{D_1\Rightarrow 0\\D_2\Rightarrow 0}},\ \mathbf{A}^{\mathbf{pp}}_{l_1l_2}\doteq\mathbf{K}^{\mathbf{vv}}\frac{\partial^{l_1+l_2}(F_{\diamond}[D_1,D_2])}{\partial D_1^{l_1}\partial D_2^{l_2}}\bigg|_{\substack{D_1\Rightarrow 0\\D_2\Rightarrow 0}},\\
&\mathbf{B}^{\mathbf{qq}}_{l_1l_2}\doteq\mathbf{M}^{\mathbf{uu}}\frac{\partial^{l_1+l_2}(F_{\diamond}[D_1,D_2])}{\partial D_1^{l_1}\partial D_2^{l_2}}\bigg|_{\substack{D_1\Rightarrow 0\\D_2\Rightarrow 0}},\ \mathbf{B}^{\mathbf{pp}}_{l_1l_2}\doteq\mathbf{M}^{\mathbf{vv}}\frac{\partial^{l_1+l_2}(F_{\diamond}[D_1,D_2])}{\partial D_1^{l_1}\partial D_2^{l_2}}\bigg|_{\substack{D_1\Rightarrow 0\\D_2\Rightarrow 0}}.
\end{aligned}\tag{29}$$

The governing equations of infinite order described in Eq. (28) can be solved through an appropriate order truncation, as will be illustrated in Section 4, or through a perturbative approach. The perturbative solution strategy is discussed in detail in Appendix C, where the ordering parameter η is introduced in Eq. (65) to categorize the orders of the averaged infinite order governing Eq. (28). The solution is sought as an asymptotic expansion in η that orders the various sensitivities of the generalized displacement vector. Such sensitivities are determined by solving hierarchical differential problems at different orders of η, and resulting in a subsequent absorption of the ordering parameter. It is noteworthy that the mathematical structure of the non-homogeneous differential equations defining the generating problem, coincides with the governing equations of a first-order gradient model or a generalized micropolar model with non-local inertias and non-zero source terms that match those of the infinite order equation. Hierarchical differential problems of higher order exhibit the same mathematical structure but include source terms involving solutions in terms of sensitivities obtained from the solutions of lower-order hierarchical differential problems. It is important to note that the generating problem of the perturbative approach coincides with that obtained from the appropriate truncation to the lowest consistent order of the infinite order equation, as illustrated in the example provided in sub-Section 5.1.

4. Continualized higher-order model and dynamic identification

The integral-differential governing Eq. (24) can be addressed through a preliminary transformation into infinite-order differential Eq. (29). Formally, these equations can be solved directly using the perturbative technique outlined in Section 3.1. Alternatively, Eq. (29) can be solved through an appropriate truncation, aiming to achieve a higher-order gradient-type continuum model. A generic N order gradient-type continuum model is described by field equations that include terms up to continualization order $2N$, namely

$$\begin{aligned}
&\sum_{r=0}^{2N}\sum_{l_1+l_2=r} -\frac{1}{l_1!l_2!}\left[\mathbf{A}^{\mathbf{qq}}_{l_1l_2}\frac{\partial^{r}\mathbf{q}^R(\mathbf{x},t)}{\partial x_1^{l_1}\partial x_2^{l_2}}+\mathbf{A}^{\mathbf{qp}}_{l_1l_2}\frac{\partial^{r}\mathbf{p}^R(\mathbf{x},t)}{\partial x_1^{l_1}\partial x_2^{l_2}}\right]+\mathbf{s}(\mathbf{x},t)=\\
&\quad=\sum_{r=0}^{2N}\sum_{l_1+l_2=r}\frac{1}{l_1!l_2!}\mathbf{B}^{\mathbf{qq}}_{l_1l_2}\frac{\partial^{r}\ddot{\mathbf{q}}^R(\mathbf{x},t)}{\partial x_1^{l_1}\partial x_2^{l_2}},\\
&\sum_{r=0}^{2N}\sum_{l_1+l_2=r} -\frac{1}{l_1!l_2!}\left[\mathbf{A}^{\mathbf{pq}}_{l_1l_2}\frac{\partial^{r}\mathbf{q}^R(\mathbf{x},t)}{\partial x_1^{l_1}\partial x_2^{l_2}}+\mathbf{A}^{\mathbf{pp}}_{l_1l_2}\frac{\partial^{r}\mathbf{p}^R(\mathbf{x},t)}{\partial x_1^{l_1}\partial x_2^{l_2}}\right]=\\
&\quad=\sum_{r=0}^{2N}\sum_{l_1+l_2=r}\frac{1}{l_1!l_2!}\mathbf{B}^{\mathbf{pp}}_{l_1l_2}\frac{\partial^{r}\ddot{\mathbf{p}}^R(\mathbf{x},t)}{\partial x_1^{l_1}\partial x_2^{l_2}}.
\end{aligned}\tag{30}$$

The Eq. (30) can be expressed in terms of the wave vector $\mathbf{k}$ and the Laplace variable s through a Fourier transform with a complex argument in the spatial domain and the bilateral Laplace transform in the temporal domain, namely

$$\begin{aligned}
&\sum_{r=0}^{2N}\sum_{l_1+l_2=r} -\frac{I^r k_1^{l_1}k_2^{l_2}}{l_1!l_2!}\left[\mathbf{A}^{\mathbf{qq}}_{l_1l_2}\widehat{\mathbf{q}}^R(\mathbf{k},s)+\mathbf{A}^{\mathbf{qp}}_{l_1l_2}\widehat{\mathbf{p}}^R(\mathbf{k},s)\right]+\widehat{\mathbf{s}}(\mathbf{k},t)=\\
&\quad=s^2\sum_{r=0}^{2N}\sum_{l_1+l_2=r}\frac{I^r k_1^{l_1}k_2^{l_2}}{l_1!l_2!}\mathbf{B}^{\mathbf{qq}}_{l_1l_2}\widehat{\mathbf{q}}^R(\mathbf{k},s),\\
&\sum_{r=0}^{2N}\sum_{l_1+l_2=r} -\frac{I^r k_1^{l_1}k_2^{l_2}}{l_1!l_2!}\left[\mathbf{A}^{\mathbf{pq}}_{l_1l_2}\widehat{\mathbf{q}}^R(\mathbf{k},s)+\mathbf{A}^{\mathbf{pp}}_{l_1l_2}\widehat{\mathbf{p}}^R(\mathbf{k},s)\right]=\\
&\quad=s^2\sum_{r=0}^{2N}\sum_{l_1+l_2=r}\frac{I^r k_1^{l_1}k_2^{l_2}}{l_1!l_2!}\mathbf{B}^{\mathbf{pp}}_{l_1l_2}\widehat{\mathbf{p}}^R(\mathbf{k},s).
\end{aligned}\tag{31}$$

From the (31) equation, focusing on the free wave propagation analysis where $\widehat{\mathbf{s}}(\mathbf{k},s)=\mathbf{0}$, and recalling that $s=I\omega$, the following eigenproblem is obtained

$$\begin{aligned}
&\mathbf{C}^{\hom}(\mathbf{k},\omega)\widehat{\mathbf{V}}^R(\mathbf{k},\omega)=\\
&\quad=\begin{bmatrix}\mathbf{C}^{\hom}_{\mathbf{qq}}(\mathbf{k},\omega) & \mathbf{C}^{\hom}_{\mathbf{qp}}(\mathbf{k},\omega)\\ \mathbf{C}^{\hom}_{\mathbf{pq}}(\mathbf{k},\omega) & \mathbf{C}^{\hom}_{\mathbf{pp}}(\mathbf{k},\omega)\end{bmatrix}\begin{Bmatrix}\widehat{\mathbf{q}}^R(\mathbf{k},\omega)\\ \widehat{\mathbf{p}}^R(\mathbf{k},\omega)\end{Bmatrix}=\begin{Bmatrix}\mathbf{0}\\ \mathbf{0}\end{Bmatrix},
\end{aligned}\tag{32}$$

where the 3×3 submatrices that compose the 6×6 $\mathbf{C}^{\hom}$ matrix are defined as follows

$$\begin{aligned}
&\mathbf{C}^{\hom}_{\mathbf{qq}}=\sum_{r=0}^{2N}\sum_{l_1+l_2=r}\frac{I^r k_1^{l_1}k_2^{l_2}}{l_1!l_2!}\left[\mathbf{A}^{\mathbf{qq}}_{l_1l_2}-\omega^2\mathbf{B}^{\mathbf{qq}}_{l_1l_2}\right],\ \mathbf{C}^{\hom}_{\mathbf{qp}}=\sum_{r=0}^{2N}\sum_{l_1+l_2=r}\frac{I^r k_1^{l_1}k_2^{l_2}}{l_1!l_2!}\mathbf{A}^{\mathbf{qp}}_{l_1l_2},\\
&\mathbf{C}^{\hom}_{\mathbf{pq}}=\sum_{r=0}^{2N}\sum_{l_1+l_2=r}\frac{I^r k_1^{l_1}k_2^{l_2}}{l_1!l_2!}\mathbf{A}^{\mathbf{pq}}_{l_1l_2},\ \mathbf{C}^{\hom}_{\mathbf{pp}}=\sum_{r=0}^{2N}\sum_{l_1+l_2=r}\frac{I^r k_1^{l_1}k_2^{l_2}}{l_1!l_2!}\left[\mathbf{A}^{\mathbf{pp}}_{l_1l_2}-\omega^2\mathbf{B}^{\mathbf{pp}}_{l_1l_2}\right].
\end{aligned}\tag{33}$$

The dynamic identification of the equivalent higher-order continuum model is determined by imposing that

$$D^{\hom}(\mathbf{k},\omega)=\det\left(\mathbf{C}^{\hom}(\mathbf{k},\omega)\right)=0.\tag{34}$$

In the specific case of a non-homogeneous wave propagation problem, where $\mathbf{k}\in\mathbb{C}^2$, $\mathbf{k}=\mathbf{k}_R+I\mathbf{k}_I=k_R\mathbf{n}_R+Ik_I\mathbf{n}_I$ with $\mathbf{k}_R$, $\mathbf{k}_I\in\mathbb{R}^2$ and $\mathbf{n}_R$, $\mathbf{n}_I$ are the directional unit vectors defined by relations (10), the characteristic equation associated with (34) can be decomposed as $D^{\hom}=D^{\hom}_R+ID^{\hom}_I=0$ and solvable in $\mathbf{k}$ by imposing the intersection of hypersurfaces to pinpoint the locus of points in space

$$\mathscr{S}^{\hom}=\left\{(k_{\mathscr{R}},k_{\mathscr{I}},\varphi_{\mathscr{R}},\varphi_{\mathscr{I}},\omega):\ \mathscr{D}^{\hom}_{\mathscr{R}}(k_{\mathscr{R}},k_{\mathscr{I}},\varphi_{\mathscr{R}},\varphi_{\mathscr{I}},\omega)=0\ \cap\ \mathscr{D}^{\hom}_{\mathscr{I}}(k_{\mathscr{R}},k_{\mathscr{I}},\varphi_{\mathscr{R}},\varphi_{\mathscr{I}},\omega)=0\right\}.\tag{35}$$

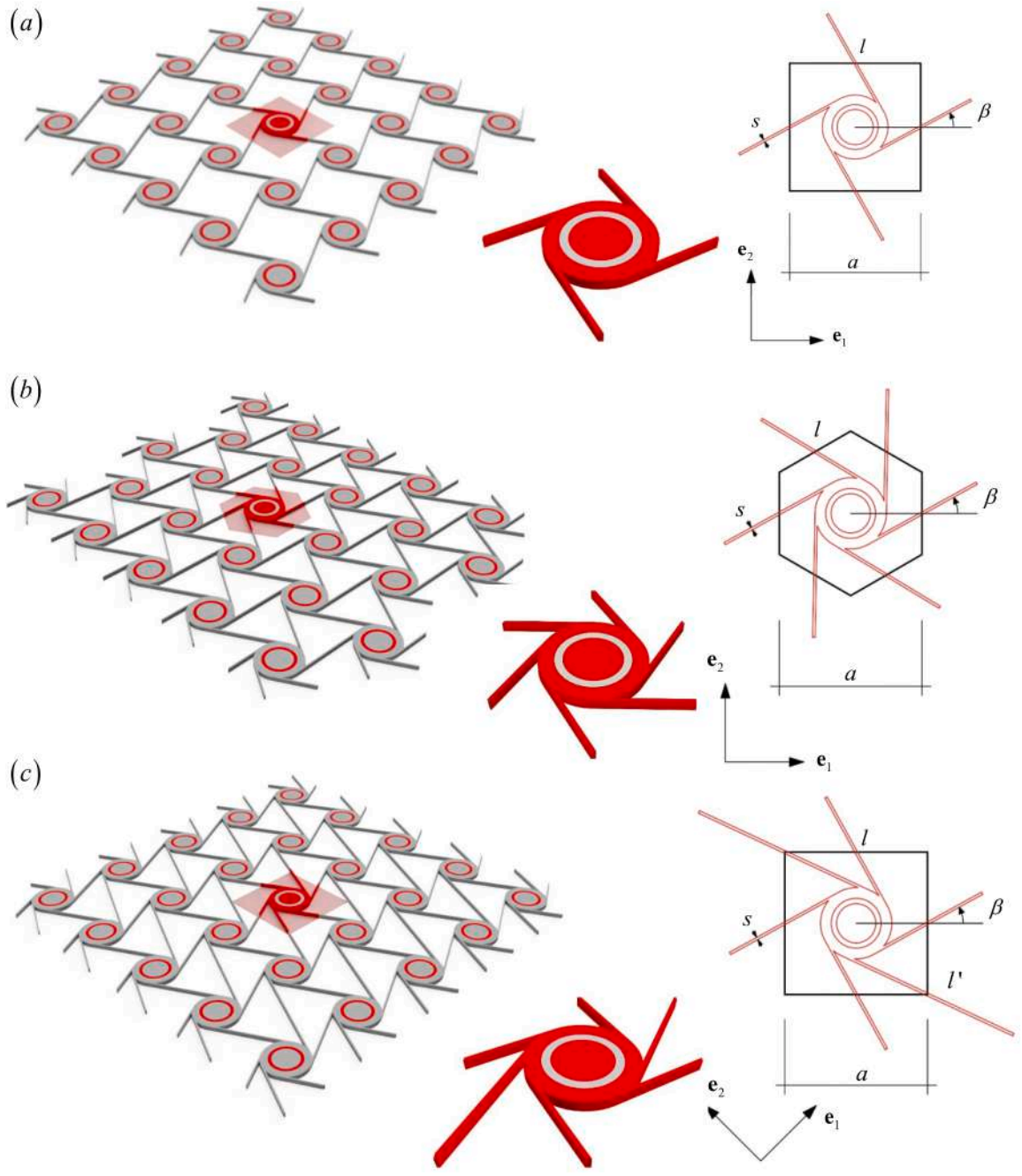

Fig. 3. Geometric description of the example topologies: a) tetrachiral lattice, b) hexachiral lattice, c) tetra-hexachiral lattice.

In the condition of homogeneous waves where $\varphi_R = \varphi_I = \varphi$, the locus of points (35) simplifies the dependencies as

$$\mathscr{S}^{\text{hom}} = \left\{ (k_{\mathscr{R}}, k_{\mathscr{I}}, \varphi, \omega) : \mathscr{D}^{\text{hom}}_{\mathscr{R}}(k_{\mathscr{R}}, k_{\mathscr{I}}, \varphi, \omega) = 0 \cap \mathscr{D}^{\text{hom}}_{\mathscr{I}}(k_{\mathscr{R}}, k_{\mathscr{I}}, \varphi, \omega) = 0 \right\}. \tag{36}$$

This condition can alternatively be resolved by formulating an equivalent polynomial eigenproblem associated with the wave vectors $\mathbf{k} = (k_R + Ik_I)\mathbf{n} = k\mathbf{n}$ with $k \in \mathbb{C}$, i.e.

$$\mathbf{C}^{\text{hom}}(k, \omega, \mathbf{n})\widehat{\mathbf{V}}^R = \left[\sum_{r=0}^{2N} \sum_{l_1+l_2=r} \left(\mathbf{C}^{\text{hom}}_{\mathbf{1},r}(\mathbf{n}) - \omega^2 \mathbf{C}^{\text{hom}}_{\mathbf{2},r}(\mathbf{n}) \right) k^r \right] \widehat{\mathbf{V}}^R = \mathbf{0}, \tag{37}$$

with k eigenvalue and $\widehat{\mathbf{V}}^R$ eigenvector, representing the wave number and the polarization vector respectively, with the direction $\mathbf{n}$ fixed. The formulation (37) is obtained by defining the components of the eigenproblem (32) with the 6×6 matrices

$$\mathbf{C}^{\text{hom}}_{\mathbf{1},r} = \begin{bmatrix} \mathbf{C}^{\text{hom}}_{\mathbf{qq},\mathbf{1}r} & \mathbf{C}^{\text{hom}}_{\mathbf{qp},\mathbf{1}r} \\ \mathbf{C}^{\text{hom}}_{\mathbf{pq},\mathbf{1}r} & \mathbf{C}^{\text{hom}}_{\mathbf{pp},\mathbf{1}r} \end{bmatrix}, \quad \mathbf{C}^{\text{hom}}_{\mathbf{2},r} = \begin{bmatrix} \mathbf{C}^{\text{hom}}_{\mathbf{qq},\mathbf{2}r} & \mathbf{0} \\ \mathbf{0} & \mathbf{C}^{\text{hom}}_{\mathbf{pp},\mathbf{2}r} \end{bmatrix}, \tag{38}$$

whose constituent submatrices of size 3×3 are defined as

$$\mathbf{C}^{\hom}_{\mathbf{qq},1r} \doteq \frac{In_1^{l_1} n_2^{l_2}}{l_1! l_2!}\mathbf{A}^{\mathbf{qq}}_{l_1 l_2},\quad \mathbf{C}^{\hom}_{\mathbf{qp},1r} \doteq \frac{In_1^{l_1} n_2^{l_2}}{l_1! l_2!}\mathbf{A}^{\mathbf{qp}}_{l_1 l_2},$$
$$\mathbf{C}^{\hom}_{\mathbf{pq},1r} \doteq \frac{In_1^{l_1} n_2^{l_2}}{l_1! l_2!}\mathbf{A}^{\mathbf{pq}}_{l_1 l_2},\quad \mathbf{C}^{\hom}_{\mathbf{pp},1r} \doteq \frac{In_1^{l_1} n_2^{l_2}}{l_1! l_2!}\mathbf{A}^{\mathbf{pp}}_{l_1 l_2},\tag{39}$$
$$\mathbf{C}^{\hom}_{\mathbf{qq},2r} \doteq \frac{n_1^{l_1} n_2^{l_2}}{Il_1! l_2!}\mathbf{B}^{\mathbf{qq}}_{l_1 l_2},\quad \mathbf{C}^{\hom}_{\mathbf{pp},2r} \doteq \frac{n_1^{l_1} n_2^{l_2}}{Il_1! l_2!}\mathbf{B}^{\mathbf{pp}}_{l_1 l_2}.$$

The eigenproblem (37) can be solved by linearization, reducing the polynomial formulation to the standard eigenproblem

$$(\mathbf{L} - k\mathbf{I})\widehat{\mathbf{W}}^R = \mathbf{0},\tag{40}$$

with $\mathbf{L} = \mathbf{L}_1^{-1}\mathbf{L}_0$ where $\mathbf{L}_1$, $\mathbf{L}_0$ matrices of size $12N \times 12N$ (of which $\mathbf{L}_1$ is invertible) and $\widehat{\mathbf{W}}^R$ eigenvector $12N \times 1$ appropriately detailed in Appendix D. By imposing the singularity of the matrix $\mathbf{L} - k\mathbf{I}$, the $12N -$ th order characteristic polynomial is determined in the form

$$\sum_{j=0}^{12N} I_j k^j = I_0 + I_1 k + \ldots + I_{12N} k^{12N} = 0,\tag{41}$$

with I_j the $j -$ th invariant determinable using the Faddeev-Leverrier method described in Appendix A. The identification related to the pure wave propagation, i.e., $\mathbf{k} = k\mathbf{n}$, with $k \in \mathbb{R}$ eigenproblem parameter and $\lambda = \omega^2$ eigenvalue, is determined by manipulating the Eq. (37) into the form

$$(\mathbf{H}_{\hom} - \lambda\mathbf{I})\widehat{\mathbf{V}}^R = \left[\left[\mathbf{C}^{\hom}_2(k,\mathbf{n})\right]^{-1}\mathbf{C}^{\hom}_1(k,\mathbf{n}) - \lambda\mathbf{I}\right]\widehat{\mathbf{V}}^R = \mathbf{0},\tag{42}$$

where the 6×6 invertible matrices $\mathbf{C}^{\hom}_1(k,\mathbf{n})$ and $\mathbf{C}^{\hom}_2(k,\mathbf{n})$ can be expressed as a linear combination of the matrices defined in (38) in the form

$$\mathbf{C}^{\hom}_1(k,\mathbf{n}) \doteq \sum_{r=0}^{2N}\sum_{l_1+l_2=r}\mathbf{C}^{\hom}_{1,r}(\mathbf{n})k^r,\ \mathbf{C}^{\hom}_2(k,\mathbf{n}) \doteq \sum_{r=0}^{2N}\sum_{l_1+l_2=r}\mathbf{C}^{\hom}_{2,r}(\mathbf{n})k^r.$$

The solution of equation Eq. (42) is obtained by determining the roots of the associated characteristic polynomial, having the same structure expressed in Eq. (41) for order 6. The coefficients of the polynomial are calculated using the Faddeev-Leverrier method, detailed in Appendix A.

5. Illustrative examples

This Section presents the static and dynamic properties of the continuum models for three different topologies, illustrated in Fig. 3. These are two-dimensional beam-lattice materials with tetrachiral (Fig. 3a), hexachiral (Fig. 3b), and tetra-hexachiral (Fig. 3c) structures, composed of a periodic repetition of unit cells with a characteristic size a that coincides with the distance between the nodes of the associated lattice (see Fig. 3). The structure consists of rigid disks with radius R and mass per unit thickness M interconnected by elastic ligaments with Young's modulus E. For the tetrachiral and hexachiral topology, the geometric parameters related to the ligaments are the slenderness $\delta = s/l$ with length l, and the ligament's thickness and depth s and b, respectively, while the angle between the coordination direction and the direction of the ligament parametrizes the chirality of geometry β. On the other hand, the ligaments of the tetra-hexachiral topology are defined by the slenderness parameters δ, $\delta' = s/l' = \delta\sqrt{\left[1 - 4(R/a)^2\right]/\left[2 - 4(R/a)^2\right]}$ with l and $l' = \sqrt{2}a\sqrt{1 - 2(R/a)^2}$ ligaments' lengths, respectively inclined by the chirality angles β, β' correlated through the following relationships $\cos\beta' = \sqrt{1 - (1 - \cos^2\beta)/2}$, $\sin\beta' = \left(\sqrt{2}\ /2\right)\sin\beta$. In the first sub-Section 5.1, the constitutive tensors of first-order gradient-type micropolar continuous are identified. In the sub-Section 5.2, the determination of the dispersive properties of the discrete Lagrangian models related to the different topologies is addressed. Subsequently, local circular resonators with radius r and mass per unit thickness m and translational and rotational stiffnesses k_v and k_θ, respectively, are centrally inserted into the rigid disks; this integration defines the metamaterials in the example geometries. In sub-Section 5.3, static and dynamic benchmark tests are explored, where the solutions derived from the introduced multifield continuum model are compared with those from discrete Lagrangian models to assess the validity of the enhanced procedure. Finally, in sub-Section 5.4, forced wave propagation is explored in the first-order gradient-type continuum model (governed by second-order truncated partial differential equations), broadening the introduced models' applicability.

5.1. Constitutive identification of the equivalent micropolar continuous

Starting from Eq. (30) related to the multifield higher-order continuum model, the expressions are simplified under the conditions of single-layer beam-lattice material without a local resonator. By omitting the inertial term, the corresponding first-order gradient-type continuum model ($N = 1$) is governed by field equations of order $2N = 2$, aligning with those of a micropolar continuous as the following specific expression

$$\frac{\mathbf{A}^{\mathbf{qq}}_{20}}{2}\frac{\partial^2\mathbf{q}^R}{\partial x_1^2} + \mathbf{A}^{\mathbf{qq}}_{11}\frac{\partial^2\mathbf{q}^R}{\partial x_1\partial x_2} + \frac{\mathbf{A}^{\mathbf{qq}}_{02}}{2}\frac{\partial^2\mathbf{q}^R}{\partial x_2^2} + \mathbf{A}^{\mathbf{qq}}_{10}\frac{\partial\mathbf{q}^R}{\partial x_1} + \mathbf{A}^{\mathbf{qq}}_{01}\frac{\partial\mathbf{q}^R}{\partial x_2} + \mathbf{A}^{\mathbf{qq}}_{00}\mathbf{q}^R = \mathbf{0}.\tag{43}$$

It is noted that the structure of the differential Eq. (43) shows a similar structure to the field equations of an equivalent micropolar continuous, if appropriately developed and defined in an equivalent operatorial form as detailed in the Eq. (81) in Appendix E. By comparison, it is obtained that

$$\mathbf{A}^{\mathbf{qq}}_{00} = \mathbf{C}_{00}\left(E_{ijhk}\right),\ \mathbf{A}^{\mathbf{qq}}_{10} = \mathbf{C}_{10}\left(E_{ijhk}\right),\ \mathbf{A}^{\mathbf{qq}}_{01} = \mathbf{C}_{01}\left(E_{ijhk}\right),$$
$$\mathbf{A}^{\mathbf{qq}}_{20} = 2\mathbf{C}_{20}\left(E_{ijhk}, S_{ij}\right),\ \mathbf{A}^{\mathbf{qq}}_{11} = \mathbf{C}_{11}\left(E_{ijhk}, S_{ij}\right),\ \mathbf{A}^{\mathbf{qq}}_{02} = 2\mathbf{C}_{02}\left(E_{ijhk}, S_{ij}\right),\tag{44}$$

where E_{ijhk}, S_{ij} are the overall elastic tensor components with $i, j, h, k = 1, 2$. The linear operators $\mathbf{A}_{bl}$ with $b,\ l = 0,\ 1,\ 2$ can be deduced using standard methods of structural mechanics concerning the various analyzed topologies, following Bacigalupo et al. in [89], while the linear operators $\mathbf{C}_{bl}$ with $b,\ l = 0, 1, 2$ are detailed in terms of components of the equivalent micropolar continuous in Appendix E.

5.1.1. Constitutive properties for the tetrachiral topology

Referring to the tetrachiral topology illustrated in Fig. 3a, the components of the coefficient matrices $\mathbf{A}_{bl}$ in (43) are specified for the directional unit vectors $\mathbf{n}_1 = \mathbf{e}_1$ and $\mathbf{n}_2 = \mathbf{e}_2$, with $\mathbf{e}_1$, $\mathbf{e}_2$ being the relative canonical basis (see Fig. 3a), and for the micromechanical parameters δ, β, a and E. The overall elastic tensor components

$$E_{1111} = E_{2222} = E\delta\left(\cos^2\beta + \delta^2\sin^2\beta\right),$$
$$E_{1121} = -E_{2212} = E\delta\left(1 - \delta^2\right)\sin\beta\cos\beta,$$
$$E_{1212} = E_{2121} = E\delta\left(\sin^2\beta + \delta^2\cos^2\beta\right),\tag{45}$$
$$S_{11} = S_{22} = \frac{1}{12}E\delta a^2\left(2\delta^2\cos^2\beta + \sin^2\beta\right),$$

are determined by exploiting the relationship (44) and manipulating the Eq. (82) in Appendix E.

5.1.2. Constitutive properties for the hexachiral topology

The coefficient matrices $\mathbf{A}_{bl}$ for the hexachiral beam-lattice material (Fig. 3b) are obtained analogously to sub-Section 5.1.1, for $\mathbf{n}_1 = \mathbf{e}_1$, $\mathbf{n}_2 = \frac{1}{2}\left(\mathbf{e}_1 + \sqrt{3}\,\mathbf{e}_2\right)$ and $\mathbf{n}_3 = \frac{1}{2}\left(-\mathbf{e}_1 + \sqrt{3}\,\mathbf{e}_2\right)$ where $\mathbf{e}_1$,$\mathbf{e}_2$ are the relative canonical basis (see Fig. 3b). Following the same procedure as presented for the tetrachiral case, the non-zero components of the elastic

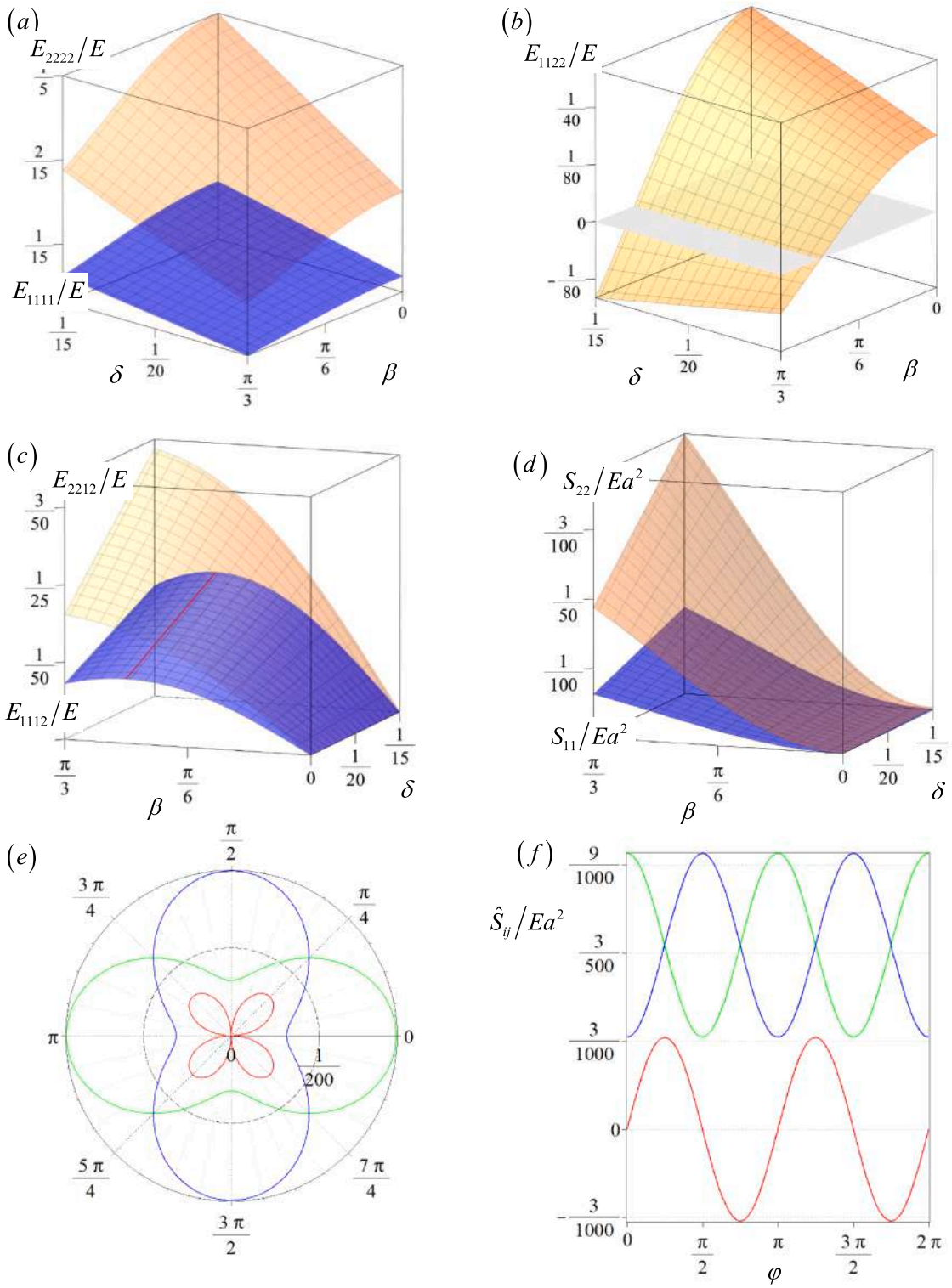

Fig. 4. Overall elastic tensor components for the tetra-hexachiral topology, a) E_{1111}/E, E_{2222}/E, b) E_{1122}/E, c) E_{2212}/E, E_{1112}/E and d) S_{11}/Ea^2, S_{22}/Ea^2. For $\beta = \pi/6$, $\delta = 1/20$, diagrams e) and f) depict the nonlocal elastic constitutive tensor $\widehat{S}_{11}/Ea^2$ (blue), $\widehat{S}_{12}/Ea^2$ (red) and $\widehat{S}_{22}/Ea^2$ (green) expressed in polar and Cartesian representations, respectively, relative to a generic orthonormal basis rotated of φ.

constitutive tensors are so determined

$$
\begin{aligned}
&E_{1111}=E_{2222}=E\delta\left[\frac{\sqrt{3}}{2}(1+\delta^2)+\frac{\sqrt{3}}{4}(1-\delta^2)\cos(2\beta)\right],\\
&E_{1122}=\frac{\sqrt{3}}{4}E\delta(1-\delta^2)\cos(2\beta),\\
&E_{1121}=E_{2221}=-E_{1112}=-E_{2212}=\frac{\sqrt{3}}{4}E\delta(1-\delta^2)\sin(2\beta),\\
&E_{1212}=E_{2121}=E\delta\left[\frac{\sqrt{3}}{4}(1+\delta^2)+\frac{\sqrt{3}}{2}(\cos^2\beta+\delta^2\sin^2\beta)\right],\\
&E_{1221}=E\delta\left[\frac{\sqrt{3}}{4}(1+\delta^2)-\frac{\sqrt{3}}{2}(\cos^2\beta+\delta^2\sin^2\beta)\right],\\
&S_{11}=S_{22}=\frac{\sqrt{3}}{12}E\delta a^2(4\delta^2\cos^2\beta+3\sin^2\beta).
\end{aligned}
\tag{46}
$$

5.1.3. Constitutive properties for the tetra-hexachiral topology

By the procedures described in 5.1.1 and 5.1.2 sub-Sections, the tetrachiral case with square elementary cell is identified for $\mathbf{n}_1=\mathbf{e}_1$ and $\mathbf{n}_2=\mathbf{e}_2$ directional unit vectors, referring to the relative canonical basis $\mathbf{e}_1$, $\mathbf{e}_2$ (Fig. 3c). The non-zero constitutive components obtained are

$$
\begin{aligned}
&E_{1111}=\frac{E_{2222}}{3}=\frac{1}{2}E\delta\left[1+\cos^2\beta+\delta^2\sin^2\beta\right],\\
&E_{1122}=E_{1221}=\frac{1}{2}E\delta(1-\delta^2)\cos(2\beta),\\
&E_{1112}=-E_{2221}=\frac{1}{2}E\delta(1-\delta^2)\sin(2\beta),\\
&E_{2212}=E\delta(1-\delta^2)\sin\beta\sqrt{1+\cos^2\beta},\\
&E_{2121}=\frac{1}{2}E\delta\left[\delta^2(1+\cos^2\beta)+\sin^2\beta\right],\\
&S_{11}=\frac{1}{12}E\delta a^2\left[2\delta^2(1+2\cos^2\beta)+3\sin^2\beta\right],\\
&S_{22}=\frac{1}{12}E\delta a^2\left[2\delta^2(1+6\cos^2\beta)+9\sin^2\beta\right],
\end{aligned}
\tag{47}
$$

which are depicted in Fig. 4 in their dimensionless form. The components of the obtained constitutive tensor exhibit strong non-linearities in relation to the chirality and slenderness parameters. Specifically, the dimensionless components E_{1111}/E and E_{2222}/E show monotonically increasing trends with increasing ligament slenderness δ and decreasing chirality angle β, following topological configurations that determine

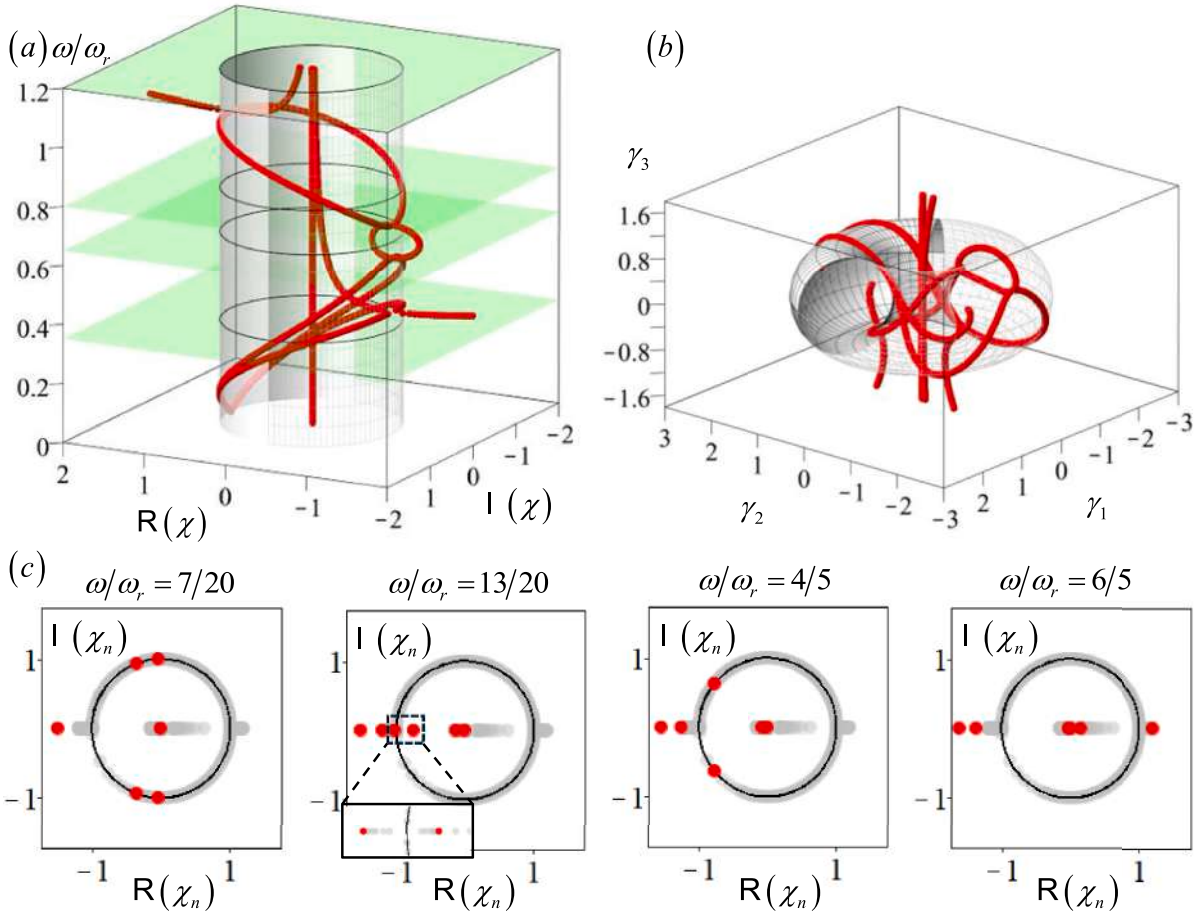

Fig. 5. Floquet multipliers χ(ω) for propagation $\mathbf{n}\equiv\mathbf{e}_2$ in the hexachiral beam-lattice material, $\delta=1/10$ and $\beta=\pi/8$. a) Curves (in red) of Floquet multipliers on the unit radius cylinder, b) curves (in red) of Floquet multipliers on the unit radius torus in the cartesian coordinate system γ_j, c) normalized Floquet multipliers $\chi_n(\omega)$ ($\psi=10/11$) on the unit circle in the complex plane. Floquet multipliers parameterized ω are indicated in gray, while red dots represent the multipliers related to the green planes' sections in Fig. 5.a.

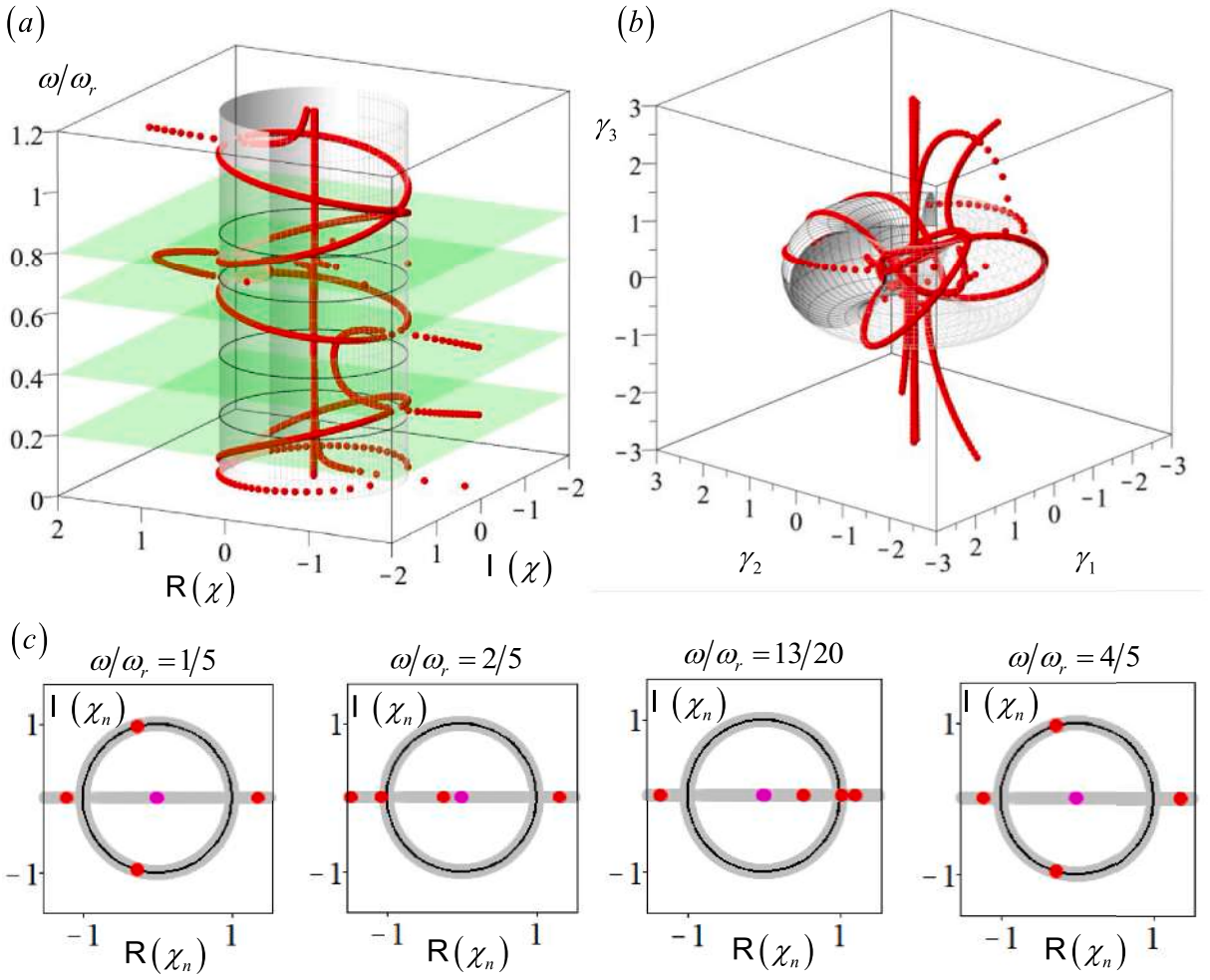

Fig. 6. Floquet multipliers $\chi(\omega)$ for propagation $\mathbf{n} \equiv \mathbf{e}_1$ in the tetrachiral metamaterial, with parameters $\delta = 1/10$, $\beta = \pi/8$, $m/M = 5/2$, $k_\nu/E \simeq 7/20$ e $k_\theta/Ea^2 \simeq 3/500$. a) Curves (in red) of Floquet multipliers on the unit radius cylinder, b) curves (in red) of Floquet multipliers on the unit radius torus in the cartesian coordinate system γ_j, c) normalized Floquet multipliers $\chi_n(\omega)$ ($\psi = 21/22$) on the unit circle in the complex plane. Floquet multipliers parameterized on ω are indicated in gray, while red dots (and magenta, in case of overlaps) represent the multipliers related to the green planes' sections in Fig. 6.a.

the overall stiffness. This monotonically increasing trend is also evident in Fig. 4b, regarding the component E_{1122}/E, which increases influenced by the decrease in the chirality of the elementary cell starting from negative values. The components correlating normal stresses with tangential strains are illustrated in Fig. 4c. In this context, the component E_{2212}/E exhibits a monotonically increasing behavior with increasing chirality β and ligament slenderness δ, while E_{1112}/E does not show a monotonic character and identifies relative maximum values represented by the red line in Fig. 4c. Due to the overall $\mathbb{Z}_2$ invariance, the non-local constitutive tensor components S_{11}/Ea^2 and S_{22}/Ea^2 are distinct for this topology, albeit with a similar increasing behavior with increasing chirality. This aspect is further explored in the diagrams in Fig. 4e and f, with a fixed ligament's slenderness $\delta = 1/20$ and chirality $\beta = \pi/6$. These diagrams represent the dimensionless non-local constitutive tensor components $\widehat{S}_{ij}/Ea^2$ referred to as a generic orthonormal basis $\{\widehat{\mathbf{e}}_1, \widehat{\mathbf{e}}_2\}$, obtained by rigidly rotating the reference basis depicted in Fig. 3c by the angle $\varphi = \mathrm{Arg}(\widehat{\mathbf{e}}_1 \cdot \mathbf{e}_1 + I\widehat{\mathbf{e}}_1 \cdot \mathbf{e}_2)$. Specifically, the second-order non-local tensor exhibits orthotropic properties owing to $\mathbb{D}_2$ invariance, with components dependent on the variation of φ.

5.2. Propagation of free Bloch homogeneous waves in the Lagrangian system

This sub-Section investigates the dynamic response of discrete Lagrangian models related to the introduced example topologies, applying the observations developed in Section 2. The attention is devoted to the propagation of homogeneous waves, where the wave vector is described as $\mathbf{k} = (k_R + Ik_I)\mathbf{n} = k\mathbf{n}$ with $k \in \mathbb{C}$ the wave number and $\mathbf{n}$ the unit propagation vector. By substituting the polar representation of the wave vector into the characteristic Eq. (9) and introducing the relation $\chi^{\pm 1} = \exp(\pm Ika_r)$ where χ denotes the (spatial) Floquet multiplier and a_r is a suitable reference length representing the microstructure, it can be verified that for specific propagation directions $\mathbf{n}$ the characteristic equation is a sixth-order palindromic polynomial in the variable $\chi \in \mathbb{C}$ expressible in the form (for details, see [90])

$$\mathscr{P}^{lag}(\chi,\omega) = \chi^6 + I_1(\omega)\chi^5 + I_2(\omega)\chi^4 + \\ + I_3(\omega)\chi^3 + I_2(\omega)\chi^2 + I_1(\omega)\chi + 1 = 0. \tag{48}$$

Referring to the Floquet multiplier's polar form $\chi = |\chi|\exp(I\mathrm{Arg}(\chi))$ and separating the real and imaginary parts of the characteristic

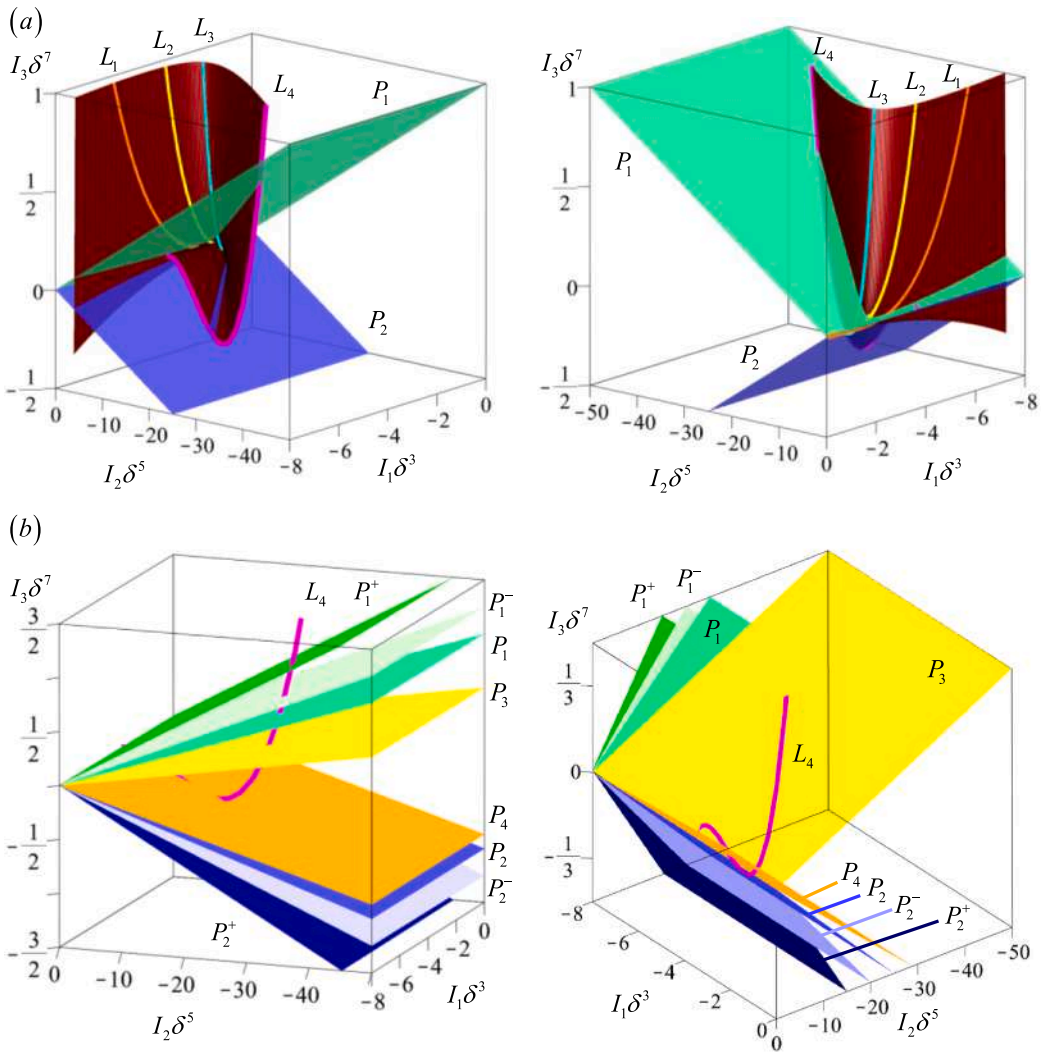

Fig. 7. a) Manifold M (red surface) and contour plots L_1, L_2, L_3 and L_4 related to the tetrachiral beam-lattice material for $\delta^d = 1/10$, in relation to planes P_1 and P_2 that express conditions of incipient damping, b) planes P_1, $P_1^{\pm}$, P_2, $P_2^{\pm}$, P_3 e P_4 and contour plots L_4 in the invariants' three-dimensional space I_1, I_2 and I_3.

polynomial, the Eq. (48) can be reformulated as follows

$$\begin{aligned}
&\mathscr{P}_{\mathscr{R}}^{lag}(\chi,\omega) = |\chi|^6\cos(6\mathrm{Arg}(\chi)) + I_1(\omega)|\chi|\left[|\chi|^4\cos(5\mathrm{Arg}(\chi)) + \cos(\mathrm{Arg}(\chi))\right] + \\
&+I_2(\omega)|\chi|^2\left[|\chi|^2\cos(4\mathrm{Arg}(\chi)) + \cos(2\mathrm{Arg}(\chi))\right] + I_3(\omega)|\chi|^3\cos(3\mathrm{Arg}(\chi)) + 1 = 0, \\
&\mathscr{P}_{\mathscr{I}}^{lag}(\chi,\omega) = |\chi|^6\sin(6\mathrm{Arg}(\chi)) + I_1(\omega)|\chi|\left[|\chi|^4\sin(5\mathrm{Arg}(\chi)) + \sin(\mathrm{Arg}(\chi))\right] + \\
&+I_2(\omega)|\chi|^2\left[|\chi|^2\sin(4\mathrm{Arg}(\chi)) + \sin(2\mathrm{Arg}(\chi))\right] + I_3(\omega)|\chi|^3\sin(3\mathrm{Arg}(\chi)) = 0,
\end{aligned} \tag{49}$$

with $I_1,\ I_2,\ I_3 \in \mathbb{R}$ since the considered systems are elastic. The procedure is general and can also be applied to the periodic beam-lattice material, neglecting the components related to the resonator's degrees of freedom $\widehat{\mathbf{v}}$ in the eigenproblem (8). The obtained characteristic equation can be converted into the polynomial form (49) following a similar approach to that adopted for the metamaterial. By solving the roots of the characteristic polynomial in the parametrization ω/ω_r with $\omega_r = \sqrt{E/M}$, it is found that the Floquet multipliers χ lie on the unit circle in the complex plane when associated with wave propagating in the metamaterial, identifying pure propagation modes. Conversely, within the spectral configurations of wave propagation's stop bands, the modulus is $|\chi| \neq 1$ exclusively at $\mathrm{Arg}(\chi) = 0, \pi$, a condition valid only in the case of elastic systems as those treated here.

Considerations regarding the Floquet multipliers emerge from the diagrams in Figs. 5 and 6, respectively concerning the hexachiral beam-lattice material and the tetrachiral metamaterial.

The results illustrated in Fig. 5 pertain to wave propagation for $\mathbf{n} \equiv \mathbf{e}_2$ and $a_r = \sqrt{3}a/2$, in relation to $\beta = \pi/8$ and $\delta = 1/10$. In particular, Fig. 5a shows the obtained Floquet multipliers $\chi(\omega)$, indicated by the red

curves encircling the unit radius cylinder, defining the frequency band structure of the hexachiral beam-lattice material. Specifically, it's feasible to identify the regions of complete or partial wave propagation or blocking, an aspect explored by the significant sections shown in Fig. 5c. For convenience of representation, these sections express the six solutions of Eq. (49) with respect to the normalized Floquet multiplier $\chi_n = \zeta(|\chi|)|\chi|\exp(I\mathrm{Arg}(\chi))$, where the auxiliary $|\chi|$- dependent function $\zeta(|\chi|) = \{|\chi|^{-\psi} \text{if} |\chi| > 1 \text{ or } 1 \text{ if } |\chi| \leq 1\}$, with $\psi \in \mathbb{Q}_{\geq 0}^{\leq 1}$ properly fixed scalar parameter, is introduced. Analogous observations can be made for Fig. 5.b, which illustrates the dynamic behavior of the system considering the modulus of χ and the arguments of χ and the introduced temporal Floquet multiplier $\upsilon = \exp(I\omega t)$ as toroidal coordinates. Referring to these coordinates, by defining the coefficients $\xi = \sinh(|\chi|)/[\cosh(|\chi|) - \cos(\mathrm{Arg}(\upsilon))]$ and $\vartheta = 1/[\cosh(|\chi|) - \cos(\mathrm{Arg}(\upsilon))]$, it is possible to determine the cartesian coordinates from the relationships $\gamma_1 = \xi\cos(\mathrm{Arg}(\chi))$, $\gamma_2 = \xi\sin(\mathrm{Arg}(\chi))$ and $\gamma_3 = \vartheta\sin(\mathrm{Arg}(\upsilon))$. The diagrams in Fig. 6 illustrate the effect induced by the presence of resonators, in the specific case of the tetrachiral metamaterial with $\beta = \pi/8$, $\delta = 1/10$ and for the wave propagation $\mathbf{n} \equiv \mathbf{e}_1$ and $a_r = a$.The introduced resonator has a mass of $m/M = 5/2$ and dimensionless stiffnesses $k_v/E \simeq 7/20$ and $k_\theta/Ea^2 \simeq 3/500$ in accordance with Bacigalupo and Gambarotta in [91]. As shown in the diagrams in Fig. 6.c, the frequencies $\omega/\omega_r = 2/5$ and $\omega/\omega_r = 13/20$ fall within total band gaps.

Moreover, the formula $\zeta(|\chi|) = \{|\chi|^{-\psi} \text{if } |\chi| > 1 \text{ or } 1 \text{ if } |\chi| \leq 1\}$ must be written in a unique row as well as the formula $\gamma_2 = \xi\sin(\mathrm{Arg}(\chi))$.

To determine the locus of points in the three-dimensional space of the invariants I_1, I_2 and I_3 where modes of pure spatial damping or conditions of incipient damping are characterized by $I(\chi) = 0$, the condition $\mathrm{Arg}(\chi) = 0, \pi$ is substituted into the real and imaginary parts of the characteristic polynomial given in the Eq. (49). This condition automatically satisfies the implicit equation $\mathscr{P}_{\mathscr{J}}^{lag}(\chi, \omega) = 0$, while the real parts specialize to the form

$$\begin{aligned}
&\mathscr{P}_{\mathscr{R}}^{0}(I_1, I_2, I_3;\ |\chi|,\ \mathrm{Arg}(\chi) = 0) = \\
&= |\chi|^6 + I_1|\chi| + I_2|\chi|^2 + I_3|\chi|^3 + 1 = 0, \\
&\mathscr{P}_{\mathscr{R}}^{\pi}(I_1, I_2, I_3;\ |\chi|,\ \mathrm{Arg}(\chi) = \pi) = \\
&= |\chi|^6 - I_1|\chi|\left(|\chi|^4 + 1\right) + I_2|\chi|^2\left(|\chi|^2 + 1\right) - I_3|\chi|^3 + 1 = 0,
\end{aligned} \tag{50}$$

identifying a pair of planes for each fixed value of $|\chi|$. Specifically, in Fig. 7 the planes corresponding to the following conditions are depicted

$$\begin{aligned}
&P_1 = \mathscr{P}_{\mathscr{R}}^{0}(I_1, I_2, I_3;\ |\chi| = 1,\ \mathrm{Arg}(\chi) = 0) = 0, \\
&P_2 = \mathscr{P}_{\mathscr{R}}^{\pi}(I_1, I_2, I_3;\ |\chi| = 1,\ \mathrm{Arg}(\chi) = \pi) = 0, \\
&P_1^{+} = \mathscr{P}_{\mathscr{R}}^{0}(I_1, I_2, I_3;\ |\chi| = 3,\ \mathrm{Arg}(\chi) = 0) = 0, \\
&P_2^{+} = \mathscr{P}_{\mathscr{R}}^{\pi}(I_1, I_2, I_3;\ |\chi| = 3,\ \mathrm{Arg}(\chi) = \pi) = 0, \\
&P_2^{-} = \mathscr{P}_{\mathscr{R}}^{0}\left(I_1, I_2, I_3;\ |\chi| = \frac{1}{2},\ \mathrm{Arg}(\chi) = 0\right) = 0, \\
&P_2^{-} = \mathscr{P}_{\mathscr{R}}^{\pi}\left(I_1, I_2, I_3;\ |\chi| = \frac{1}{2},\ \mathrm{Arg}(\chi) = \pi\right) = 0.
\end{aligned} \tag{51}$$

In the three-dimensional space of invariants, planes P_1 and P_2 identify the locus of points determining critical points in the frequency band structure. These critical points correspond to conditions of incipient spatial damping, characterized respectively by $|\chi| = 1$ and $\mathrm{Arg}(\chi) = 0, \pi$. Additionally, planes $P_i^{\pm}$ (with $i = 1, 2$) identify the points' locations which determine modes of pure damping for progressive and regressive homogeneous waves, characterized by $\mathrm{Arg}(\chi) = 0, \pi$ and $|\chi| \in \mathbb{R}_{\geq 0} \cup |\chi| \neq 1$. On the contrary, to determine the locus of points in the three-dimensional space of invariants I_1, I_2 and I_3 for which pure propagation modes characterized by $|\chi| = 1$ are identified, this condition is substituted into the Eq. (49) resulting in

$$\begin{aligned}
&\mathscr{P}_{\mathscr{R}}^{lag}(I_1, I_2, I_3;\ |\chi| = 1,\ \mathrm{Arg}(\chi)) = p_{\mathscr{R}}^{lag}(\mathrm{Arg}(\chi))\rho^{lag}(I_1, I_2, I_3;\ \mathrm{Arg}(\chi)) = \\
&= \cos(\mathrm{Arg}(\chi))\left[4\cos^2(\mathrm{Arg}(\chi)) - 3\right]\left\{I_3 + 2\cos(\mathrm{Arg}(\chi))I_2 + 2\left[2\cos^2(\mathrm{Arg}(\chi)) - 1\right]I_1 + \right. \\
&\left. + 2\cos(\mathrm{Arg}(\chi))\left[4\cos^2(\mathrm{Arg}(\chi)) - 3\right]\right\} = 0, \\
&\mathscr{P}_{\mathscr{J}}^{lag}(I_1, I_2, I_3;\ |\chi| = 1,\ \mathrm{Arg}(\chi)) = p_{\mathscr{J}}^{lag}(\mathrm{Arg}(\chi))\rho^{lag}(I_1, I_2, I_3;\ \mathrm{Arg}(\chi)) = \\
&= \sin(\mathrm{Arg}(\chi))\left[4\cos^2(\mathrm{Arg}(\chi)) - 1\right]\left\{I_3 + 2\cos(\mathrm{Arg}(\chi))I_2 + 2\left[2\cos^2(\mathrm{Arg}(\chi)) - 1\right]I_1 + \right. \\
&\left. + 2\cos(\mathrm{Arg}(\chi))\left[4\cos^2(\mathrm{Arg}(\chi)) - 3\right]\right\} = 0,
\end{aligned} \tag{52}$$

in which it is verified that the trigonometric functions $p_R^{lag}(\mathrm{Arg}(\chi))$ and $p_I^{lag}(\mathrm{Arg}(\chi))$ satisfy the condition $p_I^{lag}(\mathrm{Arg}(\chi)) = p_R^{lag}(\mathrm{Arg}(\chi) - \pi/6)$, while ρ^{lag} represents a plane in the three-dimensional space of invariants I_1, I_2 and I_3 for a fixed $\mathrm{Arg}(\chi)$. Specifically, in Fig. 7 the planes P_3 and P_4, for which $p_I^{lag} = 0$ and $p_R^{lag} = 0$ respectively, are depicted as defined by the following implicit functions

$$\begin{aligned}
&P_3 = \rho^{lag}(I_1, I_2, I_3;\ \mathrm{Arg}(\chi) = \pi/3) = I_1 - I_2 - I_3 + 2 = 0, \\
&P_4 = \rho^{lag}(I_1, I_2, I_3;\ \mathrm{Arg}(\chi) = 5\pi/6) = I_1 - \sqrt{3}I_2 + I_3 = 0.
\end{aligned} \tag{53}$$

It is important to note that the planes in the three-dimensional space of invariants defined from the Eq. (49), which identify the locus of points for which pure propagation modes, pure spatial damping modes, and conditions of incipient damping occur, are completely general and depend solely on the mathematical structure of the palindromic polynomial that governs propagation in the beam-lattice material or periodic metamaterial, considered as generic dynamic elastic-linear systems. By focusing on a particular topology, it is possible to express the invariants in closed form in terms of the angular frequency ω and the micromechanical parameters β and δ. Particularly, for the tetrachiral beam-lattice material the invariants are described as follows

$$\begin{aligned}
&I_1 = \frac{1}{\delta^3}\left\{\left(\frac{\omega}{\omega_r}\right)^2\left(\delta^2 - 2\right) - \delta\left[12\tan^2\beta + 18\delta^2\right]\right\}, \\
&I_2 = \frac{1}{\delta^5}\left\{\left(\frac{\omega}{\omega_r}\right)^2\left[\delta\left[8 - 16\delta^3 - 5\left(\frac{\omega}{\omega_r}\right)^2\right] + 12\right] + 3\delta^3\left(21\delta^2 - 16\right)\right\} \\
&+ \frac{3}{\delta^5\cos^2\beta}\left\{\left(\frac{\omega}{\omega_r}\right)^2\left[\delta\left[\left(\frac{\omega}{\omega_r}\right)^2 - 8\delta\right] - 4\right] + 16\delta^3\right\}, \\
&I_3 = \frac{1}{\delta^7}\left\{\left(\frac{\omega}{\omega_r}\right)^2\left[\begin{array}{l}\left(\frac{\omega}{\omega_r}\right)^2\left[24\delta - 14\delta^3 - 3\left(\frac{\omega}{\omega_r}\right)^2\right] + \\ + 6\delta^2\left(5\delta^4 - 2\delta^2 - 4\right)\end{array}\right] + 4\delta^5\left(18 - 23\delta^2\right)\right\} + \\
&+ \frac{3}{\delta^7\cos^2\beta}\left\{\left(\frac{\omega}{\omega_r}\right)^2\left[\begin{array}{l}\left(\frac{\omega}{\omega_r}\right)^2\left[\left(\frac{\omega}{\omega_r}\right)^2 - 2\delta^3 - 8\delta\right] + \\ + 8\delta^2\left(2\delta^2 + 1\right)\end{array}\right] - 24\delta^5\right\},
\end{aligned} \tag{54}$$

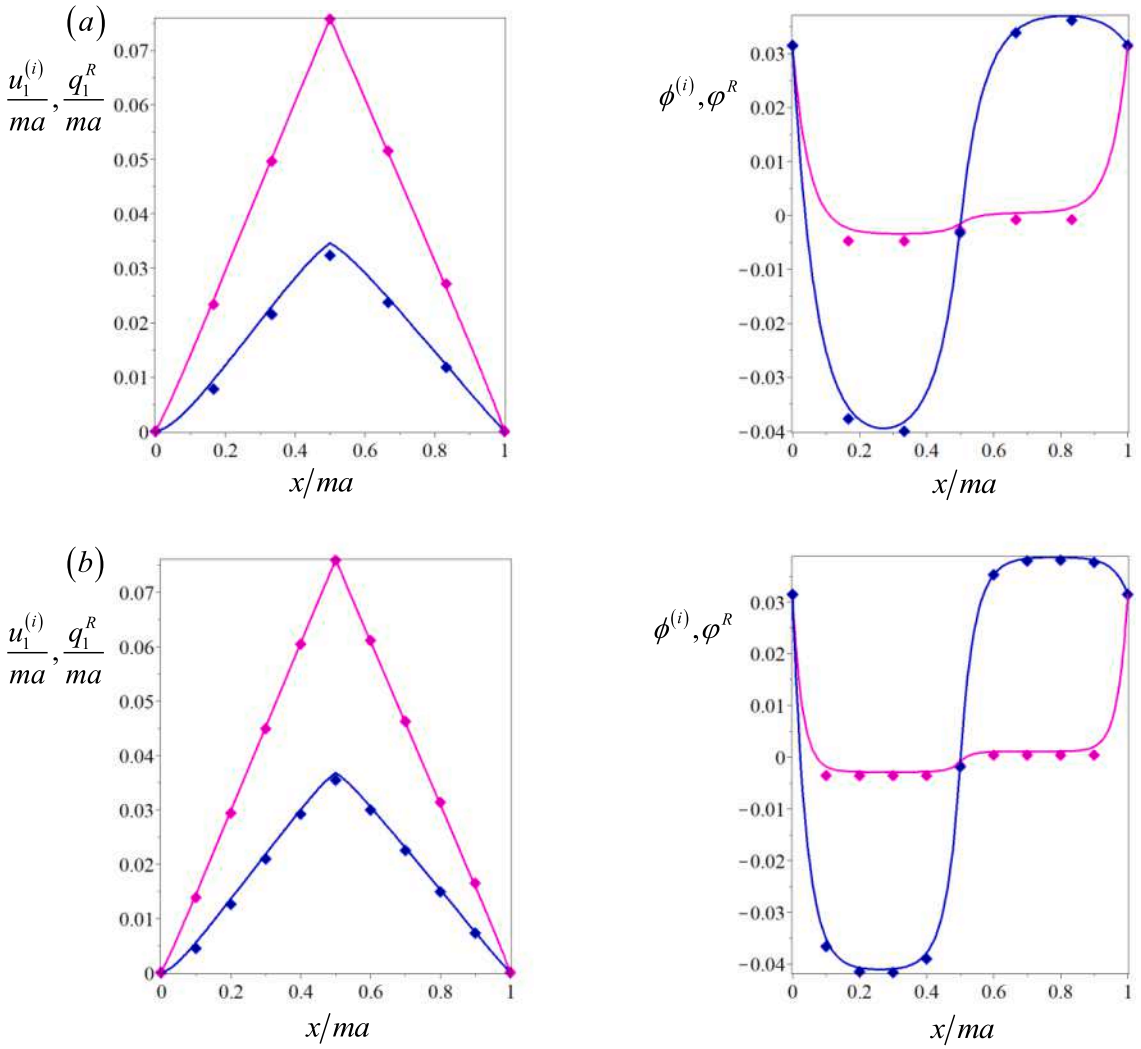

Fig. 8. Comparison of dimensionless displacements $u_1^{(i)}/ma$, q_1^R/ma and rotation $\phi^{(i)}$ and φ^R between the discrete models (markers) and continuous models (curves) for $\beta = 0$, $F/Ea^2 = 1/100$ (blue color) and $\beta = \pi/6$,$F/Ea^2 = 1/20$ (purple color), with $\eta = 1/20$, a) number of cells $m = 6$, b) number of cells $m = 10$.

which, for a fixed value of ligament slenderness δ^d, define a manifold $M = \{I_1 = f_1(\omega, \beta, \delta = \delta^d), I_2 = f_2(\omega, \beta, \delta = \delta^d), I_3 = f_3(\omega, \beta, \delta = \delta^d)\}$ parameterized in ω, β and embedded in the three-dimensional space of invariants I_1, I_2 and I_3. It is definable $L_i = \left\{I_1 = f_1\left(\omega, \beta = \beta_i^d, \delta = \delta^d\right), I_2 = f_2\left(\omega, \beta = \beta_i^d, \delta = \delta^d\right), I_3 = f_3\left(\omega, \beta = \beta_i^d, \delta = \delta^d\right)\right\}$ the contour curves of manifold M for fixed values of the chiral angle β_i^d with $i \in \mathbb{N}_{>0}$. The intersection between the manifold M and the planes $P_1, P_1^{\pm}, P_2, P_2^{\pm}$ e P_3, P_4 in (51), (53), i.e. $M \cap P_1$, $M \cap P_1^{\pm}$, $M \cap P_2$, $M \cap P_2^{\pm}$, defines curves in the three-dimensional space of invariants expressed by implicit functions of the type $f(\omega, \beta) = 0$ that identify the values of ω and the micromechanical parameter β for which pure propagation modes, pure spatial damping modes, and conditions of incipient damping (in the spectral situations defined in (51) and (53)) are realized in the tetrachiral beam-lattice material. Instead, the intersection between the curves L_i and the planes (51), (53) defines a set of points in the three-dimensional space of invariants obtained as a solution of the nonlinear equation that arises from the implicit function obtained as the intersection of M and the planes evaluated for the fixed values of chiral β_i^d i.e. $f\left(\omega, \beta = \beta_i^d\right) = 0$. Specifically, in Fig. 7 the manifold (red surface) for $\delta^d = 1/10$ and the contour curves L_1,L_2,L_3 and L_4 for $\beta_1^d = \pi/24$, $\beta_2^d = \pi/12$, $\beta_3^d = \pi/6$ e $\beta_4^d = \pi/3$, respectively, are illustrated.

5.3. *Representative benchmark tests: higher-order continualized models vs. discrete Lagrangian model*

In this sub-Section, the validation of the previously introduced higher-order gradient-type continuous models is examined to ensure their reliability in different contexts. Two validation tests are developed. The first, described in sub-Section 5.3.1, illustrates the effectiveness of the micropolar model identified in sub-Section 5.1.1 in capturing the kinematic solutions in a static problem, where a semi-indefinite domain is subjected to specific applied force conditions and boundary conditions. The second test focuses on the dispersive properties of the metamaterial and highlights how the enhanced continualization procedure can lead to continuous models capable of accurately describing the

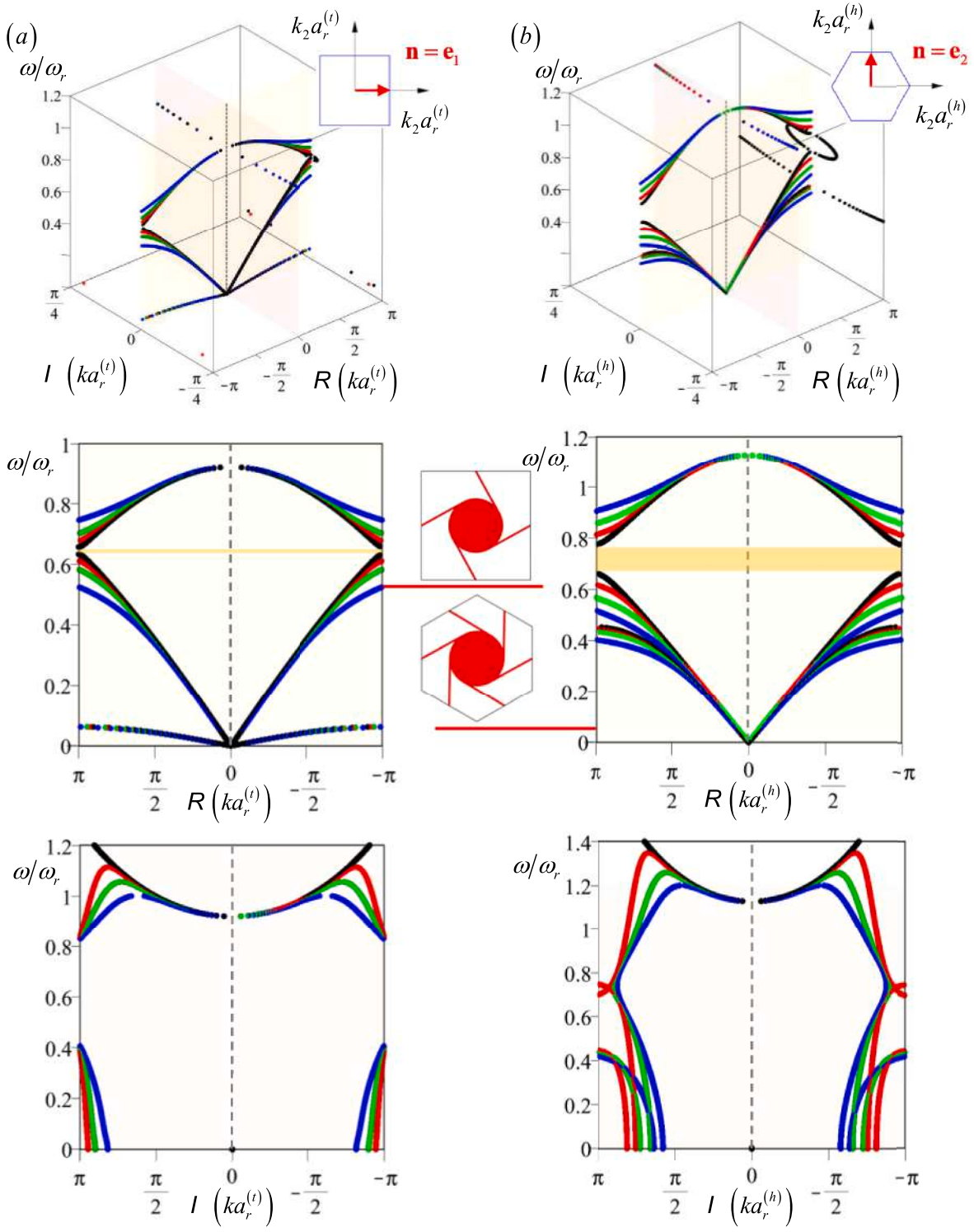

Fig. 9. Comparison between the spectra of the continualized models for the $2N = 4$ (blue), $2N = 8$ (green) and $2N = 16$ (red) order with those of the discrete Lagrangian model (black). Column a) spectra related to wave propagation for $\mathbf{n} \equiv \mathbf{e}_1$ in the tetrachiral beam-lattice material, with views and sections in the real and imaginary planes. Column b) spectra related to wave propagation for $\mathbf{n} \equiv \mathbf{e}_2$ in the hexachiral beam-lattice material, with views and sections in the real and imaginary planes. For both topologies, the micromechanical parameters are set to $\beta = \pi/8$ and $\delta = 1/10$..

associated dispersion curves.

5.3.1. Static benchmark test: an infinite strip subjected to punctual loads

It is possible to validate the constitutive identification presented in sub-Section 5.1 through a physically representative time-independent boundary problem, in which the solution obtained by the continualized model at the macroscopic scale is compared with the corresponding discrete Lagrangian one at the microscopic scale. Specifically, it is considered an infinite microstructured strip, realized through tetrachiral beam-lattice material and with height $L = \varsigma a$ where ς represents the even number of unit cells and a the size of the periodic cell (see sub-Section 5.1.1). At the horizontal upper and lower ends of the

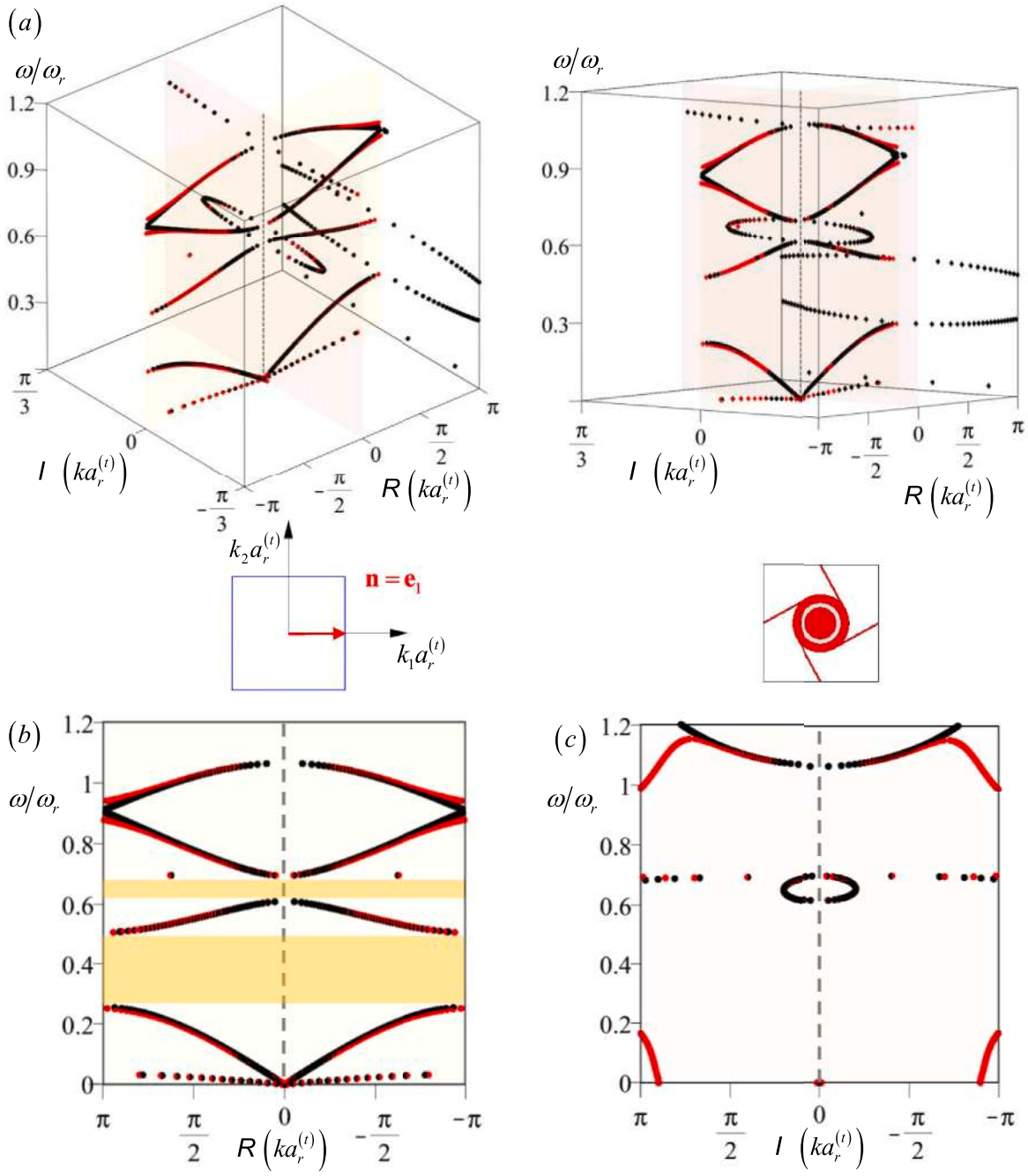

Fig. 10. Comparison of spectra between the discrete Lagrangian model (black) and the $2N = 8$ order multifield continualized model (red) referenced to the tetrachiral metamaterial for $\beta = \pi/8, \delta = 1/10$, $m/M = 5/2$, $k_\nu/E \simeq 7/20$ and $k_\theta/Ea^2 \simeq 3/500$, for fixed homogeneous wave propagation $\mathbf{n} \equiv \mathbf{e}_1$, a) views, b) real plane section, c) imaginary plane section.

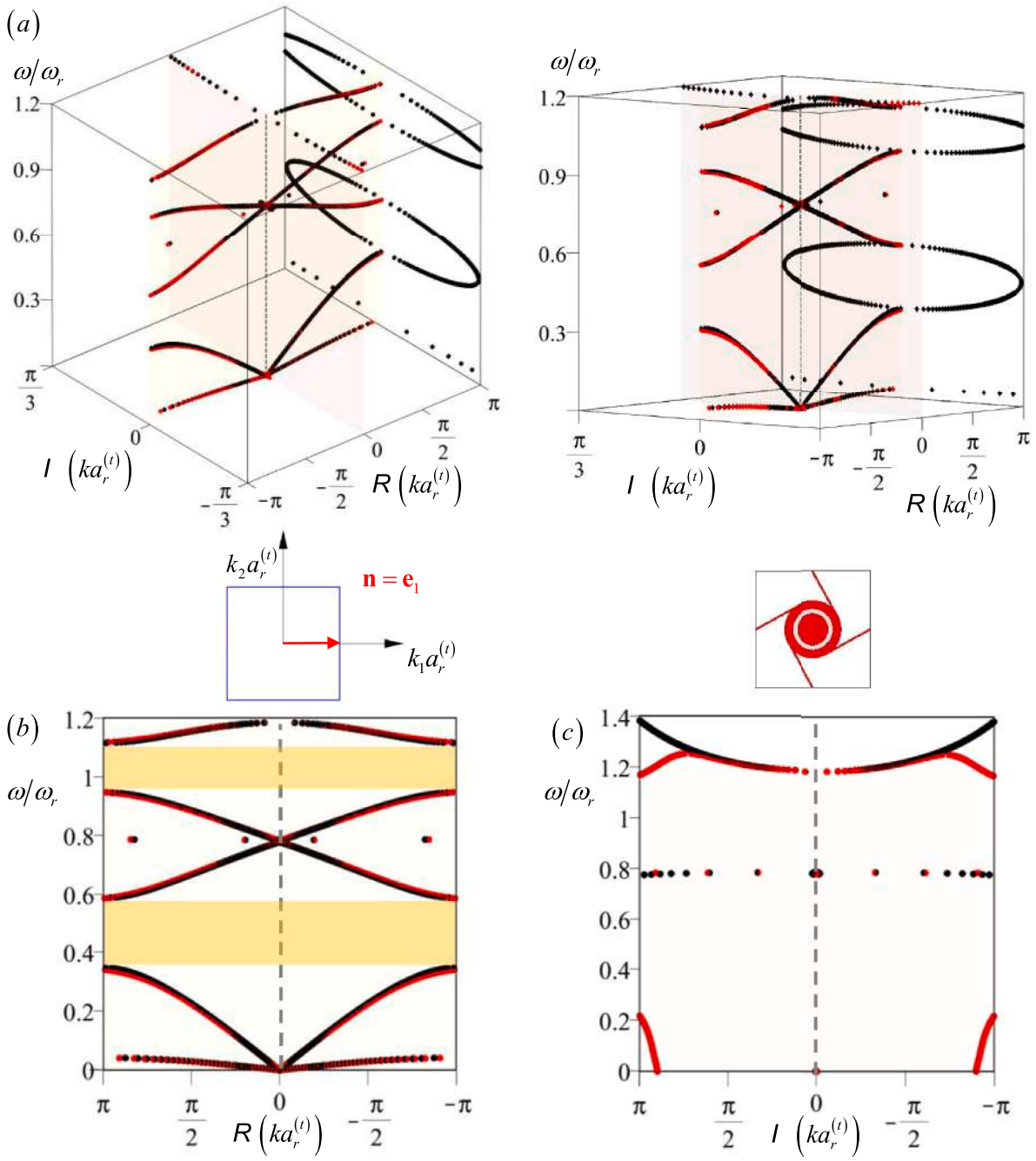

Fig. 11. Comparison of spectra between the discrete Lagrangian model (black) and the $2N = 8$ order multifield continualized model (red) referenced to the tetrachiral metamaterial for $\beta = \pi/8, \delta = 1/10, m/M = 5/4, k_\nu/E \simeq 7/20$ e $k_\theta/Ea^2 \simeq 3/500$, for fixed homogeneous wave propagation $\mathbf{n} \equiv \mathbf{e}_1$, a) views, b) real plane section, c) imaginary plane section.

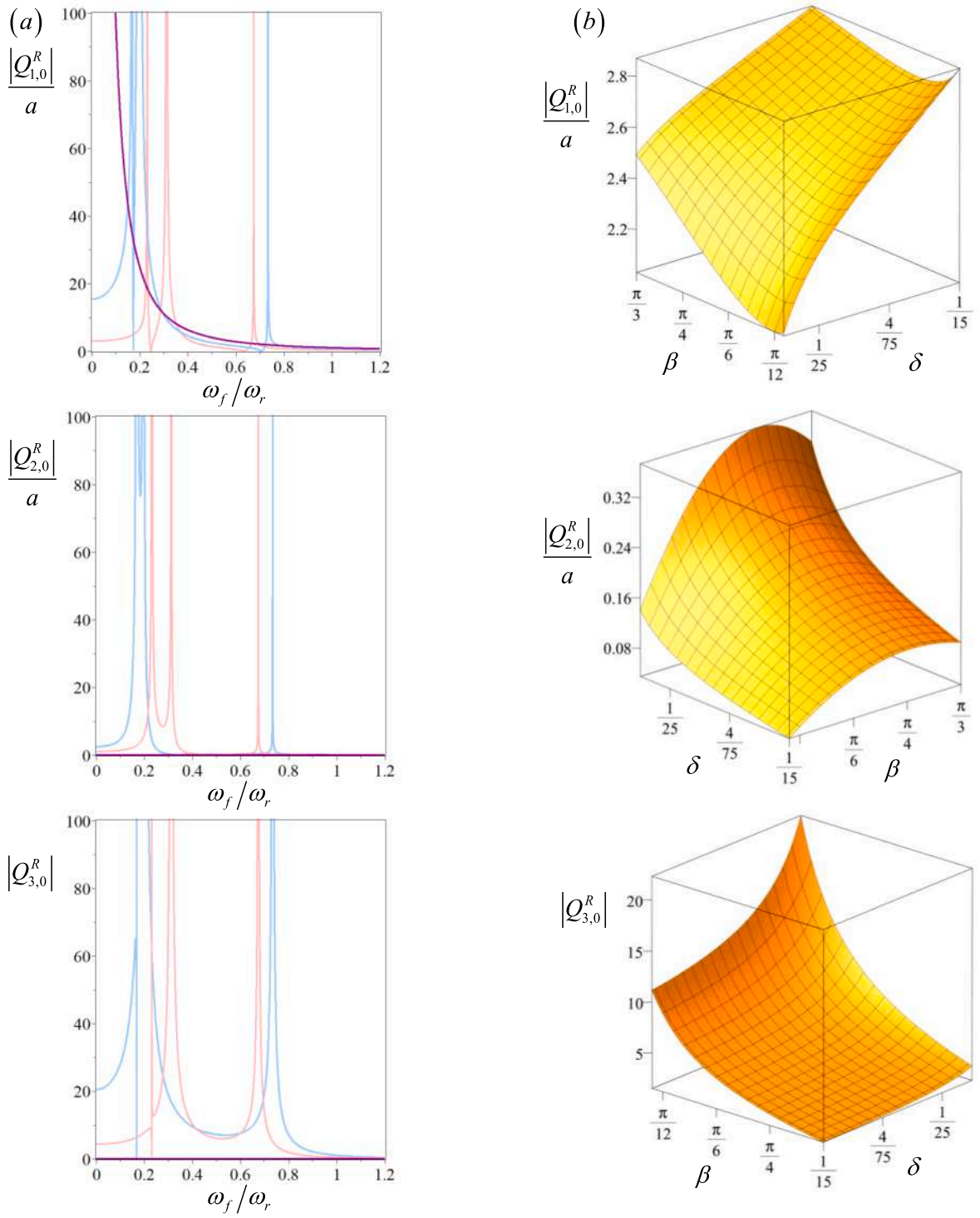

Fig. 12. Dimensionless wave amplitudes related to the solution of the forced hexachiral beam-lattice material. Column a) wave amplitudes for $k_f a_r^{(h)} = 0$ (purple curve), $k_f a_r^{(h)} = \pi/2$ (blue curve), $k_f a_r^{(h)} = \pi$ (pink curve), with micromechanical parameters $\beta = \pi/8$ and $\delta = 1/20$ fixed. Column b) variation of the amplitudes $|Q^R_{j,0}|/a$ with respect to the micromechanical parameters for $\omega_f/\omega_r = 0.5$ and $k_f a_r^{(h)} = \pi/2$..

infinite microstructured domain, the following kinematic discrete boundary conditions are applied $u_1^{(i_1,i_2=0,\varsigma)} = u_2^{(i_1,i_2=0,\varsigma)} = 0$, $\phi^{(i_1,i_2=0,\varsigma)} = \pi/100$ in any nodes lying on the upper and lower ends identified with the label $^{(i_1,i_2=0)}$ and $^{(i_1,i_2=\varsigma)}$, respectively. Moreover, a series of punctual horizontal forces, with the same intensity F, is applied in the nodes lying in the averaging alignment of the strip identified with the label $^{(i_1,i_2=\varsigma/2)}$. Due to the indeterminacy along the horizontal direction exists an invariance of the solution along the same direction. Consequently, the boundary algebraic difference problem can be reduced in a one-dimensional model.

At the macroscopic level, it is considered the infinite strip realised by homogeneous materials characterized by the constitutive point of view from the elastic tensor components reported in sub-Section 5.1.1 and any of its material points is kinematically described by the regularized field vector $\mathbf{q}^R = \begin{pmatrix} q_1^R & q_2^R & \phi^R \end{pmatrix}^T$. Also in this case, due to the indeterminacy along the horizontal direction exists an invariance of the solution along the same direction. Consequently, the boundary differential problem can be described by a one-dimensional model governed by the equations

$$\begin{aligned}
&\left[\left(1-\eta^2\right)\cos^2\beta - 1\right]\left(\frac{\mathrm{d}^2}{\mathrm{d}{x_2}^2}q_1^R(x_2) + \frac{\mathrm{d}}{\mathrm{d}x_2}\varphi^R(x_2)\right) + \\
&\quad + \frac{1}{2}\sin(2\beta)\left(\eta^2-1\right)\frac{\mathrm{d}^2}{\mathrm{d}{x_2}^2}q_2^R(x_2) - \frac{F}{E\eta a^3}\delta\left(x_2 - \frac{L}{2}\right) = 0, \\
&\left[\left(\eta^2-1\right)\cos^2\beta - \eta^2\right]\frac{\mathrm{d}^2}{\mathrm{d}{x_2}^2}q_2^R(x_2) + \\
&\quad + \frac{1}{2}\sin(2\beta)\left(\eta^2-1\right)\left(\frac{\mathrm{d}}{\mathrm{d}x_2}\varphi^R(x_2) + \frac{\mathrm{d}^2}{\mathrm{d}{x_2}^2}q_1^R(x_2)\right) = 0, \\
&\left[\frac{1}{2} + \left(\eta^2 - \frac{1}{2}\right)\cos^2\beta\right]a^2\frac{\mathrm{d}^2}{\mathrm{d}{x_2}^2}\varphi^R(x_2) + 6\left[\left(1-\eta^2\right)\cos^2\beta - 1\right]\frac{\mathrm{d}}{\mathrm{d}x_2}q_1^R(x_2) + \\
&\quad + 3\left(\eta^2-1\right)\sin(2\beta)\frac{\mathrm{d}}{\mathrm{d}x_2}q_2^R(x_2) - 12\varphi^R(x_2)\left[1 + \left(\eta^2-1\right)\cos^2\beta\right] = 0,
\end{aligned} \tag{55}$$

where $\delta(x_2 - L/2)$ is the Dirac delta function. It is important to note that the source term appears in (55) is obtained by using the bridging scale relationship in the $\mathbf{k}-$ space for the source terms reported in (21) in relation to the punctual load distribution at the microscopic level. Moreover, the consistent boundary conditions applied at the horizontal upper and lower ends of the infinite homogeneous domain are determined starting by the down-scaling relation expressed in differential form reported in the Eq. (64) of Appendix B. Specifically, via its appropriate truncation in agreement with the order of the governing equations of the continuous model the kinematic boundary conditions are determined in the form $q_1^R(x_2 = 0, L) = 0$, $q_2^R(x_2 = 0, L) = 0$, $\varphi^R(x_2 = 0, L) = \pi/100$..

The results analytically obtained for the parameters $\eta = 1/20$ and $\beta = 0$ (blue curves) and $\beta = \pi/6$ (purple curves) are illustrated for $\varsigma = 6$ and $\varsigma = 10$ respectively in Figs. 8a and b. The dimensionless concentrated forces applied to the discrete model are $F/Ea^2 = 1/100$ and $F/Ea^2 = 1/20$ for the cases with chirality $\beta = 0$ and $\beta = \pi/6$. The diagrams in Fig. 8 show good agreement with the discrete Lagrangian solutions, which can be further improved via higher-order continuous models. It is also important to note that an ulterior better deal with the discrete Lagrangian solution exists between the local generalized displacement of the homogenized model obtained via the pseudo-differential down-scaling relationships shown in Eq. (64) of Appendix B and the corresponding solution obtained by the discrete Lagrangian model (see for details [81]). The achirality ($\beta = 0$) and chirality ($\beta = \pi/6$) of the topologies lead to distinctly different responses, influenced respectively by the non-auxetic and auxetic intrinsic properties of each model, leading to lower rotation values under chiral conditions, even though the applied force is greater. Moreover as expected, the non-local effects of the static response tend to decrease as the height of the infinite strip increases.

5.3.2. *Dynamic benchmark tests: comparison of dispersive spectra*

Highlighting the effectiveness of the higher-order continualized models introduced in Section 4, the formulations of the continuum model are applied to various significant examples and compared with the corresponding discrete Lagrangian models. Specifically, Fig. 9 illustrates the dimensionless spectra for two example topologies: the tetrachiral beam-lattice material (Fig. 9, column a) and the hexachiral beam-lattice material (Fig. 9, column b) for $\beta = \pi/8$ and $\delta = 1/10$ analyzing the homogeneous free wave directions $\mathbf{n} \equiv \mathbf{e}_1$ and $\mathbf{n} \equiv \mathbf{e}_2$, respectively. For the tetrachiral beam-lattice material where $a_r = a_r^{(t)} = a$ and for the hexachiral topology where $a_r = a_r^{(h)} = \sqrt{3}a/2$, it can be observed that the dispersion curves for the enhanced continualized models, described by Eq. (30) reduced to the case of beam-lattice material and truncated to the $2N = 4$ (blue), $2N = 8$ (green) and $2N = 16$ (red) order (with N being the order of the gradient-type continuum model), show a progressive convergence with the curves associated with the discrete Lagrangian model (black) as the order of approximation increases. The sections of the real and imaginary planes reported in rows 2 and 3 in Fig. 9 highlight the effectiveness of the continualized models in approximating the curves related to pure propagation and pure damping. Focusing on the results obtained for the $\mathscr{R}\left(ka_r^{(t)}\right)$ and $\mathscr{R}\left(ka_r^{(h)}\right)$, the dispersion curves determine two respective band gaps. The first band gap is observed for the tetrachiral beam-lattice material at the dimensionless frequency centered in $\omega/\omega_r = 13/2$, while the second is identified for the hexachiral topology in the interval $\omega/\omega_r \in [3/5, 4/5]$. Once the effectiveness of higher-order continuum models has been verified, it is possible to extend the continualization procedure to the metamaterial. Taking into consideration the geometric and constitutive characteristics of the tetrachiral metamaterial introduced in sub-Section 5.2, Figs. 10 and 11 illustrate the spectra related to the corresponding truncated multifield continualized model at $2N = 8$ order. The spectra, evaluated under homogeneous free wave conditions for $\mathbf{n} \equiv \mathbf{e}_1$, are referred to two different resonator/structure mass ratios, $m/M = 5/2$ and $m/M = 5/4$, respectively. It is important to note that the $2N = 8$ order gradient-type continuum model (red) is once again validated, showing a clear convergence to the discrete Lagrangian model (black) for both mass ratio configurations. By comparing the solutions obtained for the tetrachiral beam-lattice material (Fig. 9a) and the tetrachiral metamaterial (Figs. 10 and 11), the continualization procedure described demonstrates the ability to provide a continuum model capable of approximating the variation of band gaps by alternating model parameters. As expected, this allows for the detection of the effectiveness of resonators and distinguishing the effects produced by modifying the system's mass relationships.

Specifically, it is important to note that the first pass-band amplitude associated with the Bloch wave propagating along the coordination direction in both the configurations of the tetrachiral metamaterial is substantially minor than the corresponding one in the associate tetrachiral beam-lattice material determining the opening of a large partial low-frequency band gap between the acoustic branches and the first optical one. Moreover, it is also possible to remark that the solution obtained via the continualized models, being able to convergently approximate the actual frequency spectrum of the discrete Lagrangian model, is also able to detect accurately the frequency band structures in terms of pass- and stop-band amplitudes.

5.4. *Experimental virtual test: harmonically forced wave propagation in the continualized second-order model*

After validating the multi-field continuum models under free wave conditions, this Sub-section aims to develop a virtual experimental test

by analytically solving the first set of differential equations used in the perturbative approach introduced in Eq. (71) of Appendix C. This involves characterizing the response of the continualized model governed by second-order differential equations ($j = 2$ in Eq. (71)) of the beam-lattice material subjected to a harmonic forcing of type $\mathbf{g}_0(x_1) = G_0\left(\exp\left[I(k_f x_1 - \omega_f t)\right] \quad 0 \quad 0\right)^T$, where k_f and ω_f represent the wavenumber and angular frequency of the forcing, respectively, while G_0 denotes its relative amplitude. Considering the spatial dependence of the forcing and taking into account the indeterminacy of the model in the physical space along the x_i directions with $i = 1, 2$, only the strip along x_1 is analyzed. Based on these assumptions and recalling the definitions in Appendix C of the linear differential operators (68) and developing the Eq. (71) is obtained

$$\mathbf{A}_{00}^{\mathbf{qq}}\mathbf{q}_0^R + \mathbf{B}_{00}^{\mathbf{qq}}\frac{\partial^2 \mathbf{q}_0^R}{\partial t^2} + \mathbf{A}_{10}^{\mathbf{qq}}\frac{\partial \mathbf{q}_0^R}{\partial x_1} + \mathbf{B}_{10}^{\mathbf{qq}}\frac{\partial^2}{\partial t^2}\left(\frac{\partial \mathbf{q}_0^R}{\partial x_1}\right) + \\ + \frac{1}{2}\mathbf{A}_{20}^{\mathbf{qq}}\frac{\partial^2 \mathbf{q}_0^R}{\partial x_1^2} + \frac{1}{2}\mathbf{B}_{20}^{\mathbf{qq}}\frac{\partial^2}{\partial t^2}\left(\frac{\partial^2 \mathbf{q}_0^R}{\partial x_1^2}\right) = \mathbf{g}_0. \tag{56}$$

The solution of the Eq. (56), characterizing the steady-state response of the mechanical system, has the following structure

$$\mathbf{q}_0^R(x_1, t) = \left(\mathbf{C}^{\hom,2}\right)^{-1}\mathbf{g}_0(x_1, t) = \frac{\operatorname{cof}\left(\mathbf{C}^{\hom,2}\right)^T}{\det\left(\mathbf{C}^{\hom,2}\right)}\mathbf{g}_0(x_1, t), \tag{57}$$

in which the term $\mathbf{C}^{\hom,2}\left(k_f, \omega_f\right)$, dependent on the problem parameters k_f and ω_f (due to the harmonic nature of the forcing), is expressed by the relation

$$\mathbf{C}^{\hom,2}\left(k_f, \omega_f\right) = \left[\mathbf{A}_{00}^{\mathbf{qq}} + Ik_f\mathbf{A}_{10}^{\mathbf{qq}} - \frac{k_f^2}{2}\mathbf{A}_{20}^{\mathbf{qq}} - \omega_f^2\left(\mathbf{B}_{00}^{\mathbf{qq}} + Ik_f\mathbf{B}_{10}^{\mathbf{qq}} - \frac{k_f^2}{2}\mathbf{B}_{20}^{\mathbf{qq}}\right)\right], \tag{58}$$

while the term $\operatorname{cof}\left(\mathbf{C}^{\hom,2}\right)$ represents the corresponding cofactor matrix. As expected, the Eq. (57) determines parametric singularities for k_f and ω_f such that $\det\left(\mathbf{C}^{\hom,2}\right) = 0$, corresponding to wavenumber and angular frequency values related to the Floquet spectra associated with the continualized model governed by a second-order differential equation. Characterizing the problem for the hexachiral beam-lattice material, it is possible to determine the dimensionless wave solution amplitudes $|Q_{j,0}^R|$ with $j = 1, 2, 3$, as functions of the micromechanical and dynamic parameters in the steady state regime, as illustrated in Fig. 12. From the diagrams in column 12.a, it is observed that for $k_f = 0$ a wave solution is obtained where the oscillation modes are pure translation and rotation. In this case, an excitation like $\mathbf{g}_0(x_1)$ does not affect displacements along x_2 and rotations, unlike when $k_f \neq 0$. Furthermore, the diagrams in column 12.b show that for $k_f a_r^{(h)} = \pi/2$ and $\omega/\omega_r = 0.5$, the magnitude of the amplitude component $|Q_{1,0}^R|$ exhibits a monotonically increasing trend with increasing δ. This behavior is replicated for $|Q_{3,0}^R|$ with increasing δ and β, while $|Q_{2,0}^R|$ does not exhibit a monotonic surface.

6. Conclusions

A novel enhanced high-frequency continualization scheme is introduced, delivering a thermodynamically consistent characterization of the constitutive and dispersive properties of periodic beam-lattice inertial metamaterials. The proposed continualization scheme is based on a completely general mathematical framework grounded on integral transforms and/or pseudo-differential operators which consents to describe in a very accurate way the essential aspects of the physical problem under investigation governed by the difference (in space) - differential (in time) equations. More specifically, by employing the Z-transform on the discrete spatial variable and the bilateral Laplace transform on the temporal variable, the eigenproblem governing the dynamic behaviour of the discrete Lagrangian system is formulated. This continualization approach formally equates the spatial Z-transform, reinterpreted in reciprocal space and applied to the micro-variables of the discrete system, with the spatial Fourier transform applied to the macro-variables of the equivalent integral-type continuum multifield model. Thermodynamic consistency is ensured by incorporating an appropriate regularization kernel, inducing inertial nonlocality in the integral-type continuum model, thereby aligning the frequency band structure with that of the discrete Lagrangian model.

By incorporating pseudo-differential operators and leveraging Taylor series expansions, the infinite-order gradient-type continuum multifield model is derived and resolved through two different methodologies. The first method employs a perturbative approach to tackle the infinite-order averaged differential equations asymptotically equivalent to the discrete Lagrangian equations to describe the forced Bloch wave propagation in the metamaterial. The second method addresses the problem by determining a higher-order gradient-type continuum model through appropriate truncation of the corresponding differential equations, aiming to characterize the dispersive properties of the metamaterial in both high- and low-frequency regimes. The analytical multifield continualization procedure is then applied to two-dimensional periodic microstructures with tetrachiral, hexachiral, and hexa-tetrachiral topologies. The applications highlight the ability of the obtained equivalent continuum models to describe the effective constitutive properties of the inertial metamaterial with periodic microstructure and to define a dynamic response that converges to that of the discrete Lagrangian model as the truncation order increases. Subsequently, a universal/general characterization of the frequency band structure of the metamaterials is furnished for a generic lattice with a monoatomic periodic cell elastically coupled with local resonators and elastically connected with the adjacent atoms/cells. A comprehensive characterization of the frequency band structure of the metamaterials is provided for a generic lattice with a monoatomic periodic cell that is elastically coupled with local resonators and elastically connected to adjacent atoms or cells. For these cases, under the conditions of free homogeneous elastic wave propagation of Bloch waves and for a fixed propagation direction, the dynamic problem is governed by a palindromic characteristic polynomial related to the Floquet multiplier. This framework allows for the observation of properties in analogy with the Floquet theory and provides significant representations in the three-dimensional space of invariants. By identifying notable conditions of pure propagation, pure spatial damping, and incipient damping modes through implicit functions, these conditions are subsequently compared with the invariants obtained in a closed form specific to a particular topology. Moreover, the modes of pure propagation are identified as the branches of the complex spectra that lie within the cylinder or torus manifolds, while the modes of spatial damping are identified as the branches that extend outward from these manifolds. Extending the application of the introduced continuum models, the resolution procedure for forced wave propagation has also been described, examining how the solution amplitudes vary with the micromechanical and dynamic parameters of the studied lattice.

CRediT authorship contribution statement

Andrea Bacigalupo: Writing – review & editing, Writing – original draft, Validation, Supervision, Software, Methodology, Investigation, Formal analysis, Conceptualization. **Paolo Badino:** Writing – review & editing, Writing – original draft, Validation, Supervision, Software, Methodology, Investigation, Formal analysis, Conceptualization. **Vito Diana:** Writing – review & editing, Writing – original draft, Validation, Supervision, Software, Methodology, Investigation, Formal analysis, Conceptualization. **Luigi Gambarotta:** Writing – review & editing, Writing – original draft, Validation, Supervision, Software, Methodology, Investigation, Formal analysis, Conceptualization.

Declaration of competing interest

The authors declare that they have no known competing financial interests or personal relationships that could have appeared to influence the work reported in this paper.

Data availability

No data was used for the research described in the article.

Acknowledgments

A.Bacigalupo is member of INdAM-GNFM. The authors gratefully acknowledge the National Group of Mathematical Physics (GNFM-INdAM, Italy) and the financial support of the European Union - Next Generation EU, component M4C2, investment 1.1 for the project PRIN PNRR 2022-P2022HLHHB-D53D23018260001: "A digital framework for the cutting of soft tissues: A first step towards virtual surgery".

Appendix A

One method used to determine the invariants I_j as well as coefficients of the associated characteristic polynomial is the Faddeev-Leverrier method. The characteristic polynomial associated with the standard eigenproblem related to a generic n order matrix $\mathbf{A}$ can be written in the form $\det(\mathbf{A}-\lambda\mathbf{I}) = \sum_{j=0}^{n} I_j \lambda^j$, where $I_0 = (-1)^n \det(\mathbf{A})$ while $I_n = 1$. The invariants I_{n-k}(with $k \in \mathbb{N}$ parameter identifying the $k-$ th phase of the scheme) can be determined by introducing the auxiliary matrices $\mathbf{M}_k$, defined as follows

$$\mathbf{M}_k \doteq \begin{cases} \mathbf{0} & k=0 \\ \mathbf{A}\mathbf{M}_{k-1} + I_{n-k+1}\mathbf{I} & k=1,\dots,n \end{cases}, \tag{59}$$

from which the invariants I_{n-k} of the matrix $\mathbf{A}$ are derived with respect to the relation

$$I_{n-k} = \begin{cases} 1 & k=0 \\ -\dfrac{1}{k}\mathrm{tr}(\mathbf{A}\mathbf{M}_k) & k=1,\dots,n \end{cases}. \tag{60}$$

Characterizing the eigenvalue problem for $n = 6$, the corresponding invariants are obtained

$$\begin{aligned}
I_6 &= 1, \\
I_5 &= -\mathrm{tr}(\mathbf{A}), \\
I_4 &= -\frac{1}{2}\mathrm{tr}(\mathbf{A}^2) + \frac{1}{2}(\mathrm{tr}(\mathbf{A}))^2, \\
I_3 &= -\frac{1}{3}\mathrm{tr}(\mathbf{A}^3) + \frac{1}{2}\mathrm{tr}(\mathbf{A}^2)\mathrm{tr}(\mathbf{A}) - \frac{1}{6}(\mathrm{tr}(\mathbf{A}))^3, \\
I_2 &= -\frac{1}{4}\mathrm{tr}(\mathbf{A}^4) + \frac{1}{3}\mathrm{tr}(\mathbf{A})\mathrm{tr}(\mathbf{A}^3) + \frac{1}{8}(\mathrm{tr}(\mathbf{A}^2))^2 - \frac{1}{4}\mathrm{tr}(\mathbf{A}^2)(\mathrm{tr}(\mathbf{A}))^2 + \frac{1}{24}(\mathrm{tr}(\mathbf{A}))^4, \\
I_1 &= -\frac{1}{5}\mathrm{tr}(\mathbf{A}^5) + \frac{1}{4}\mathrm{tr}(\mathbf{A})\mathrm{tr}(\mathbf{A}^4) + \frac{1}{6}\mathrm{tr}(\mathbf{A}^2)\mathrm{tr}(\mathbf{A}^3) - \frac{1}{6}(\mathrm{tr}(\mathbf{A}))^2\mathrm{tr}(\mathbf{A}^3) + \\
&\quad - \frac{1}{8}(\mathrm{tr}(\mathbf{A}^2))^2\mathrm{tr}(\mathbf{A}) + \frac{1}{12}(\mathrm{tr}(\mathbf{A}))^3\mathrm{tr}(\mathbf{A}^2) - \frac{1}{120}(\mathrm{tr}(\mathbf{A}))^5, \\
I_0 &= \det(\mathbf{A}),
\end{aligned} \tag{61}$$

and by substituting the matrices $\mathbf{H}_{lag}$ and $\mathbf{H}_{\mathrm{hom}}$ for matrix $\mathbf{A}$ in Eq. (61), the coefficients of the characteristic polynomial associated with the eigenproblems (13) and (50) in the main text are obtained, respectively. Furthermore, if $\mathbf{A} = \mathbf{L}$ and $n = 12N$, the $12N+1$ invariants are recursively obtained following the method described in Eqs. (59) and (60), knowing that $I_{12N} = 1$ and $I_0 = (-1)^{12N}\det(\mathbf{H}_{\mathrm{hom}})$.

Appendix B

The formal equality (26) can be suitably specialized in the case of tetrachiral beam-lattice material for $\mathbf{n}_1 = \mathbf{e}_1$ and $\mathbf{n}_2 = \mathbf{e}_2$ (see Fig. 3a). Under these conditions, the formal Taylor expansion of the pseudo-differential regularization operator becomes

$$\begin{aligned}
F_\circ[D_1, D_2] &= \frac{a^2 D_1 D_2}{\sinh(aD_1)\sinh(aD_2)} \sim \\
&\sim \sum_{\substack{r=2n \\ n\in\mathbb{N}}} \sum_{\substack{|\alpha|=r \\ l_1+l_2=r}} \frac{1}{r!}\binom{r}{l_1, l_2} \frac{\partial^{|\alpha|}}{\partial D_{\alpha_1}\dots\partial D_{\alpha_r}} \left(\frac{a^2 D_1 D_2}{\sinh(aD_1)\sinh(aD_2)}\right)\Bigg|_{\substack{D_1\Rightarrow 0 \\ D_2\Rightarrow 0}} D_{\alpha_1}\dots D_{\alpha_r} = \\
&= 1 - \frac{1}{6}a^2(D_1^2 + D_2^2) + \frac{7}{360}a^4(D_1^4 + D_2^4) + \frac{1}{36}a^4 D_1^2 D_2^2 + \dots .
\end{aligned} \tag{62}$$

By applying the relation (62) to the down-scaling relationships introduced in Eq. (26) it is possible to obtain

$$\mathbf{U}_{(i_1,i_2)}(t) \sim \left(\sum_{\substack{r=2n \\ n\in\mathbb{N}}} \sum_{\substack{l_1,l_2\in\mathbb{N} \\ l_1+l_2=r}} \frac{1}{l_1!l_2!\partial D_1^{l_1}\partial D_2^{l_2}} \left(\frac{a^2 D_1 D_2}{\sinh(aD_1)\sinh(aD_2)} \right) \Big|_{\substack{D_1\Rightarrow 0 \\ D_2\Rightarrow 0}} D_1^{l_1} D_2^{l_2} \mathbf{Q}^R(\mathbf{x},t) \right) \Big|_{\mathbf{x}\in X} =$$
$$= \left(\sum_{\substack{r=2n \\ n\in\mathbb{N}}} \sum_{\substack{l_1,l_2\in\mathbb{N} \\ l_1+l_2=r}} \frac{1}{l_1!l_2!\partial D_1^{l_1}\partial D_2^{l_2}} \left(\frac{a^2 D_1 D_2}{\sinh(aD_1)\sinh(aD_2)} \right) \Big|_{\substack{D_1\Rightarrow 0 \\ D_2\Rightarrow 0}} \frac{\partial^r \mathbf{Q}^R(\mathbf{x},t)}{\partial x_1^{l_1}\partial x_2^{l_2}} \right) \Big|_{\mathbf{x}\in X}. \tag{63}$$

Moreover, in the mechanical problems governed by one-dimensional differential equations, as in the case of the infinite strip treated in sub-Section 5.3.1, the down-scaling relationship (63) can be specialized in the compact form

$$\mathbf{U}_{(i_1,i_2)}(t) \sim \left(\frac{aD_2}{\sum_{n\in\mathbb{N}} \frac{a^{2n+1}D_2^{2n+1}}{(2n+1)!}} \mathbf{Q}^R(x_2,t) \right) \Big|_{\mathbf{x}\in X} = \left(\sum_{n\in\mathbb{N}} a^{2n} e_n \frac{\partial^{2n}}{\partial x^{2n}} \mathbf{Q}^R(x_2,t) \right) \Big|_{\mathbf{x}\in X}, \tag{64}$$

where the term e_n is given by the recursive relation $e_n = -\frac{1}{a_0}\sum_{j=0}^{n-1} a_{n-j}e_j$, where $a_n = 1/(2n+1)!$ with $n \in \mathbb{N}$. It is important to note that being the macroscopic field is x_1-indipendent also the associated microscopic discrete field turns out to be invariante with respect the index i_1 involved in the sub-set X that characterize the position of the nodes of the lattice (see for details the nomenclature indroduced in Section 2).

Appendix C

In this Appendix, an alternative perturbative solution procedure for the integro-differential equations defined in Eq. (28) is proposed. Firstly, the ordering parameter η is introduced into the governing equations

$$\begin{aligned}
&\sum_{\substack{l_1,l_2\in\mathbb{N} \\ l_1+l_2=r}} -\frac{\eta^{h(j)r}}{l_1!l_2!}\left[\mathbf{A}^{\mathbf{qq}}_{l_1l_2} \frac{\partial^r \mathbf{q}^R(\mathbf{x},t)}{\partial x_1^{l_1}\partial x_2^{l_2}} + \mathbf{A}^{\mathbf{qp}}_{l_1l_2} \frac{\partial^r \mathbf{p}^R(\mathbf{x},t)}{\partial x_1^{l_1}\partial x_2^{l_2}} \right] + \mathbf{s}(\mathbf{x},t) = \sum_{\substack{l_1,l_2\in\mathbb{N} \\ l_1+l_2=r}} \frac{\eta^{h(j)r}}{l_1!l_2!} \mathbf{B}^{\mathbf{qq}}_{l_1l_2} \frac{\partial^r \ddot{\mathbf{q}}^R(\mathbf{x},t)}{\partial x_1^{l_1}\partial x_2^{l_2}}, \\
&\sum_{\substack{l_1,l_2\in\mathbb{N} \\ l_1+l_2=r}} -\frac{\eta^{h(j)r}}{l_1!l_2!}\left[\mathbf{A}^{\mathbf{pq}}_{l_1l_2} \frac{\partial^r \mathbf{q}^R(\mathbf{x},t)}{\partial x_1^{l_1}\partial x_2^{l_2}} + \mathbf{A}^{\mathbf{pp}}_{l_1l_2} \frac{\partial^r \mathbf{p}^R(\mathbf{x},t)}{\partial x_1^{l_1}\partial x_2^{l_2}} \right] = \sum_{\substack{l_1,l_2\in\mathbb{N} \\ l_1+l_2=r}} \frac{\eta^{h(j)r}}{l_1!l_2!} \mathbf{B}^{\mathbf{pp}}_{l_1l_2} \frac{\partial^r \ddot{\mathbf{p}}^R(\mathbf{x},t)}{\partial x_1^{l_1}\partial x_2^{l_2}},
\end{aligned} \tag{65}$$

where $h(j) = \{0 \text{ if } l_1+l_2 = r < j \text{ or } 1 \text{ if } l_1+l_2 = r \geq j\}$ is the discrete step function, with $j \in \mathbb{N}_{>0}$, which rewrites the Eq. (65) as

$$\begin{aligned}
&\sum_{\substack{l_1,l_2\in\mathbb{N} \\ l_1+l_2=r<j}} -\frac{1}{l_1!l_2!}\left\{ \mathbf{A}^{\mathbf{qq}}_{l_1l_2} \frac{\partial^r \mathbf{q}^R(\mathbf{x},t)}{\partial x_1^{l_1}\partial x_2^{l_2}} + \mathbf{A}^{\mathbf{qp}}_{l_1l_2} \frac{\partial^r \mathbf{p}^R(\mathbf{x},t)}{\partial x_1^{l_1}\partial x_2^{l_2}} + \mathbf{B}^{\mathbf{qq}}_{l_1l_2} \frac{\partial^r \ddot{\mathbf{q}}^R(\mathbf{x},t)}{\partial x_1^{l_1}\partial x_2^{l_2}} \right\} + \mathbf{s}(\mathbf{x},t) + \\
&- \sum_{\substack{l_1,l_2\in\mathbb{N} \\ l_1+l_2=r\geq j}} \frac{\eta^r}{l_1!l_2!}\left\{ \mathbf{A}^{\mathbf{qq}}_{l_1l_2} \frac{\partial^r \mathbf{q}^R(\mathbf{x},t)}{\partial x_1^{l_1}\partial x_2^{l_2}} + \mathbf{A}^{\mathbf{qp}}_{l_1l_2} \frac{\partial^r \mathbf{p}^R(\mathbf{x},t)}{\partial x_1^{l_1}\partial x_2^{l_2}} + \mathbf{B}^{\mathbf{qq}}_{l_1l_2} \frac{\partial^r \ddot{\mathbf{q}}^R(\mathbf{x},t)}{\partial x_1^{l_1}\partial x_2^{l_2}} \right\} = \mathbf{0}, \\
&\sum_{\substack{l_1,l_2\in\mathbb{N} \\ l_1+l_2=r<j}} -\frac{1}{l_1!l_2!}\left\{ \mathbf{A}^{\mathbf{pq}}_{l_1l_2} \frac{\partial^r \mathbf{q}^R(\mathbf{x},t)}{\partial x_1^{l_1}\partial x_2^{l_2}} + \mathbf{A}^{\mathbf{pp}}_{l_1l_2} \frac{\partial^r \mathbf{p}^R(\mathbf{x},t)}{\partial x_1^{l_1}\partial x_2^{l_2}} + \mathbf{B}^{\mathbf{pp}}_{l_1l_2} \frac{\partial^r \ddot{\mathbf{p}}^R(\mathbf{x},t)}{\partial x_1^{l_1}\partial x_2^{l_2}} \right\} + \\
&- \sum_{\substack{l_1,l_2\in\mathbb{N} \\ l_1+l_2=r\geq j}} \frac{\eta^r}{l_1!l_2!}\left\{ \mathbf{A}^{\mathbf{pq}}_{l_1l_2} \frac{\partial^r \mathbf{q}^R(\mathbf{x},t)}{\partial x_1^{l_1}\partial x_2^{l_2}} + \mathbf{A}^{\mathbf{pp}}_{l_1l_2} \frac{\partial^r \mathbf{p}^R(\mathbf{x},t)}{\partial x_1^{l_1}\partial x_2^{l_2}} + \mathbf{B}^{\mathbf{pp}}_{l_1l_2} \frac{\partial^r \ddot{\mathbf{p}}^R(\mathbf{x},t)}{\partial x_1^{l_1}\partial x_2^{l_2}} \right\} = \mathbf{0}.
\end{aligned} \tag{66}$$

It is important to note that the parameter η only categorizes the orders in the infinite order mean governing equations. The solution of the Eq. (66) is sought as a power series expansion concerning the parameter η, in the form

$$\begin{aligned}
&\mathbf{q}^R(\mathbf{x},t) \sim \mathbf{q}_0^R(\mathbf{x},t) + \eta\mathbf{q}_1^R(\mathbf{x},t) + \eta^2\mathbf{q}_2^R(\mathbf{x},t) + \ldots = \sum_{m\in\mathbb{N}_{>0}} \eta^m \mathbf{q}_m^R(\mathbf{x},t), \\
&\mathbf{p}^R(\mathbf{x},t) \sim \mathbf{p}_0^R(\mathbf{x},t) + \eta\mathbf{p}_1^R(\mathbf{x},t) + \eta^2\mathbf{p}_2^R(\mathbf{x},t) + \ldots = \sum_{m\in\mathbb{N}_{>0}} \eta^m \mathbf{p}_m^R(\mathbf{x},t),
\end{aligned} \tag{67}$$

where $\mathbf{q}_m^R$, $\mathbf{p}_m^R$ represent $m-$th sensitivities of generalized displacements. The sensitivities given in (67) are derived by solving hierarchical differential problems at different orders of η. From the mathematical structure of Eq. (66) linear differential operators with double and single arguments can be defined

$$\mathscr{W}^{\mathbf{1},\mathbf{q}}_{l_1l_2}(\mathbf{y}_1,\mathbf{y}_2)\doteq\mathbf{A}^{\mathbf{qq}}_{l_1l_2}\frac{\partial^r\mathbf{y}_1}{\partial x_1^{l_1}\partial x_2^{l_2}}+\mathbf{A}^{\mathbf{qp}}_{l_1l_2}\frac{\partial^r\mathbf{y}_2}{\partial x_1^{l_1}\partial x_2^{l_2}},\quad \mathscr{W}^{\mathbf{1},\mathbf{p}}_{l_1l_2}(\mathbf{y}_1,\mathbf{y}_2)\doteq\mathbf{A}^{\mathbf{pq}}_{l_1l_2}\frac{\partial^r\mathbf{y}_1}{\partial x_1^{l_1}\partial x_2^{l_2}}+\mathbf{A}^{\mathbf{pp}}_{l_1l_2}\frac{\partial^r\mathbf{y}_2}{\partial x_1^{l_1}\partial x_2^{l_2}},$$
$$\mathscr{W}^{\mathbf{2},\mathbf{q}}_{l_1l_2}(\mathbf{y}_1)\doteq\mathbf{B}^{\mathbf{qq}}_{l_1l_2}\frac{\partial^2}{\partial t^2}\left(\frac{\partial^r\mathbf{y}_1}{\partial x_1^{l_1}\partial x_2^{l_2}}\right),\quad \mathscr{W}^{\mathbf{2},\mathbf{p}}_{l_1l_2}(\mathbf{y}_1)\doteq\mathbf{B}^{\mathbf{pp}}_{l_1l_2}\frac{\partial^2}{\partial t^2}\left(\frac{\partial^r\mathbf{y}_1}{\partial x_1^{l_1}\partial x_2^{l_2}}\right), \tag{68}$$

with $\mathbf{y}_1$, $\mathbf{y}_2$ being generic vector fields of appropriate dimension. It is possible to rewrite Eq. (66) by introducing the power series expansions expressed in (67), thus obtaining

$$\begin{aligned}
&\sum_{\substack{l_1,l_2\in\mathbb{N}\\ l_1+l_2=r<j}}-\frac{1}{l_1!l_2!}\left\{\mathscr{W}^{\mathbf{1},\mathbf{q}}_{l_1l_2}\left(\sum_{m\in\mathbb{N}_{>0}}\eta^m\mathbf{q}^R_m,\sum_{m\in\mathbb{N}_{>0}}\eta^m\mathbf{p}^R_m\right)+\mathscr{W}^{\mathbf{2},\mathbf{q}}_{l_1l_2}\left(\sum_{m\in\mathbb{N}_{>0}}\eta^m\mathbf{q}^R_m\right)\right\}+\mathbf{s}+\\
&-\sum_{\substack{l_1,l_2\in\mathbb{N}\\ l_1+l_2=r\geq j}}\frac{\eta^r}{l_1!l_2!}\left\{\mathscr{W}^{\mathbf{1},\mathbf{q}}_{l_1l_2}\left(\sum_{m\in\mathbb{N}_{>0}}\eta^m\mathbf{q}^R_m,\sum_{m\in\mathbb{N}_{>0}}\eta^m\mathbf{p}^R_m\right)+\mathscr{W}^{\mathbf{2},\mathbf{q}}_{l_1l_2}\left(\sum_{m\in\mathbb{N}_{>0}}\eta^m\mathbf{q}^R_m\right)\right\}=\mathbf{0},\\
&\sum_{\substack{l_1,l_2\in\mathbb{N}\\ l_1+l_2=r<j}}-\frac{1}{l_1!l_2!}\left\{\mathscr{W}^{\mathbf{1},\mathbf{p}}_{l_1l_2}\left(\sum_{m\in\mathbb{N}_{>0}}\eta^m\mathbf{q}^R_m,\sum_{m\in\mathbb{N}_{>0}}\eta^m\mathbf{p}^R_m\right)+\mathscr{W}^{\mathbf{2},\mathbf{p}}_{l_1l_2}\left(\sum_{m\in\mathbb{N}_{>0}}\eta^m\mathbf{p}^R_m\right)\right\}+\\
&-\sum_{\substack{l_1,l_2\in\mathbb{N}\\ l_1+l_2=r\geq j}}\frac{\eta^r}{l_1!l_2!}\left\{\mathscr{W}^{\mathbf{1},\mathbf{p}}_{l_1l_2}\left(\sum_{m\in\mathbb{N}_{>0}}\eta^m\mathbf{q}^R_m,\sum_{m\in\mathbb{N}_{>0}}\eta^m\mathbf{p}^R_m\right)+\mathscr{W}^{\mathbf{2},\mathbf{p}}_{l_1l_2}\left(\sum_{m\in\mathbb{N}_{>0}}\eta^m\mathbf{p}^R_m\right)\right\}=\mathbf{0}.
\end{aligned} \tag{69}$$

Due to the linearity of the newly introduced differential operators and manipulating the expressions appropriately, one obtains

$$\begin{aligned}
&\sum_{\substack{l_1,l_2\in\mathbb{N}\\ l_1+l_2=r<j}}\sum_{m\in\mathbb{N}_{>0}}-\frac{\eta^m}{l_1!l_2!}\left\{\mathscr{W}^{\mathbf{1},\mathbf{q}}_{l_1l_2}(\mathbf{q}^R_m,\mathbf{p}^R_m)+\mathscr{W}^{\mathbf{2},\mathbf{q}}_{l_1l_2}(\mathbf{q}^R_m)\right\}-\sum_{\substack{l_1,l_2\in\mathbb{N}\\ l_1+l_2=r<j}}\frac{1}{l_1!l_2!}\left\{\mathscr{W}^{\mathbf{1},\mathbf{q}}_{l_1l_2}(\mathbf{q}^R_0,\mathbf{p}^R_0)+\mathscr{W}^{\mathbf{2},\mathbf{q}}_{l_1l_2}(\mathbf{q}^R_m)\right\}+\\
&+\mathbf{s}+\sum_{\substack{l_1,l_2\in\mathbb{N}\\ l_1+l_2=r\geq j}}\sum_{m\in\mathbb{N}_{>0}}-\frac{\eta^{r+m-1}}{l_1!l_2!}\left\{\mathscr{W}^{\mathbf{1},\mathbf{q}}_{l_1l_2}(\mathbf{q}^R_{m-1},\mathbf{p}^R_{m-1})+\mathscr{W}^{\mathbf{2},\mathbf{q}}_{l_1l_2}(\mathbf{q}^R_{m-1})\right\}=\mathbf{0},\\
&\sum_{\substack{l_1,l_2\in\mathbb{N}\\ l_1+l_2=r<j}}\sum_{m\in\mathbb{N}_{>0}}-\frac{\eta^m}{l_1!l_2!}\left\{\mathscr{W}^{\mathbf{1},\mathbf{p}}_{l_1l_2}(\mathbf{q}^R_m,\mathbf{p}^R_m)+\mathscr{W}^{\mathbf{2},\mathbf{p}}_{l_1l_2}(\mathbf{p}^R_m)\right\}-\sum_{\substack{l_1,l_2\in\mathbb{N}\\ l_1+l_2=r<j}}\frac{1}{l_1!l_2!}\left\{\mathscr{W}^{\mathbf{1},\mathbf{p}}_{l_1l_2}(\mathbf{q}^R_0,\mathbf{p}^R_0)+\mathscr{W}^{\mathbf{2},\mathbf{p}}_{l_1l_2}(\mathbf{p}^R_0)\right\}+\\
&+\sum_{\substack{l_1,l_2\in\mathbb{N}\\ l_1+l_2=r\geq j}}\sum_{m\in\mathbb{N}_{>0}}-\frac{\eta^{r+m-1}}{l_1!l_2!}\left\{\mathscr{W}^{\mathbf{1},\mathbf{p}}_{l_1l_2}(\mathbf{q}^R_{m-1},\mathbf{p}^R_{m-1})+\mathscr{W}^{\mathbf{2},\mathbf{p}}_{l_1l_2}(\mathbf{p}^R_{m-1})\right\}=\mathbf{0}.
\end{aligned} \tag{70}$$

It is observable that the generating solution $\mathbf{q}_0$, $\mathbf{p}_0$ can be derived from the Eq. (70) truncated to order 0 in the following manner

$$\begin{aligned}
&\sum_{\substack{l_1,l_2\in\mathbb{N}\\ l_1+l_2=r<j}}-\frac{1}{l_1!l_2!}\left\{\mathscr{W}^{\mathbf{1},\mathbf{q}}_{l_1l_2}(\mathbf{q}^R_0,\mathbf{p}^R_0)+\mathscr{W}^{\mathbf{2},\mathbf{q}}_{l_1l_2}(\mathbf{q}^R_0)\right\}+\mathbf{g}_0=\mathbf{0},\\
&\sum_{\substack{l_1,l_2\in\mathbb{N}\\ l_1+l_2=r<j}}-\frac{1}{l_1!l_2!}\left\{\mathscr{W}^{\mathbf{1},\mathbf{p}}_{l_1l_2}(\mathbf{q}^R_0,\mathbf{p}^R_0)+\mathscr{W}^{\mathbf{2},\mathbf{p}}_{l_1l_2}(\mathbf{p}^R_0)\right\}+\mathbf{h}_0=\mathbf{0}.
\end{aligned} \tag{71}$$

The first system of differential equations includes source terms aligned with the dominant order, corresponding to the forces exerted on the real system, namely $\mathbf{g}_0=\mathbf{s}$ and $\mathbf{h}_0=\mathbf{0}$. By considering only terms of order $s<j$, the differential equations become

$$\begin{aligned}
&\sum_{\substack{l_1,l_2\in\mathbb{N}\\ l_1+l_2=r<j}}-\frac{1}{l_1!l_2!}\left\{\mathscr{W}^{\mathbf{1},\mathbf{q}}_{l_1l_2}(\mathbf{q}^R_u,\mathbf{p}^R_u)+\mathscr{W}^{\mathbf{2},\mathbf{q}}_{l_1l_2}(\mathbf{q}^R_u)\right\}=\mathbf{0},\\
&\sum_{\substack{l_1,l_2\in\mathbb{N}\\ l_1+l_2=r<j}}-\frac{1}{l_1!l_2!}\left\{\mathscr{W}^{\mathbf{1},\mathbf{p}}_{l_1l_2}(\mathbf{q}^R_u,\mathbf{p}^R_u)+\mathscr{W}^{\mathbf{2},\mathbf{p}}_{l_1l_2}(\mathbf{p}^R_u)\right\}=\mathbf{0},
\end{aligned} \tag{72}$$

where, after successive simplifications, the differential equations system obtained is homogeneous. Consequently, the solution for Eq. (72) reduces to the trivial solution $\mathbf{q}^R_u=\mathbf{p}^R_u=\mathbf{0}$. At order j, the differential equations system becomes

$$\begin{aligned}
&\sum_{\substack{l_1,l_2\in\mathbb{N}\\ l_1+l_2=r<j}}-\frac{1}{l_1!l_2!}\left\{\mathscr{W}^{\mathbf{1},\mathbf{q}}_{l_1l_2}\left(\mathbf{q}^R_j,\mathbf{p}^R_j\right)+\mathscr{W}^{\mathbf{2},\mathbf{q}}_{l_1l_2}\left(\mathbf{q}^R_j\right)\right\}+\mathbf{g}_j(\mathbf{q}^R_0,\mathbf{p}^R_0)=\mathbf{0},\\
&\sum_{\substack{l_1,l_2\in\mathbb{N}\\ l_1+l_2=r<j}}-\frac{1}{l_1!l_2!}\left\{\mathscr{W}^{\mathbf{1},\mathbf{p}}_{l_1l_2}\left(\mathbf{q}^R_j,\mathbf{p}^R_j\right)+\mathscr{W}^{\mathbf{2},\mathbf{p}}_{l_1l_2}\left(\mathbf{p}^R_j\right)\right\}+\mathbf{h}_j(\mathbf{q}^R_0,\mathbf{p}^R_0)=\mathbf{0},
\end{aligned} \tag{73}$$

with $\mathbf{g}_j$, $\mathbf{h}_j$ source terms at order j dependent on the generating solutions obtained at order 0, explicitly characterized by the following relations

$$\begin{aligned}\mathbf{g}_j(\mathbf{q}_0^R,\mathbf{p}_0^R) &= \sum_{\substack{l_1,l_2\in\mathbb{N}\\ l_1+l_2=r=j}} -\frac{1}{l_1!l_2!}\left\{\mathscr{W}^{\mathbf{1},\mathbf{q}}_{l_1l_2}(\mathbf{q}_0^R,\mathbf{p}_0^R)+\mathscr{W}^{\mathbf{2},\mathbf{q}}_{l_1l_2}(\mathbf{q}_0^R)\right\},\\ \mathbf{h}_j(\mathbf{q}_0^R,\mathbf{p}_0^R) &= \sum_{\substack{l_1,l_2\in\mathbb{N}\\ l_1+l_2=r=j}} -\frac{1}{l_1!l_2!}\left\{\mathscr{W}^{\mathbf{1},\mathbf{p}}_{l_1l_2}(\mathbf{q}_0^R,\mathbf{p}_0^R)+\mathscr{W}^{\mathbf{2},\mathbf{p}}_{l_1l_2}(\mathbf{p}_0^R)\right\}.\end{aligned} \tag{74}$$

Moreover, by dealing with equations at order n with $n>j$, one obtains

$$\begin{aligned}&\sum_{\substack{l_1,l_2\in\mathbb{N}\\ l_1+l_2=r<j}} -\frac{1}{l_1!l_2!}\left\{\mathscr{W}^{\mathbf{1},\mathbf{q}}_{l_1l_2}(\mathbf{q}_n^R,\mathbf{p}_n^R)+\mathscr{W}^{\mathbf{2},\mathbf{q}}_{l_1l_2}(\mathbf{q}_n^R)\right\}+\mathbf{g}_n\left(\mathbf{q}_0^R,\mathbf{p}_0^R,...,\mathbf{q}_{n-j}^R,\mathbf{p}_{n-j}^R\right)=\mathbf{0},\\ &\sum_{\substack{l_1,l_2\in\mathbb{N}\\ l_1+l_2=r<j}} -\frac{1}{l_1!l_2!}\left\{\mathscr{W}^{\mathbf{1},\mathbf{p}}_{l_1l_2}(\mathbf{q}_n^R,\mathbf{p}_n^R)+\mathscr{W}^{\mathbf{2},\mathbf{p}}_{l_1l_2}(\mathbf{p}_n^R)\right\}+\mathbf{h}_n\left(\mathbf{q}_0^R,\mathbf{p}_0^R,...,\mathbf{q}_{n-j}^R,\mathbf{p}_{n-j}^R\right)=\mathbf{0},\end{aligned} \tag{75}$$

with $\mathbf{g}_n$, $\mathbf{h}_n$ forcing terms resulting from the combination of various components summed over the term $r=l_1+l_2$ distinguished for the value of j, namely

$$\begin{aligned}\mathbf{g}_n\left(\mathbf{q}_0^R,\mathbf{p}_0^R,...,\mathbf{q}_{n-j}^R,\mathbf{p}_{n-j}^R\right) &= \sum_{\substack{l_1,l_2\in\mathbb{N}\\ l_1+l_2=r<j}} -\frac{1}{l_1!l_2!}\left\{\mathscr{W}^{\mathbf{1},\mathbf{q}}_{l_1l_2}\left(\mathbf{q}_j^R,\mathbf{p}_j^R\right)+\mathscr{W}^{\mathbf{2},\mathbf{q}}_{l_1l_2}\left(\mathbf{q}_j^R\right)\right\}+...+\\ &-\sum_{\substack{l_1,l_2\in\mathbb{N}\\ j\le l_1+l_2\le n}}\frac{1}{l_1!l_2!}\left\{\mathscr{W}^{\mathbf{1},\mathbf{q}}_{l_1l_2}(\mathbf{q}_0^R,\mathbf{p}_0^R)+\mathscr{W}^{\mathbf{2},\mathbf{q}}_{l_1l_2}(\mathbf{q}_0^R)\right\}+...-\sum_{\substack{l_1,l_2\in\mathbb{N}\\ l_1+l_2=j}}\frac{1}{l_1!l_2!}\left\{\mathscr{W}^{\mathbf{1},\mathbf{q}}_{l_1l_2}\left(\mathbf{q}_{n-j}^R,\mathbf{p}_{n-j}^R\right)+\mathscr{W}^{\mathbf{2},\mathbf{q}}_{l_1l_2}\left(\mathbf{q}_{n-j}^R\right)\right\},\\ \mathbf{h}_n\left(\mathbf{q}_0^R,\mathbf{p}_0^R,...,\mathbf{q}_{n-j}^R,\mathbf{p}_{n-j}^R\right) &= \sum_{\substack{l_1,l_2\in\mathbb{N}\\ l_1+l_2=r<j}} -\frac{1}{l_1!l_2!}\left\{\mathscr{W}^{\mathbf{1},\mathbf{p}}_{l_1l_2}\left(\mathbf{q}_j^R,\mathbf{p}_j^R\right)+\mathscr{W}^{\mathbf{2},\mathbf{p}}_{l_1l_2}\left(\mathbf{p}_j^R\right)\right\}+...+\\ &-\sum_{\substack{l_1,l_2\in\mathbb{N}\\ j\le l_1+l_2\le n}}\frac{1}{l_1!l_2!}\left\{\mathscr{W}^{\mathbf{1},\mathbf{p}}_{l_1l_2}(\mathbf{q}_0^R,\mathbf{p}_0^R)+\mathscr{W}^{\mathbf{2},\mathbf{p}}_{l_1l_2}(\mathbf{p}_0^R)\right\}+...-\sum_{\substack{l_1,l_2\in\mathbb{N}\\ l_1+l_2=j}}\frac{1}{l_1!l_2!}\left\{\mathscr{W}^{\mathbf{1},\mathbf{p}}_{l_1l_2}\left(\mathbf{q}_{n-j}^R,\mathbf{p}_{n-j}^R\right)+\mathscr{W}^{\mathbf{2},\mathbf{p}}_{l_1l_2}\left(\mathbf{p}_{n-j}^R\right)\right\},\end{aligned} \tag{76}$$

which arise from the expansion of Eq. (70) into the following relationships

$$\begin{aligned}&\sum_{\substack{l_1,l_2\in\mathbb{N}\\ l_1+l_2=r<j}} -\frac{\eta^j}{l_1!l_2!}\left\{\mathscr{W}^{\mathbf{1},\mathbf{q}}_{l_1l_2}\left(\mathbf{q}_j^R,\mathbf{p}_j^R\right)+\mathscr{W}^{\mathbf{2},\mathbf{q}}_{l_1l_2}\left(\mathbf{q}_j^R\right)\right\}-\sum_{\substack{l_1,l_2\in\mathbb{N}\\ l_1+l_2=r<j}}\frac{\eta^{j+1}}{l_1!l_2!}\left\{\mathscr{W}^{\mathbf{1},\mathbf{q}}_{l_1l_2}\left(\mathbf{q}_{j+1}^R,\mathbf{p}_{j+1}^R\right)+\mathscr{W}^{\mathbf{2},\mathbf{q}}_{l_1l_2}\left(\mathbf{q}_{j+1}^R\right)\right\}+\\ &+...-\sum_{\substack{l_1,l_2\in\mathbb{N}\\ l_1+l_2=r<j}}\frac{\eta^n}{l_1!l_2!}\left\{\mathscr{W}^{\mathbf{1},\mathbf{q}}_{l_1l_2}(\mathbf{q}_n^R,\mathbf{p}_n^R)+\mathscr{W}^{\mathbf{2},\mathbf{q}}_{l_1l_2}(\mathbf{q}_n^R)\right\}-\sum_{\substack{l_1,l_2\in\mathbb{N}\\ j\le l_1+l_2\le n}}\frac{\eta^r}{l_1!l_2!}\left\{\mathscr{W}^{\mathbf{1},\mathbf{q}}_{l_1l_2}(\mathbf{q}_0^R,\mathbf{p}_0^R)+\right.\\ &\left.+\mathscr{W}^{\mathbf{2},\mathbf{q}}_{l_1l_2}(\mathbf{q}_0^R)\right\}-\sum_{\substack{l_1,l_2\in\mathbb{N}\\ j\le l_1+l_2\le n-1}}\frac{\eta^{r+1}}{l_1!l_2!}\left\{\mathscr{W}^{\mathbf{1},\mathbf{q}}_{l_1l_2}(\mathbf{q}_1^R,\mathbf{p}_1^R)+\mathscr{W}^{\mathbf{2},\mathbf{q}}_{l_1l_2}(\mathbf{q}_1^R)\right\}+...+\\ &-\sum_{\substack{l_1,l_2\in\mathbb{N}\\ l_1+l_2=j}}\frac{\eta^n}{l_1!l_2!}\left\{\mathscr{W}^{\mathbf{1},\mathbf{q}}_{l_1l_2}\left(\mathbf{q}_{n-j}^R,\mathbf{p}_{n-j}^R\right)+\mathscr{W}^{\mathbf{2},\mathbf{q}}_{l_1l_2}\left(\mathbf{q}_{n-j}^R\right)\right\}=\mathbf{0},\\ &\sum_{\substack{l_1,l_2\in\mathbb{N}\\ l_1+l_2=r<j}} -\frac{\eta^j}{l_1!l_2!}\left\{\mathscr{W}^{\mathbf{1},\mathbf{p}}_{l_1l_2}\left(\mathbf{q}_j^R,\mathbf{p}_j^R\right)+\mathscr{W}^{\mathbf{2},\mathbf{p}}_{l_1l_2}\left(\mathbf{p}_j^R\right)\right\}-\sum_{\substack{l_1,l_2\in\mathbb{N}\\ l_1+l_2=r<j}}\frac{\eta^{j+1}}{l_1!l_2!}\left\{\mathscr{W}^{\mathbf{1},\mathbf{p}}_{l_1l_2}\left(\mathbf{q}_{j+1}^R,\mathbf{p}_{j+1}^R\right)+\mathscr{W}^{\mathbf{2},\mathbf{p}}_{l_1l_2}\left(\mathbf{p}_{j+1}^R\right)\right\}+\\ &+...-\sum_{\substack{l_1,l_2\in\mathbb{N}\\ l_1+l_2=r<j}}\frac{\eta^n}{l_1!l_2!}\left\{\mathscr{W}^{\mathbf{1},\mathbf{p}}_{l_1l_2}(\mathbf{q}_n^R,\mathbf{p}_n^R)+\mathscr{W}^{\mathbf{2},\mathbf{p}}_{l_1l_2}(\mathbf{p}_n^R)\right\}-\sum_{\substack{l_1,l_2\in\mathbb{N}\\ j\le l_1+l_2\le n}}\frac{\eta^r}{l_1!l_2!}\left\{\mathscr{W}^{\mathbf{1},\mathbf{p}}_{l_1l_2}(\mathbf{q}_0^R,\mathbf{p}_0^R)+\right.\\ &\left.+\mathscr{W}^{\mathbf{2},\mathbf{p}}_{l_1l_2}(\mathbf{p}_0^R)\right\}-\sum_{\substack{l_1,l_2\in\mathbb{N}\\ j\le l_1+l_2\le n-1}}\frac{\eta^{r+1}}{l_1!l_2!}\left\{\mathscr{W}^{\mathbf{1},\mathbf{p}}_{l_1l_2}(\mathbf{q}_1^R,\mathbf{p}_1^R)+\mathscr{W}^{\mathbf{2},\mathbf{p}}_{l_1l_2}(\mathbf{p}_1^R)\right\}+...+\\ &-\sum_{\substack{l_1,l_2\in\mathbb{N}\\ l_1+l_2=j}}\frac{\eta^n}{l_1!l_2!}\left\{\mathscr{W}^{\mathbf{1},\mathbf{p}}_{l_1l_2}\left(\mathbf{q}_{n-j}^R,\mathbf{p}_{n-j}^R\right)+\mathscr{W}^{\mathbf{2},\mathbf{p}}_{l_1l_2}\left(\mathbf{p}_{n-j}^R\right)\right\}=\mathbf{0}.\end{aligned} \tag{77}$$

Appendix D

Defining the coefficient terms $\mathbf{C}_r^{\hom}(\mathbf{n},\omega) \doteq \left(\mathbf{C}_{\mathbf{1},r}^{\hom}(\mathbf{n}) - \omega^2 \mathbf{C}_{\mathbf{2},r}^{\hom}(\mathbf{n})\right)$ for simplicity of notation, the linearization of the eigenproblem (37) can be addressed by observing that

$$\left[\sum_{r=0}^{2N}\sum_{l_1+l_2=r} \mathbf{C}_r^{\hom}(\mathbf{n},\omega)k^r\right]\widehat{\mathbf{V}}^R = k\mathbf{C}_{2N}^{\hom}k^{2N-1}\widehat{\mathbf{V}}^R + \mathbf{C}_{2N-1}^{\hom}k^{2N-1}\widehat{\mathbf{V}}^R + \ldots + \mathbf{C}_0^{\hom}\widehat{\mathbf{V}}^R = (k\mathbf{L}_1 + \mathbf{L}_0)\widehat{\mathbf{W}}^R = \mathbf{0}, \tag{78}$$

with $\widehat{\mathbf{W}}^R \doteq \left(k^{2N-1}\widehat{\mathbf{V}}^R \quad \ldots \quad k\widehat{\mathbf{V}}^R \quad \widehat{\mathbf{V}}^R\right)^T$ eigenvector $12N\times 1$, while $\mathbf{L}_1$ and $\mathbf{L}_0$ are matrices $12N\times 12N$ defined as

$$\mathbf{L}_1 = \begin{bmatrix} \mathbf{C}_{2N}^{\hom} & \mathbf{0} & \cdots & \cdots & \cdots & \mathbf{0} \\ \mathbf{0} & \mathbf{I} & \ddots & \cdots & \cdots & \vdots \\ \vdots & \ddots & \ddots & \ddots & \cdots & \vdots \\ \vdots & \cdots & \ddots & \ddots & \ddots & \vdots \\ \vdots & \cdots & \cdots & \ddots & \ddots & \mathbf{0} \\ \mathbf{0} & \cdots & \cdots & \cdots & \mathbf{0} & \mathbf{I} \end{bmatrix}, \quad \mathbf{L}_0 = \begin{bmatrix} \mathbf{C}_{2N-1}^{\hom} & \mathbf{C}_{2N-2}^{\hom} & \cdots & \mathbf{C}_r^{\hom} & \cdots & \mathbf{C}_0^{\hom} \\ -\mathbf{I} & \mathbf{0} & \cdots & \cdots & \cdots & \mathbf{0} \\ \mathbf{0} & \ddots & \ddots & \cdots & \cdots & \vdots \\ \vdots & \ddots & \ddots & \ddots & \cdots & \vdots \\ \vdots & \cdots & \ddots & \ddots & \ddots & \vdots \\ \mathbf{0} & \cdots & \cdots & \mathbf{0} & -\mathbf{I} & \mathbf{0} \end{bmatrix}. \tag{79}$$

Due to the invertibility of the matrix $\mathbf{L}_1$, the linear polynomial eigenproblem (78) can be defined in the standard form $\left(\mathbf{L}_1^{-1}\mathbf{L}_0 - k\mathbf{I}\right)\widehat{\mathbf{W}}^R = \mathbf{0}$, whose solution in terms of eigenvalues coincides with what can be obtained in the Eq. (78).

Appendix E

The in-plane field equations for the Cosserat micropolar continuum for a homogeneous material can be defined as

$$\begin{aligned} &\mathrm{E}_{\mathrm{ijhk}}\left(u_{\mathrm{h,k}} - \delta_{3\mathrm{ji}}\phi\right)_{,\mathrm{j}} = 0 \\ &\mathrm{S}_{\mathrm{ij}}\phi_{,\mathrm{ji}} + \delta_{3\mathrm{ji}}\mathrm{E}_{\mathrm{ijhk}}\left(\mathrm{u}_{\mathrm{h,k}} - \delta_{3\mathrm{kh}}\phi\right) = 0, \end{aligned} \tag{80}$$

In the particular static and unforced condition, for $i, j, h, k = 1, 2$. The partial differential Eq. (80) (where the symbol $\bullet$, represents the spatial partial derivative) are related to the translational component $\mathrm{u_h}$, micro-rotation ϕ, and the overall elastic tensor components $\mathrm{E_{ijhk}}$ and $\mathrm{S_{ij}}$. The Eq. (80) can be rewritten in the following matrix form

$$\mathbf{C}_{20}\frac{\partial^2 \mathbf{q}_{\mathrm{m}}}{\partial \mathrm{x}_1^2} + \mathbf{C}_{11}\frac{\partial^2 \mathbf{q}_{\mathrm{m}}}{\partial \mathrm{x}_1 \partial \mathrm{x}_2} + \mathbf{C}_{02}\frac{\partial^2 \mathbf{q}_{\mathrm{m}}}{\partial \mathrm{x}_2^2} + \mathbf{C}_{10}\frac{\partial \mathbf{q}_{\mathrm{m}}}{\partial \mathrm{x}_1} + \mathbf{C}_{01}\frac{\partial \mathbf{q}_{\mathrm{m}}}{\partial \mathrm{x}_2} + \mathbf{C}_{00}\mathbf{q}_{\mathrm{m}} = 0 \tag{81}$$

where $\mathbf{q}_{\mathrm{m}} = \left(\mathrm{u}_1^{\mathrm{m}} \quad \mathrm{u}_2^{\mathrm{m}} \quad \phi^{\mathrm{m}}\right)^{\mathrm{T}}$ generalized displacement vector refers to the micropolar continuum, while the non-zero components of the 3×3 coefficient matrices take the form

$$\begin{aligned} &[\mathbf{C}_{20}]_{11} = E_{1111},\ [\mathbf{C}_{20}]_{12} = [\mathbf{C}_{20}]_{21} = E_{1121},\ [\mathbf{C}_{20}]_{22} = E_{2121}, [\mathbf{C}_{20}]_{33} = S_{11}, \\ &[\mathbf{C}_{11}]_{11} = 2E_{1211},\ [\mathbf{C}_{11}]_{12} = E_{1221} + E_{1122},\ [\mathbf{C}_{11}]_{21} = E_{1122} + E_{1221},\ [\mathbf{C}_{11}]_{22} = 2E_{2122},\ [\mathbf{C}_{11}]_{33} = 2S_{12}, \\ &[\mathbf{C}_{02}]_{11} = E_{1212},\ [\mathbf{C}_{02}]_{12} = [\mathbf{C}_{02}]_{21} = E_{1222},\ [\mathbf{C}_{02}]_{22} = E_{2222},\ [\mathbf{C}_{02}]_{33} = S_{22}, \\ &[\mathbf{C}_{10}]_{13} = E_{1211} - E_{1121},\ [\mathbf{C}_{10}]_{23} = E_{1221} - E_{2121},\ [\mathbf{C}_{10}]_{31} = E_{2111} - E_{1211},\ [\mathbf{C}_{10}]_{32} = E_{2121} - E_{1221}, \\ &[\mathbf{C}_{01}]_{13} = E_{1212} - E_{1221},\ [\mathbf{C}_{01}]_{23} = E_{1222} - E_{2122},\ [\mathbf{C}_{01}]_{31} = E_{1221} + E_{1221}, \\ &[\mathbf{C}_{00}]_{33} = 2E_{1221} + E_{1212} - E_{2121}, \end{aligned} \tag{82}$$

in reference to the major symmetry properties of the elasticity tensors.

References

[1] Fleck NA, Deshpande VS, Ashby MF. Micro-architectured materials: past, present and future. Proceedings of the Royal Society A: Mathematical, Physical and Engineering Sciences 2010;466(2121):2495–516.

[2] Jia Z, Liu F, Jiang X, Wang L. Engineering lattice metamaterials for extreme property, programmability, and multifunctionality. J Appl Phys 2020;127(15): 150901.

[3] Wang C, Vangelatos Z, Grigoropoulos CP, Ma Z. Micro-engineered architected metamaterials for cell and tissue engineering. Mater Today Adv 2022;13:100206.

[4] Jiao P, Mueller J, Raney JR, Zheng X, Alavi AH. Mechanical metamaterials and beyond. Nat Commun 2023;14(1):6004.

[5] Zhang X, Han Y, Zhu M, Chu Y, Li W, Zhang Y, Zhang Y, Luo J, Tao R, Qi J. Bio-inspired 4d printed intelligent lattice metamaterials with tunable mechanical property. Int J Mech Sci 2024;272:109198.

[6] Zheng X, Zhang X, Chen T-T, Watanabe I. Deep learning in mechanical metamaterials: from prediction and generation to inverse design. Adv Mater 2023; 35(45):2302530.

[7] Sood M, Wu C-M. Influence of structural arrangements on static and dynamic properties of additively manufactured polyester elastomer lattice metamaterials. Applied Materials Today 2023;35:101933.

[8] Xia X, Spadaccini CM, Greer JR. Responsive materials architected in space and time. Nat Rev Mater 2022;7(9):683–701.

[9] Muhammad CWLim, Li JT, Zhao Z. Lightweight architected lattice phononic crystals with broadband and multiband vibration mitigation characteristics. Extreme Mechanics Letters 2020;41:100994.

[10] Fantoni F, Bosco E, Bacigalupo A. Multifield nested metafilters for wave propagation control. Extreme Mechanics Letters 2022;56:101885.

[11] Li Y, Wang Y, Yao S. Multipolar resonance and bandgap formation mechanism of star-shaped lattice structure. Int J Mech Sci 2021;193:106163.

[12] Mei C, Li L, Li X, Jiang Y, Han X, Tang H, Wang X, Hu Y. Spatiotemporal damping of dissipative metamaterial. Int J Mech Sci 2023;254:108393.

[13] Prall D, Lakes R. Properties of a chiral honeycomb with a Poisson's ratio of -1. Int J Mech Sci 1997;39(3):305–14.

[14] Wang H, Zhao D, Jin Y, Wang M, Mukhopadhyay T, You Z. Modulation of multi-directional auxeticity in hybrid origami metamaterials. Applied Materials Today 2020;20:100715.

[15] Mizzi L, Salvati E, Spaggiari A, Tan J-C, Korsunsky AM. 2d auxetic metamaterials with tuneable micro-/nanoscale apertures. Applied Materials Today 2020;20:100780.
[16] Mukhopadhyay T, Kundu D. Mixed-mode multidirectional Poisson's ratio modulation in auxetic 3d lattice metamaterials. Adv Eng Mater 2022;24(5):2101183.
[17] Aguzzi G, Kanellopoulos C, Wiltshaw R, Craster RV, Chatzi EN, Colombi A. Octet lattice-based plate for elastic wave control. Sci Rep 2022;12:1088.
[18] Wang Z-P, Poh LH, Zhu Y, Dirrenberger J, Forest S. Systematic design of tetra-petals auxetic structures with stiffness constraint. Materials & Design 2019;170:107669.
[19] Srivastava C, Mahesh V, Pitchai P, Guruprasad P, Petrinic N, Scarpa F, Harursampath D, Ponnusami SA. Effective mechanical properties of auxetic materials: numerical predictions using variational asymptotic method based homogenization. J Appl Mech 2023;90(11).
[20] Li Y, Wang X, Yan G. Analytical dispersion curves and bandgap boundaries for quadrilateral lattices. European Journal of Mechanics/A Solids 2023;97:104835.
[21] Chen Y, Li T, Scarpa F, Wang L. Lattice metamaterials with mechanically tunable Poisson's ratio for vibration control. Phys Rev Appl 2017;7(2):024012.
[22] Gao W-T, Yang C, Tan Y-T, Ren J. Reversible topological non-reciprocity by positive– negative Poisson's ratio switch in chiral metamaterials. Appl Phys Lett 2022;121(7).
[23] Carta G, Jones I, Movchan N, Movchan A. Wave polarization and dynamic degeneracy in a chiral elastic lattice. Proceedings of the Royal Society A 2019;475(2232):20190313.
[24] Kheybari M, Daraio C, Bilal OR. Tunable auxetic metamaterials for simultaneous attenuation of airborne sound and elastic vibrations in all directions. Appl Phys Lett 2022;121(8).
[25] Bacigalupo A, De Bellis ML, Misseroni D. Design of tunable acoustic metamaterials with periodic piezoelectric microstructure. Extreme Mechanics Letters 2020;40:100977.
[26] Nassar H, Chen H, Norris A, Haberman M, Huang G. Non-reciprocal wave propagation in modulated elastic metamaterials. Proceedings of the Royal Society A: Mathematical, Physical and Engineering Sciences 2017;473(2202):20170188.
[27] Matlack KH, Serra-Garcia M, Palermo A, Huber SD, Daraio C. Designing perturbative metamaterials from discrete models. Nat Mater 2018;17(4):323–8.
[28] Wang Y-Z, Li F-M, Wang Y-S. Influences of active control on elastic wave propagation in a weakly nonlinear phononic crystal with a monoatomic lattice chain. Int J Mech Sci 2016;106:357–62.
[29] Li DZ, Li SP, Ma NN, Wang HM, Zang CL, Chen WQ. Propagation characteristics of elastic longitudinal wave in a piezoelectric semiconductor metamaterial rod and its tuning. Int J Mech Sci 2024;266:108977.
[30] Mazzotti M, Foehr A, Bilal OR, Bergamini A, Bosia F, Daraio C, Pugno NM, Miniaci M. Bio-inspired non self-similar hierarchical elastic metamaterials. Int J Mech Sci 2023;241:107915.
[31] Masiani R, Rizzi N, Trovalusci P. Masonry as structured continuum. Meccanica 1995;30(6):673–83.
[32] Bertoldi K, Bigoni D, Drugan W. Nacre: an orthotropic and bimodular elastic material. Compos Sci Technol 2008;68(6):1363–75.
[33] Bollineni RK, Ahmed MS, Shahab S, Mirzaeifar R. Nacre-like block lattice metamaterials with targeted phononic band gap and mechanical properties. J Mech Behav Biomed Mater 2024;154:106511.
[34] Chen Y, Wang L. Tunable band gaps in bio-inspired periodic composites with nacre-like microstructure. J Appl Phys 2014;116(6):063506.
[35] Morsali S, Qian D, Minary-Jolandan M. Designing bioinspired brick-and-mortar composites using machine learning and statistical learning. Communications Materials 2020;1(1):1–11.
[36] Bacigalupo A, De Bellis ML, Gnecco G, Nutarelli F. On dispersion curve coloring for mechanical metafilters. Sci Rep 2022;12:20019.
[37] Diana V, Bacigalupo A, Gambarotta L. Dynamic continualization of masonry-like structured materials. Mathematics and Mechanics of Solids 2024;29(3):577–95.
[38] Jiang B, Wang Y, H Niu, Cheng X, Zhao P, Bao J. GNNs for mechanical properties prediction of strut-based lattice structures. Int J Mech Sci 2024;269:109082.
[39] Bacigalupo A, De Bellis ML, Vasta M. Design of tunable hierarchical waveguides based on Fibonacci-like microstructure. Int J Mech Sci 2022;224:107280.
[40] Liu H, Zhang ET, Wang G, Ng BF. In-plane crushing behavior and energy absorption of a novel graded honeycomb from hierarchical architecture. Int J Mech Sci 2022;221:107202.
[41] Gasparetto VEL, ElSayed MSA. Multiscale optimization of specific elastic properties and microscopic frequency band-gaps of architectured microtruss lattice materials. Int J Mech Sci 2021;197:106320.
[42] Zheng L-Y, et al. Acoustic graphene network loaded with Helmholtz resonators: a first-principle modeling, Dirac cones, edge and interface waves. New J Phys 2020;22:013029.
[43] Casolo S. A linear-elastic heuristic-molecular modelling for plane isotropic micropolar and auxetic materials. Int J Solids Struct 2021;224:111042.
[44] Bacigalupo A, Gambarotta L. Dispersive wave propagation in two-dimensional rigid periodic blocky materials with elastic interfaces. J Mech Phys Solids 2017;102:165–86.
[45] Bacigalupo A, Gambarotta L. Chiral two-dimensional periodic blocky materials with elastic interfaces: auxetic and acoustic properties. Extreme Mechanics Letters 2020;39:100769.
[46] Spadoni A, Ruzzene M. Elasto-static micropolar behavior of a chiral auxetic lattice. J Mech Phys Solids 2012;60(1):156–71.
[47] Kumar RS, McDowell DL. Generalized continuum modeling of 2-d periodic cellular solids. Int J Solids Struct 2004;41(26):7399–422.
[48] Liu X, Huang G, Hu G. Chiral effect in plane isotropic micropolar elasticity and its application to chiral lattices. J Mech Phys Solids 2012;60(11):1907–21.
[49] Ostoja-Starzewski M. Lattice models in micromechanics. Appl Mech Rev 2002;55(1):35–59.
[50] Diana V, Bacigalupo A, Gambarotta L. Continuum-molecular modeling of planar micropolar media: anisotropy, chiral properties and length-scale effects. Int J Solids Struct 2024;295:112810.
[51] Yilmaz C, Hulbert GM. Dynamics of locally resonant and inertially amplified lattice materials. Dynamics of lattice materials 2017:233–58.
[52] Huang H, Sun C, Huang G. On the negative effective mass density in acoustic metamaterials. Int J Eng Sci 2009;47(4):610–7.
[53] Huang H, Sun C. Wave attenuation mechanism in an acoustic metamaterial with negative effective mass density. New J Phys 2009;11(1):013003.
[54] Lai Y, Wu Y, Sheng P, Zhang Z-Q. Hybrid elastic solids. Nat Mater 2011;10(8):620–4.
[55] Raghavan L, Phani AS. Local resonance bandgaps in periodic media: theory and experiment. J Acoust Soc Am 2013;134(3):1950–9.
[56] Krushynska AO, Miniaci M, Bosia F, Pugno NM. Coupling local resonance with Bragg band gaps in single-phase mechanical metamaterials. Extreme Mechanics Letters 2017;12:30–6.
[57] Krushynska AO, Kouznetsova VG, Geers MG. Towards optimal design of locally resonant acoustic metamaterials. J Mech Phys Solids 2014;71:179–96.
[58] Liu X-N, Hu G-K, Huang G-L, Sun C-T. An elastic metamaterial with simultaneously negative mass density and bulk modulus. Appl Phys Lett 2011;98(25).
[59] Baravelli E, Ruzzene M. Internally resonating lattices for bandgap generation and low-frequency vibration control. J Sound Vib 2013;332(25):6562–79.
[60] Zhu R, Liu X, Hu G, Sun C, Huang G. A chiral elastic metamaterial beam for broadband vibration suppression. J Sound Vib 2014;333(10):2759–73.
[61] Zhu R, Liu X, Hu G, Sun C, Huang G. Negative refraction of elastic waves at the deep- subwavelength scale in a single-phase metamaterial. Nat Commun 2014;5(1):5510.
[62] Xiao L, Iqbal M, Yu X. Quasi-static band gaps in metamaterial pipes with negative stiffness resonators. Int J Mech Sci 2024;261:108668.
[63] Fan X, Li J, Zhang X, Li F. Multi-bandgaps metamaterial plate design using complex mass-beam resonator. Int J Mech Sci 2022;236:107742.
[64] Li Y, Gao Z, Cai K, Luo Y. Design of multi-state tunable phononic crystals based on the reconstruction mechanism of guide-rail lattice. Int J Mech Sci 2023;254:108442.
[65] Liu X, Hu G, Sun C, Huang G. Wave propagation characterization and design of two- dimensional elastic chiral metacomposite. J Sound Vib 2011;330(11):2536–53.
[66] Zhu D, Huang X, Hua H, Zheng H. Vibration isolation characteristics of finite periodic tetrachiral lattice coating filled with internal resonators. Proc Inst Mech Eng Part C J Mech Eng Sci 2016;230(16):2840–50.
[67] Bacigalupo A, Gambarotta L. Identification of non-local continua for lattice-like materials. Int J Eng Sci 2021;159:103430.
[68] Lu M-H, Feng L, Chen Y-F. Phononic crystals and acoustic metamaterials. Mater Today 2009;12(12):34–42.
[69] Rosenau P. Hamiltonian dynamics of dense chains and lattices: or how to correct the continuum. Phys Lett A 2003;311(1):39–52.
[70] Askes H, Metrikine AV. Higher-order continua derived from discrete media: continualisation aspects and boundary conditions. Int J Solids Struct 2005;42(1):187–202.
[71] Askes H, Suiker A, Sluys L. A classification of higher-order strain-gradient models–linear analysis. Archive of Applied Mechanics 2002;72(2):171–88.
[72] Bacigalupo A, Gambarotta L. Wave propagation in non-centrosymmetric beam-lattices with lumped masses: discrete and micropolar modeling. Int J Solids Struct 2017;118-119:128–45.
[73] Andrianov I, Awrejcewicz J. Continuous models for 2d discrete media valid for higher-frequency domain. Comput Struct 2008;86(1–2):140–4.
[74] Collins MA. A quasicontinuum approximation for solitons in an atomic chain. Chem Phys Lett 1981;77(2):342–7.
[75] Rosenau P. Dynamics of dense lattices. Phys Rev B 1987;36(11):5868.
[76] Kevrekidis P, Kevrekidis I, Bishop A, Titi E. Continuum approach to discreteness. Phys Rev E 2002;65(4):046613.
[77] Jia L, Jie Y, Sritawat K, Huaping W. A dynamic homogenization model for long-wavelength wave propagation in corrugated sandwich plates. Int J Mech Sci 2018;149:27–37.
[78] Andrianov IV, Starushenko GA, Weichert D. Numerical investigation of 1d continuum dynamical models of discrete chain. ZAMM-Journal of Applied Mathematics and Mechanics/Zeitschrift für Angewandte Mathematik und Mechanik 2012;92(11–12):945–54.
[79] Charlotte M, Truskinovsky L. Lattice dynamics from a continuum viewpoint. J Mech Phys Solids 2012;60(8):1508–44.
[80] Kunin IA. Elastic media with microstructure I: one-dimensional models, 26. New York: Springer Berlin Heidelberg; 1982.
[81] Bacigalupo A, Gambarotta L. Generalized micropolar continualization of 1d beam lattices. Int J Mech Sci 2019;155:554–70.
[82] Gómez-Silva F, Zaera R. Analysis of low order non-standard continualization methods for enhanced prediction of the dispersive behaviour of a beam lattice. Int J Mech Sci 2021;196:106296.
[83] Gómez-Silva F, Fernández-Sáez J, Zaera R. Nonstandard continualization of 1d lattice with next-nearest interactions. low order odes and enhanced prediction of the dispersive behavior. Mech Adv Mater Struct 2020;29(6):923–32.
[84] Le Verrier U. Sur les variations séculaires des éléments des orbites pour les sept planètes principales. J. de Math. 1840;5(1):230.

[85] Horst P. A method for determining the coefficients of a characteristic equation. Ann Math Stat 1935;6:83–4.
[86] Faddeev DK, Faddeeva VN. Computational methods of linear algebra. W.H. Freeman San Francisco; 1980.
[87] Maslov VP. Asymptotic methods of solution of pseudodifferential equations. Moskow: Nauka; 1987.
[88] Davies EB. Spectral theory and differential operators. Cambridge University Press; 1995.
[89] Bacigalupo A, Badino P, Diana V, Gambarotta L. Overall constitutive properties of stratified lattices with alternating chirality. Philosophical Transactions of the Royal Society A 2024;382:20230355.
[90] Fantoni F, Bacigalupo A, Gambarotta L. Dynamic multifield continualization of multilayered lattice-like metamaterials. Int J Solids Struct 2024;304:113015.
[91] Bacigalupo A, Gambarotta L. Simplified modeling of chiral lattice materials with local resonators. Int J Solids Struct 2016;83:126–41.